DEVELOPMENT OF AN IN SITU SYSTEM

FOR MEASURING GROUND THERMAL

PROPERTIES

by

WARREN ADAM AUSTIN, III

Bachelor of Science

Oklahoma State University

Stillwater, Oklahoma

1995

Submitted to the Faculty of the
Graduate College of the
Oklahoma State University
in partial fulfillment of
the requirements for
the Degree of
MASTER OF SCIENCE
Oklahoma State University
May, 1998

DEVELOPMENT OF AN IN SITU SYSTEM

FOR MEASURING GROUND THERMAL

PROPERTIES

Thesis Approved:

_____
Thesis Adviser

_____

Ronald L. Dougherty
_____

Wayne B. Powell
_____
Dean of Graduate College

ACKNOWLEDGMENTS

TABLE OF CONTENTS

LIST OF TABLES

LIST OF FIGURES

1. Introduction

1.1. Overview

Ground Source Heat Pump systems (GSHP) have a number of desirable characteristics, including high efficiency, low maintenance costs, and low life cycle cost. However, the high initial costs of GSHP systems sometimes cause a building owner to reject the GSHP system alternative. For commercial applications, vertical ground loop heat exchangers (boreholes) are typically used, and for large buildings, the large number of boreholes required can be quite expensive.

Each vertical heat exchanger consists of three main components, as shown in figure 1-1. The three components are the pipe, grout material around the pipe, and soil around the grout. The vertical borehole is a drilled cylindrical hole that can vary in diameter and depth.

The pipe, which typically ranges from ¾" nominal diameter to 1 ½" nominal diameter is high density polyethylene (HDPE). The pipe is inserted in a "U" shape, with a "U-bend" at the bottom of the borehole.

The next component is the material surrounding the pipe, usually "grout". The grout plays an important role in heat transfer between the soil and the fluid flowing within the pipe. It is preferable for the grout to have a high thermal conductivity. Different grout materials have different thermal conductivity values, typically ranging from 0.3 to 0.9 Btu/ft-hr-°F.

The goal of this thesis project is to develop an apparatus and procedure for estimating the thermal properties of the soil surrounding a drilled hole. The uncertainty of the soil's thermal properties is often the most significant problem facing GSHP

1. Introduction

1.1. Overview

Ground Source Heat Pump systems (GSHP) have a number of desirable characteristics, including high efficiency, low maintenance costs, and low life cycle cost. However, the high initial costs of GSHP systems sometimes cause a building owner to reject the GSHP system alternative. For commercial applications, vertical ground loop heat exchangers (boreholes) are typically used, and for large buildings, the large number of boreholes required can be quite expensive.

Each vertical heat exchanger consists of three main components, as shown in figure 1-1. The three components are the pipe, grout material around the pipe, and soil around the grout. The vertical borehole is a drilled cylindrical hole that can vary in diameter and depth.

The pipe, which typically ranges from ¾" nominal diameter to 1 ½" nominal diameter is high density polyethylene (HDPE). The pipe is inserted in a "U" shape, with a "U-bend" at the bottom of the borehole.

The next component is the material surrounding the pipe, usually "grout". The grout plays an important role in heat transfer between the soil and the fluid flowing within the pipe. It is preferable for the grout to have a high thermal conductivity. Different grout materials have different thermal conductivity values, typically ranging from 0.3 to 0.9 Btu/ft-hr-°F.

The goal of this thesis project is to develop an apparatus and procedure for estimating the thermal properties of the soil surrounding a drilled hole. The uncertainty of the soil's thermal properties is often the most significant problem facing GSHP

designers and engineers. The thermal properties that designers are concerned with are the thermal conductivity (k), thermal diffusivity (α), and volumetric heat capacity (ρc_p). The properties are related by the following equation:

$$\alpha_{soil} = \frac{k_{soil}}{\rho_{soil} c_{p_{soil}}}$$

(1-1)

The number of boreholes and depth per borehole is highly dependent on the soil thermal properties. Depending on geographic location and the drilling cost for that particular area, the soil thermal properties highly influence the initial cost to install a ground source heat pump system.
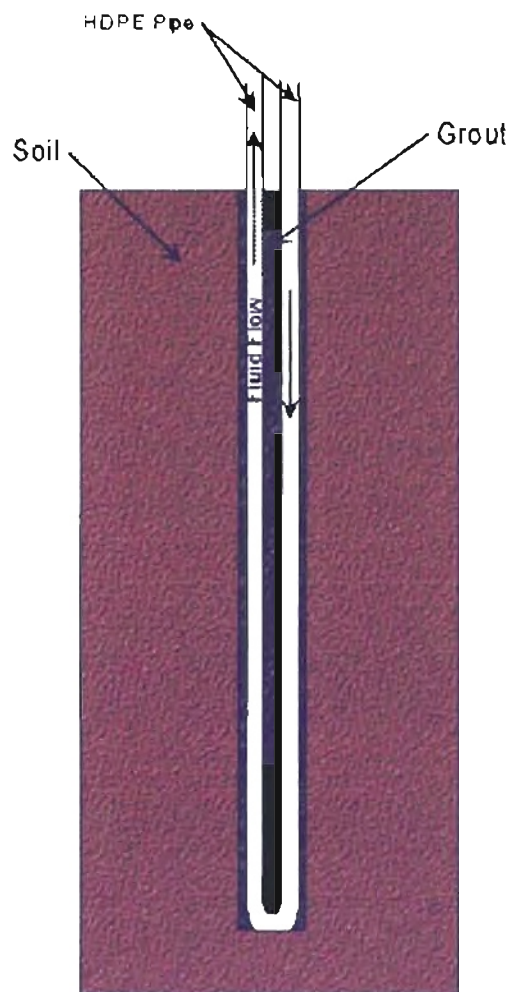
Figure 1-1. Typical Vertical Ground Loop Heat Exchanger with a U-bend Pipe Configuration

Designers of the ground loop heat exchangers have a very difficult job when estimating the soil thermal conductivity (k) and soil volumetric heat capacity (ρc_p). Both soil thermal properties are generally required when the designer is sizing the ground loop heat exchanger depth and number of boreholes using software programs such as GLHEPRO for Windows (Spitler, et al. 1996).

The borehole field can be an array of boreholes often configured in a rectangular grid. In order to design the borehole field, designers and engineers must begin with values for the soil parameters. Some engineers and designers use soil and rock classification manuals containing soil property data to design GSHP systems. One popular manual used is the Soil and Rock Classification for the Design of Ground-Coupled Heat Pump Systems Field Manual (EPRI, 1989). Figures 1-2a and 1-2b are excerpts from the manual of typical thermal conductivities for the rock classifications. The horizontal band associated with each soil/rock type indicates the range of thermal conductivity. The typical designer must choose a thermal conductivity value within that band range depending on the soil composition of the project.
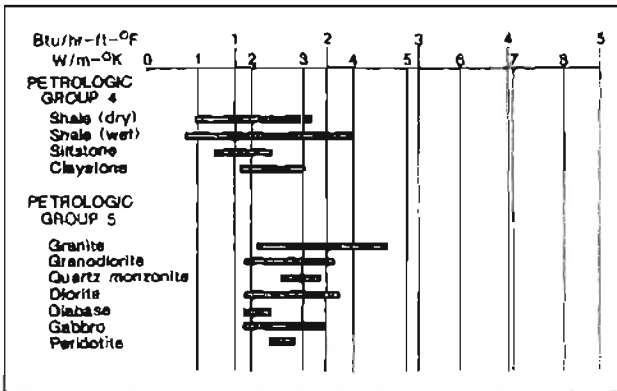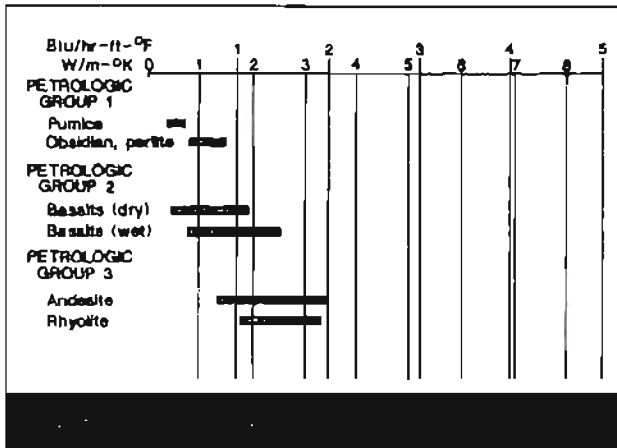
FIGURE 11-1. Thermal Conductivities of Typical Rocks (2 of 3)

Figure 1-2a. Rock Thermal Conductivity Values Taken from
Soil and Rock Classification Field Manual (EPRI, 1989)
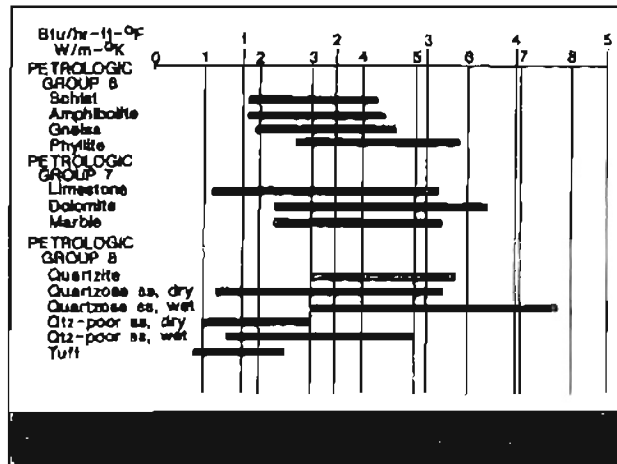
Figure 1-2b. Rock Thermal Conductivity Values taken from
Soil and Rock Classification Field Manual (EPRI, 1989)

4

Consider Quartzose sandstone (ss) wet in Figure 1-2b. According to the figure, the thermal conductivity ranges from 1.8 Btu/ft-hr-°F (~3 W/m-K) to 4.5 Btu/hr-ft-°F (~7.85 W/m-K). A conservative and prudent designer would choose the thermal conductivity value of 1.8 Btu/hr-ft-°F (~3 W/m-K) or some value close to the low end of the band. The lower conductivity value results in more total borehole length. At the other end of the spectrum, the high value of 4.5 Btu/hr-ft-°F (~7.85 W/m-K) yields the smallest total borehole length.

As an example, twelve boreholes in a rectangle are sized for a 9,000 ft^2 daycare center. Using the sizing option of GLHEPRO for Windows and a thermal conductivity value of 4.5 Btu/hr-ft-°F (~7.85 W/m-K), the required depth for each borehole is 152 ft (~46 m). With the same configuration, changing the thermal conductivity to 1.8 Btu/hr-ft-°F (~3 W/m-K) requires a ground loop heat exchanger depth per borehole of 217 ft (~66 m). This is a per borehole depth difference of 65 ft (~43 m), nearly a 43% increase. The change in depth greatly effects the change in cost. The borehole will incur additional drilling cost, pipe cost, grout cost, and header cost. Estimating a cost of $10 per foot for the total installation, the additional ground loop heat exchanger depth will cost $7,800 for the twelve boreholes.

To even further complicate the problem, the designer must deal with soil rock formations that consist of multiple layers. In order to overcome this uncertainty, the designer may require that a well log as a single test borehole is drilled. Unfortunately, well logs are often extremely vague ("...12 feet of sandy silt, 7 feet of silty sand...") and difficult to interpret. When the uncertainties in the soil or rock type are coupled with the

uncertainties in the soil thermal properties, the designer must, again, be conservative and prudent when sizing the borefield.

This thesis focuses on methods for experimentally measuring the ground thermal properties using a test borehole, then using the experimental results to develop methods to better estimate the ground thermal properties. All of the tested boreholes were part of commercial installations and research sites in Stillwater, OK, Chickasha, OK, and Bartlesville, OK, and South Dakota State University, SD. This thesis will describe the development an experimental apparatus to collect data and the development of a computational model to evaluate the data collected and estimate the soil thermal properties.

1.2. Literature Review- Test Methods

There are several methods for estimating soil thermal conductivity that might be applied to boreholes. These include soil and rock identification, experimental testing of drill cuttings, in situ probes, and inverse heat conduction models.

1.2.1. Soil and Rock Identification

One technique to determine the soil thermal properties is described by the IGSHPA Soil and Rock Classification manual. The manual contains procedures to determine the type of soil and the type of rock encountered at a project location. The procedure begins by classifying the soil by visual inspection.

6

The next few steps can be followed by the flow chart depicted in figure 3-1 of the Soil and Rock Classification Field Manual (EPRI 1989). Once the soil type has been determined, the reference manual offers the values shown in Table 1-1 for the different soil types:

Table 1-1 Soil Thermal Properties				
Thermal Texture Class	Thermal Conductivity		Thermal Diffusivity	
	W/m-°K	Btu/hr-ft-°F	cm²/sec	ft²/day
Sand (or Gravel)	0.77	0.44	0.0045	0.42
Silt	1.67	0.96	-	-
Clay	1.11	0.64	0.0054	0.50
Loam	0.91	0.52	0.0049	0.46
Saturated Sand	2.50	1.44	0.0093	0.86
Saturate Silt or Clay	1.67	0.96	0.0066	0.61

Alternatively, if the underlying ground at the site also contains various rock formations, it is then necessary to classify the rock type(s) into eight different categories based upon several different elements. The eight categories are termed Petrologic groups. Figure 1-2a and 2b show the thermal conductivity values for each rock type. Even though the rock identification procedures are somewhat complicated, the designer is still left with a wide range of thermal conductivities and to be prudent, must choose a low value.

1.2.2. Experimental Testing of Drill Cuttings

Another method used to determine the thermal conductivity of the rock was approached from the viewpoint that the conductivity can be determined from the drill cuttings. Sass (1971) stated at that time that thermal conductivity is difficult to determine

7

by standard methods due to the lack of cores or outcrop samples from the drill. The only available samples to use were the drill cuttings that could vary in size from a fine powder (air-drilled displacement) to millimeter sized particles (coarse-toothed rotary bits). Sass (1971) began his procedure by collecting the drill cuttings of a well into a plastic cell using a spatula to pack the particles inside the cell. The plastic cell is then weighed (dry). Then water is added into the plastic cell and weighed again (wet). The difference in weight can be used to find the volume fraction of water. Next, the cell is placed in a divided-bar apparatus and the effective thermal conductivity is determined. The plastic cell is a long plastic tube approximately 0.63 cm thick, fitted to machined copper bases as shown in Figure 1-3. The outer diameter is the same as the divided bar at an outer diameter of 3.81 cm and an inner diameter of 3.49 cm. The plastic cell has a volume of 6 cm^3. A constant temperature drop is maintained across the sample and copper standard. The thermal conductivity is then estimated by using a rock fragment and water mixture in a steady-state divided-bar apparatus.
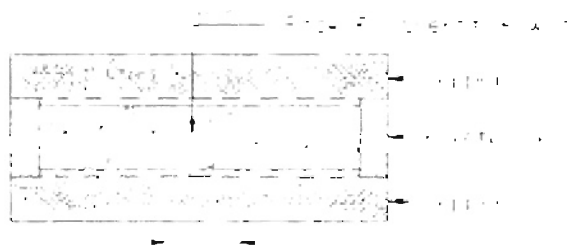
Figure 1-3. Illustrated Thermal Conductivity Cell

The model for this approach begins with the assumption that the thermal resistance of the full cell can be represented by the thermal resistance of the aggregate and the plastic cell wall in parallel given in equation 1-2.

$$K_a = \frac{D^2}{d^2} K_c - \frac{D^2 - d^2}{d^2} K_p \qquad (1\text{-}2)$$

Where, K_p *is the thermal conductivity of the plastic wall*

D is the Outer diameter of the Cell Wall (3.81 cm)

d is the Inner Diameter of the Cell Wall (3.49 cm)

K_c *is the measured conductivity of the Cell and Contents*

K_a *is the conductivity of the water-saturated aggregate.*

In the second part of this model, the aggregate can be represented by a geometric mean of conductivities of its constituents. Where the constituent conductivities do not contrast by more than one order of magnitude, this model appears to have been successful for applications of this kind. For an aggregate in which the *i*th constituent occupies volume fraction ϕ,

$$K_a = K_1^{\phi 1} K_2^{\phi 2} \dots K_n^{\phi n} \qquad (1\text{-}3)$$

If n-1 of the constituents are solid fragments, and the remaining constituent is water with conductivity K_w and volume fraction ϕ, then K_a becomes:

$$K_a = K_r^{1-\phi} K_w^{\phi} \qquad (1\text{-}4)$$

Where. K_r *is the geometric mean conductivity of the solid constituents*

Combining equation 1-1 and 1-3 gives:

$$K_r = K_w \left\{ \frac{D^2}{d^2} \frac{K_c}{K_w} - \frac{D^2 - d^2}{d^2} \frac{K_p}{K_w} \right\}^{1/(1-\phi)} \qquad (1\text{-}5)$$

Substituting the known numerical values and the known values of the apparatus, equation 1-5 can be reduced to:

9

$$K_r = 1.46\{0.815K_c - 0.104\}^{1/(1-\phi)} \tag{1-6}$$

Equation 1-6 gives an estimate of the conductivity of a nonporous isotropic rock in terms of the effective conductivity of a cell containing its water-saturated fragments and of the porosity of the cell's contents.

The results of using this method to determine the thermal conductivity are debatable due to the assumption of rock/soil continuity. If several different layers of rock and/or soil are present, it is difficult to determine with certainty the thermal conductivity value obtained using the drill cuttings. [1]

1.2.3. In Situ Probes

The idea of using measuring probes has been around for some time. According to Choudary (1976), sampling the ground parameters for thermal conductivity and diffusivity in situ using a probe could reduce measurement error of the ground thermal conductivity. This concept was first suggested by a German physicist named Schleiremachen in 1833. It wasn't until around the 1950's that the probes were developed to the point of being usable for testing drilled wells.

The general construction of an in situ probe consists of an internal heater and at least one embedded temperature sensor all set in a ceramic insulator or epoxy. All of

---

[1] Experimental Testing of Borehole Cored Samples

Concurrent research under way at Oklahoma State University in estimating the thermal conductivity of the soil uses the concept of cored samples taken from a borehole drilled for use in a ground loop heat exchanger. This new innovative method takes cored samples from the drill and utilizes a guarded hot plate experimental test apparatus. Each core sample tested is the size of small cylinder with approximately 3 ½" radius and 3" in length. The sample is carefully handled to maintain the moisture content by sealing the sample with a very thin layer of epoxy.

these components are then encased by a metal sheath, usually stainless steel on modern probes.

Most probes used for this type of application today are about 6 to 12 inches long. These types of small probes are usually placed in a bucket size sample of the drilled soil at a laboratory. The probe in the middle of the bucket then heats the soil. The probe then measures the temperature response to the heat input. Some newer probe models incorporate the heater and temperature sensor within the same probe. Based upon the temperature measurement in the middle of the probe and the measured heat input, the results are used in models such as the Line Source Model for determining the thermal conductivity of the soil.

1.3. Literature Review- Models

Several different models have been utilized for estimating the performance of vertical ground loop heat exchangers. They are of interest here for possible inverse use—estimating the ground thermal properties from the performance rather than the performance from the ground thermal properties. Specifically, we are interested in imposing a heat pulse of "short" duration (1-7 days) and determining the ground thermal properties from the results.

1.3.1. Line Source Model

This model is based on approximating the borehole as a line source, assuming end effects are small. The soil acts as a heat rejection medium that has an assumed uniform and constant initial temperature (T_o). The original model was first developed by Lord Kelvin and it is sometimes called Kelvin Line Source Theory. Ingersoll and Plass (1948) applied the model to ground loop heat exchangers. Mogensen (1983) further enhances their findings by applying the model to estimate the ground thermal conductivity. Ingersoll and Plass begin with this general line source equation:

$$\Delta T(r,t) = \frac{\dot{Q}}{2\pi k} \int\limits_{\frac{r}{2\pi k}}^{\infty} \frac{e^{-\beta}}{\beta} d\beta \tag{1-7}$$

Where,

  $\Delta T(r,t)$ = Temperature Rise beginning at T_o (°F)

  r = Radius from Line Source (ft)

  t = Time after start of Heat Injection (hr)

  $\dot{Q}$ = Heat Injection Rate per unit borehole length (Btu/hr-ft)

  k = Thermal Conductivity (Btu/hr-ft-°F)

  α = Thermal Diffusivity (ft²/hr)

Mogensen (1983) suggested approximating the integral portion of equation 1-7 as:

$$\int\limits_{\frac{r}{2\pi k}}^{\infty} \frac{e^{-\beta^2}}{\beta} d\beta = \ln\left(\frac{4\alpha t}{R^2}\right) - C \tag{1-8}$$

Where,   C = Euler's Number (0.5772...).

12

In this case, r = R is the borehole wall radius given by Mogensen (1983). It is also required to include the thermal resistance between the fluid within the pipe and the borehole wall. Mogensen (1983) stated this thermal resistance as 'm_{TR}'.

The thermal resistance has the units of hr-ft-°F/Btu. The addition of thermal resistance into the equation yields:

$$\Delta T(R,t) = \dot{Q} m_{TR} + \frac{\dot{Q}}{4\pi k}\left[\ln\left(\frac{4\alpha t}{R^2}\right) - C\right] \tag{1-9}$$

Collecting terms and rearranging the equation to a more usable form, it becomes easily evaluated for an effective thermal conductivity of the soil for a given length of time, near constant heat injection rate, and near constant change in temperature. The resulting equation for this evaluation is:

$$\Delta T(R,t) = \dot{Q} m_{TR} + \frac{\dot{Q}}{4\pi k}\left[\ln\left(\frac{4\alpha}{R^2}\right) - C\right] + \frac{\dot{Q}}{4\pi k}\ln t \tag{1-10}$$

Notice the first two terms on the right hand side of the equation are constant as long as the heat injection rate is near constant. The only variable in the equation is ln(t). The equation is then reduced to simplest form by taking the constants and ln(t) into a general linear form,

$$y = mx + b \tag{1-11}$$

Where,

     $y = \Delta T$ the change in temperature

     b = the two constant terms on the RHS of the equation

     $m = \dfrac{\dot{Q}}{4\pi k}$

     $x = \ln t$

After obtaining experimental data of delta T, time, and the heat injection rate, a simple plot of temperature versus the natural log of time will yield the slope of the line. This slope is equated to 'm' and the thermal conductivity can be determined.

This model is very easy to use once the derivation is reduced to the final equation (1-11). The Line Source Model does have some disadvantages. This model is applied in Chapter 5. As shown in Chapter 5, there are significant difficulties associated with applying the model in practice.

1.3.2. Cylindrical Source Model

The model was first implemented by Carslaw and Jaeger and presented by Ingersoll (1948, 1954). The description here relies primarily on Kavanaugh (1984, 1991). The model was developed by using a finite cylinder in an infinite medium of constant properties. The cylinder source model begins with the analytical solution to the 2-D heat conduction equation:

$$\Delta T_g = T_{ff} - T_{rn} = \frac{q_{gc}}{k_s L} G(z, p) \tag{1-12}$$

$$\text{Where, } G(z,p) = \frac{1}{\pi^2} \int_0^\infty \frac{e^{-\beta^2 z} - 1}{J_1^2(\beta) + Y_1^2(\beta)} \left[J_0(p\beta) Y_1(\beta) - J_1(\beta) Y_0(p\beta) \right] \frac{d\beta}{\beta^2} \tag{1-13}$$

T_{ff} *is the far-field temperature*

T_{ro} *is the temperature at the cylinder wall*

T_g *is the temperature of ground*

q_{gc} *is the heat flux or heat pulse to the ground*

k_s *is the thermal conductivity of the soil*

L *is the length of the cylinder*

The dependent variables within the 'G' or cylinder source function are given as:

$$z = \frac{\alpha_{soil} t}{r^2}$$

(1-14)

$$p = \frac{r}{r_o}$$

(1-15)

The term z in equation 1-14 is known as the Fourier number. Equation 1-12 is based on a constant heat flux to the ground. For the purposes of experimentation and the fact that applications do not operate in the constant heat flux mode, equation 1-12 can be modified to adjust for the abnormalities that occur. Kavanaugh (1991) has developed an equation to estimate equation 1-12, broken down into piece-wise time intervals. The resulting equation is:

$$\Delta T_g = \frac{1}{k_{soil} L} \left\{ \begin{array}{l} RF_1 q_{RG_1} \left[G(z,p)_n - G(z,p)_{n-1} \right] + RF_2 q_{RG_2} \left[G(z,p)_{n-1} - G(z,p)_{n-2} \right] + \\ ...+RF_n q_{RG_n} \left[G(z,p)_1 \right] \end{array} \right\}$$

(1-16)

Where,   *RF is the run fraction that modifies the heat rate into the ground (Kavanaugh, 1984)*

n is the time interval

In order to adapt the cylinder source model to a borehole with a U-bend pipe configuration, an equivalent diameter was suggested to correct this error. The diameter of the two pipe leads can be represented by an approximation of an equivalent diameter for the given pipe's diameter (Bose, 1984).

$$D_{equivalent} = \sqrt{2} \, D_o$$

(1-17)

This diameter equivalence of equation 1-17 yields a single diameter pipe, which approximates the heat transfer from two pipes in a cylindrical borehole. The two pipes are represented as a single cylinder with diameter $D_{equivalent}$. If the grout properties are assumed to be the same as the soil properties, the temperature at the edge of the

15

equivalent pipe can be estimated using $G(z,1)$. The resistance between the fluid and the edge of the equivalent pipe must be estimated. The internal structure is composed of the resistance of the pipe conductivity and the resistance of convection due to the fluid movement inside the pipe. The pipe resistance can be represented [2] by:

$$R_p = \frac{r_o \ln\left(\frac{r_o}{r_i}\right)}{2k_p} \tag{1-18}$$

The conductivity of the pipe (k_p) is required as part of the input for equation 1-18. The convection resistance can represented similarly by:

$$R_c = \frac{1}{h_i \frac{r_i}{r_o}} \tag{1-19}$$

The convection coefficient (h_i) in equation 1-19 is determined from the following two equations that deal with heat transfer in internal fluid flow pipes. Equation 1-20 is the convection coefficient for turbulent flow.

$$h_i = Nu_{D_i} \frac{k_w}{D_i} \tag{1-20}$$

The Nusselt number (Nu) is given by Dittus (1930) as a function of the Reynold's number and Prandtl number. The Nusselt equation is given as:

$$Nu_{D_i} = 0.023 \, Re_{D_i}^{4/5} \, Pr^n \tag{1-21}$$

The Prandtl power coefficient is dependent on the direction of the temperature field. For heating ($T_{pipe\ surface} > T_{mean\ fluid\ temp}$), $n = 0.4$. For cooling ($T_{pipe\ surface} < T_{mean\ fluid\ temp}$), n 0.3.

---

[2] Kavanaugh does not insert a 2 in the denominator, but it appears that it should be there to account for the fact that there are two pipes in parallel. Cf. Paul (1996).

After calculating the convection coefficient in equations 1-20, equation 1-18 and 1-19 can be combined into an equivalent heat transfer coefficient of the total heat transfer from the fluid to the outside cylinder pipe wall. Kavanaugh (1991) represents the equivalent pipe resistance as:

$$h_{eq} = \frac{1}{R_p + R_c}$$

(1-22)

The temperature difference between the outside wall of the cylinder and fluid inside the pipe can be calculated using equation 1-23.

$$\Delta T_p = \frac{q_{sc}}{C * N_t * h_{eq} * A_o}$$

(1-23)

Where, $A_o = 2\pi r_o L$ is the outer surface area of contact
$C = 0.85$ is the short circuit factor
N_t is the number of tubes used

The combination of two pipes configured in a U-bend borehole are close together if not touching at some places. Since the result is some heat transfer from one pipe to the other (thermal short-circuiting), Kavanaugh (1984) has incorporated a coefficient to account for this. The coefficient is $C = 0.85$ for a single U-bend ground loop design. There is also a need to account for the actual number of pipes. Occasionally, more than one U-tube is inserted into a borehole, the coefficient N_t accounts for the additional actual surface of the multiple pipe leads.

After determining all of the variables, equations 1-12, 1-22 and the far-field temperature (T_{ff}) can be summed to yield the average water temperature.

$$T_{avg} = T_{ff} + \Delta T_g + \Delta T_p$$

(1-24)

As presented, the cylinder source model does not account for the grout thermal properties, but they could be taken into account. Kavanaugh (1997) suggests a trial-and-error approach to determine k_{soil} from an experimental data set. This is not wholly satisfying, as it is time consuming and relies on user judgement as to what is the best solution.

1.4. Objectives

Based on the need for measurement of ground thermal properties, the following objectives have been developed:

1. Develop a portable, reasonable-cost, in situ test system that can be replicated by others in the ground source heat pump industry. Also, determine a suitable test procedure.

2. Develop a numerical model to represent a borehole, incorporating variable power input, convection resistance, conduction through the pipe, conduction through the grout, and conduction through the soil. The model will be used to determine the thermal response of the borehole and ground for various choices of soil and grout thermal properties. By adjusting the value of the soil and grout thermal properties, a best "fit" to the experimental data can be found. The adjustment process, when done systematically, is known as parameter estimation.

3. Determine the best parameter estimation procedure for analyzing the experimentally obtained results of the soil thermal properties.

2. Experimental Apparatus

2.1. Description of Experimental Apparatus

The experimental apparatus is contained within an enclosed single axle trailer. The trailer contains all necessary components to perform a test. The apparatus has two barb fittings on the exterior of the trailer to allow attachment of two HDPE tubes which are protruding from a vertical borehole. The trailer houses stainless steel plumbing, water heater elements, water supply/purge tank and pump, circulation pumps and valves, an SCR power controller, and two 7000 watt power generators (not inside the trailer during testing). All necessary instrumentation and data acquisition equipment are also contained within the trailer. The instrumentation and data acquisition equipment include a flow meter, two thermistor probes, a watt transducer, two thermocouples, and a data logger. The experimental apparatus is described as a set of subsystems: the trailer, the water supply, the power supply, water heating, pipe insulation, temperature measurement, flow sensing/control equipment, and data acquisition.

2.2. In Situ Trailer Construction

The in situ trailer must be able to operate independently of water and electric utilities, since many of the test locations are undeveloped. The trailer must also be capable of housing every component of the experimental apparatus. The mobile unit containing the experimental apparatus is a Wells Cargo general-purpose trailer. Figures 2-1 and 2-2 are scaled drawings of the Wells Cargo/In Situ trailer. Both figures depict

20

exterior views of the trailer, and show the original condition of the trailer with one modification, the Coleman 13,500 Btu/hr Air Conditioner mounted on top of the roof.
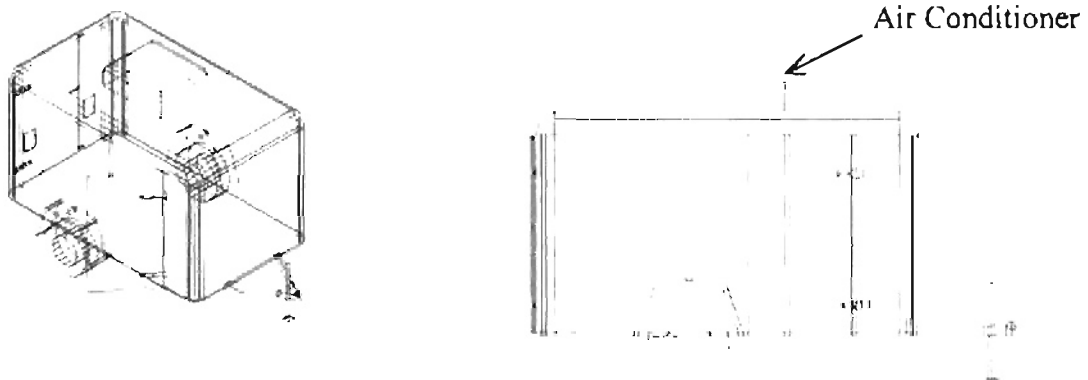
Figure 2-1. Exterior Views of In Situ trailer
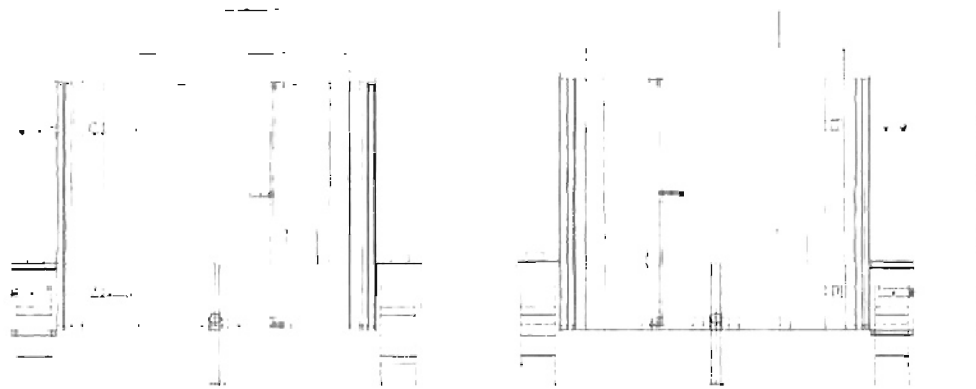
Figure 2-2. Exterior Views of In Situ trailer

The dimensions of the trailer play a very important role in equipment placement. All other parts of the experimental apparatus must fit into the trailer at the same time. The inside trailer dimensions are 10 ft x 6 ft x 5 ½ ft, shown in Figures 2-3 and 2-4.
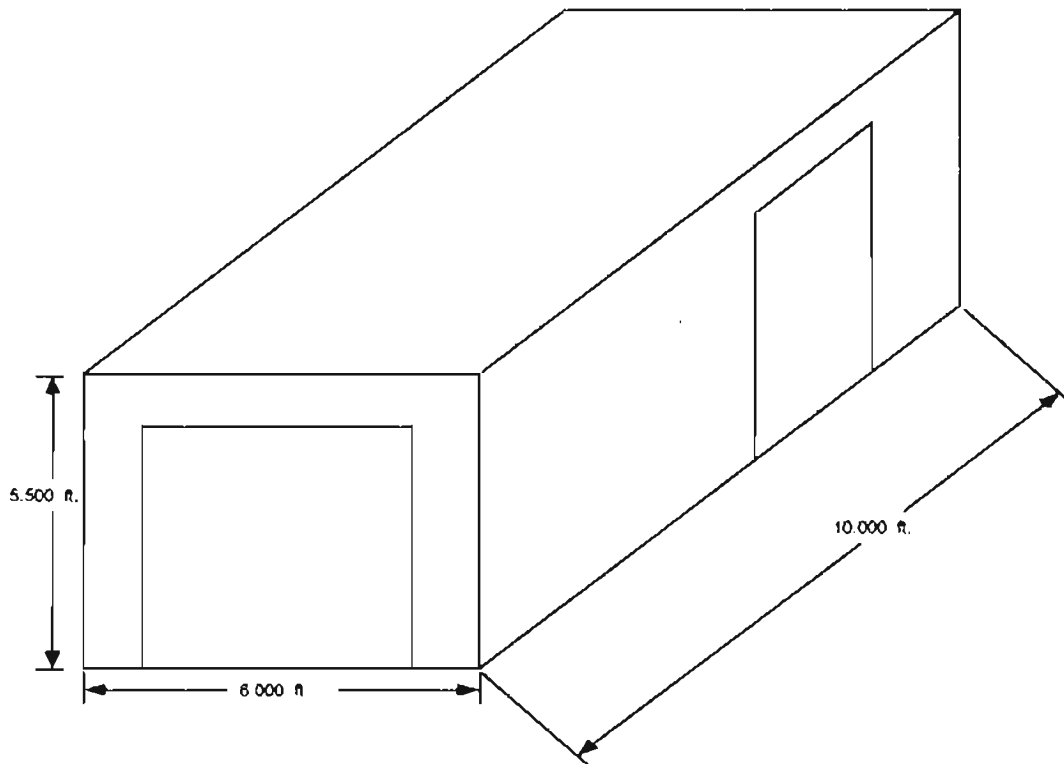
Figure 2-3. In Situ Trailer Dimensions
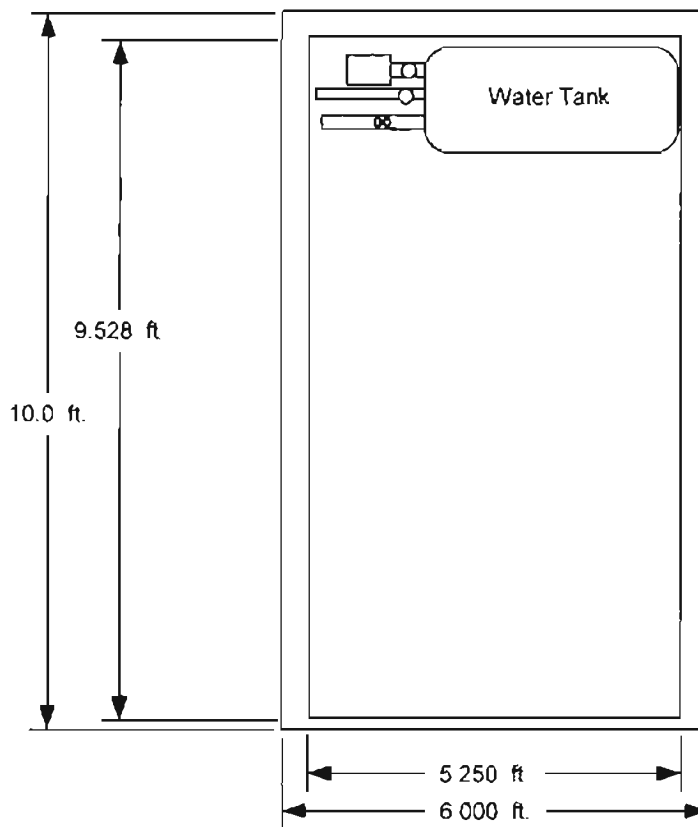
Figure 2-4. Top View of Trailer

Interior and exterior modifications are required to the trailer for the experimental equipment. The first modification to the trailer is the interior wall reconstruction. The trailer was acquired with 1/16" aluminum exterior siding and 1 ¼" steel frame beams to support the siding and interior walls. The interior walls were 1/8" plywood mounted to the steel beams. Insulated walls were not included with the purchase of the trailer. With the interior walls as delivered, there was not any room for installation of the insulation and electrical wiring designed for the space nor was the wall capable of supporting the plumbing mounted directly to the inside wall. To overcome these problems, several changes and additions are made to the trailer.

First the steel frame beams are extended in order to create more space in between the interior and exterior walls. Wood studs are mounted to the steel beams on the inside surface of the beam. Since the frame beams are a U-channel shape, the studs fit in the middle of the U-channel. As the studs are mounted to the beams, the studs wedge into the channel creating a sturdy wall. Figure 2-5 is an overhead view of a cross section of the new left side wall construction. The studs are 3 ½" wide and 1 ½" thick, a normal 2x4 construction grade stud. This gives a new total distance between the exterior aluminum siding and the inside surface of the interior wall of approximately 4 ½". The gap is filled with two layers of R-11 insulation (compressed), to minimize heat loss through the wall to the outside air (the total R-value of the wall is about 24). In addition, conduit is installed through the wood studs for the required electrical wiring.
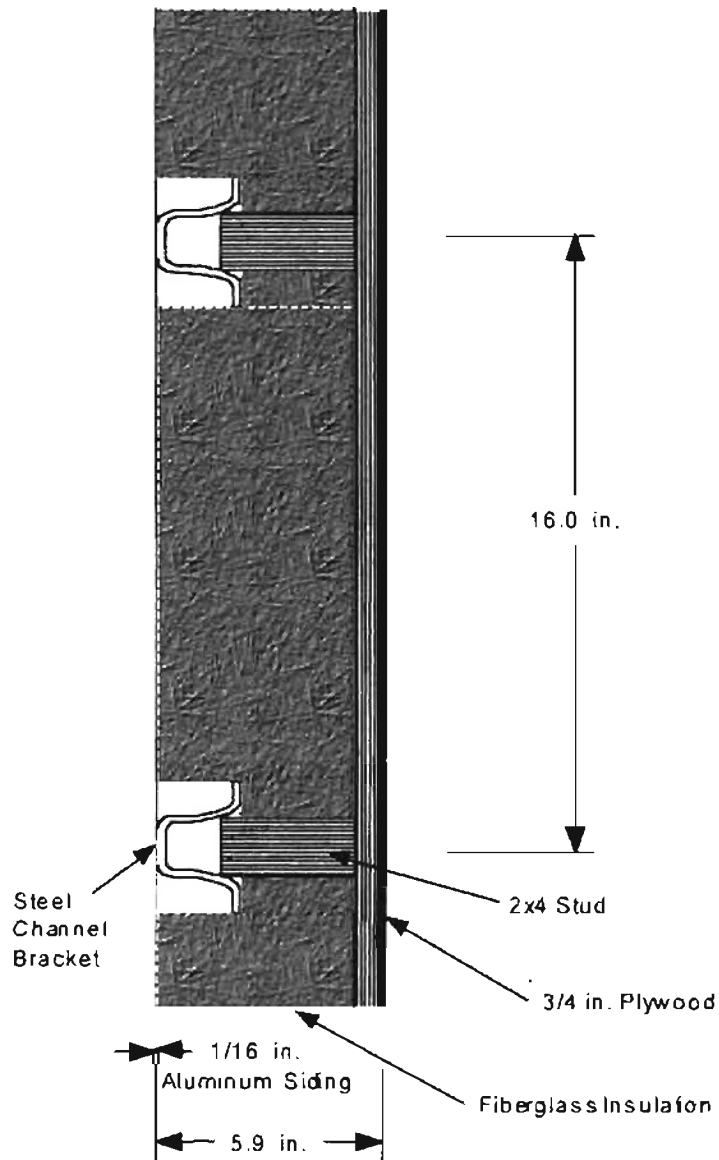
Figure 2-5. Overhead View of the Left Wall Cross Section

The inner layer of the trailer in Figure 2-5 is ¾" plywood which provides

structural support for mounting brackets and screws. It is essential since the stainless

steel plumbing weighs approximately 80 lbs.

The rest of the interior walls of the trailer are constructed in the same manner as

in Figure 2-5. The only difference for the other internal walls is the ¾" plywood is

replaced with ½" plywood to allow for attachment of other items. The rear and side

access doors were not modified; they are already insulated and did not require changes.

Another modification for the trailer is the installation of the Coleman Air Conditioner. Some temperature measurement devices, e.g. thermocouples with cold junction compensation, are sensitive to temperature fluctuations. When the local temperature fluctuates, a temperature differential is created between the thermocouple junction and the cold junction compensation temperature, causing an error. The experimental test requires at least one person to operate the experiment. The air conditioner is capable of producing 13,500 Btu/hr or 1.125 tons of cooling. For the size of the trailer, the air conditioner has more than enough capacity to meet the space requirements. To minimize these errors, a constant conditioned space temperature is desirable. Therefore, a second design need is met with the air conditioner.

2.3. Water Supply System

In order to keep the experimental apparatus mobile, a water supply tank and purging system must accompany the system. If water is not readily available at a test site, the water supply tank can be used to fill the plumbing system inside the trailer and, if required, the borehole pipe loop. The water supply system is composed of six different components:

1. Water Storage
2. Water Purging
3. Water Flow Rate
4. Water Filtering
5. Water Circulating
6. Water Valve Control

2.3.1. Water Storage Tank

The first component of the water supply system is the water storage tank. The tank is molded out of ¼" thick, chemical resistant polyethylene. The water storage tank is rectangular in shape and has the dimensions of 18"h x 17.5"w x 36.5"l. It is capable of storing a maximum of 45 gallons of water. The tank has 3 inlet/outlet ports. Figure 2-6 is a drawing of the tank with the location of the three ports relative to the position of the tank inside the trailer depicted. The tank is located on the front wall of the trailer. The top view in Figure 2-6 is illustrated looking towards the front wall of the trailer inside of the trailer. The bottom view is the left side view of the tank and the inlet/outlet ports. The water supply and return ports connect to a flow center* mounted on the left side trailer wall.
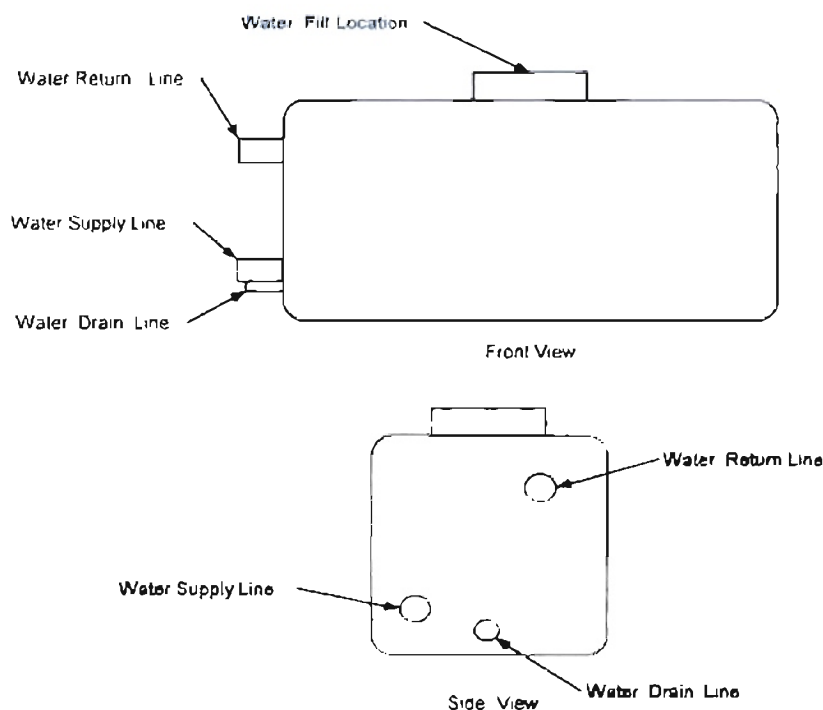
Figure 2-6. Water Supply Flow Ports

---

* A "flow center" is a metal cabinet containing 2 pumps, each connected to a 3-way valve. They are commonly used in residential GSHP installations.

One port is the water supply line, located at the bottom of the water storage tank. This allows the purge pump to draw water that does not contain air bubbles. The second port is the water return line, located near the top of the water storage tank. This allows any air in the water purged from the borehole or the plumbing system inside the trailer to bubble out the top portion of the tank. Returning water to the top of the tank minimizes the air bubbles in the water being drawn out of the bottom of the tank. The third port is the drain line, located at the bottom of the tank near the water supply line. The water drain line in the water tank can drain the entire system if it is needed. Each port has a PVC ball valve on the exterior left side of the tank. The ball valves allow an operator to shut off the tank ports after the completion of the purge test.

2.3.2. *Water Purging*

The second component of the water supply system is the purge pump system. The two purge pumps are connected to the water supply tank via the water supply line. Figure 2-7 is a frontal view of the water supply system. The pumps are mounted in-line and vertically with the 1" PVC plumbing. The pumps serve to circulate the working fluid during the purging operation of a test. The Grundfos pumps are located on the left side of the ball valve on the water supply line. The Grundfos pumps are UP26-99F series pumps rated at 230V and 1.07A. Under normal working conditions they supply 8 gpm to the plumbing inside the trailer at 10 psig and produce 7 gpm to a 250ft borehole at an unmeasured pressure. The flanges for the pumps connect with 1" nipple pipe thread (NPT)-1"PVC 40 nominal schedule fittings.

27

2.3.3. Water Flow Rate

The third component of the water supply system is the visual flow meter. It is a CalQflo flow meter and serves to evaluate the flow rate when the borehole line or the internal plumbing is purging (A separate, high quality flow meter, described below, is used to measure flow rate during the experiment.). The location of the flow meter is down stream from the purge pump. The reading from the visual meter is an indicator of correct flushing speed. There is not any data collection during the purging operation. The flow in the internal plumbing during purging is moving in the opposite direction of the instrument flow meter; therefore that reading can not be reliable because the flow meter is unidirectional. The overall reason for using the visual flow meter is to determine if flow rate is fast enough to purge the system. There is a minimum requirement of 2 feet per second to purge air out of a system line (IGSHPA, 1991). If the minimum requirement is not met, then air remaining in the system will interfere with the flow rate measurement.

2.3.4. Water Filtering

The fourth component of the water supply system is the water filter. The water filter is in between the visual flow meter and the purge pumps in the water supply line. The water filter is a standard in-line filter cartridge normally used with household water systems to remove excess rust and sediment. The water filter serves as a particle removal filter, removing sediment, rust, or other foreign particles such as HDPE

28

shavings flushed from the U-tube or the rest of the system. The filter also aids in

maintaining a minimum constant head on the purge pump.
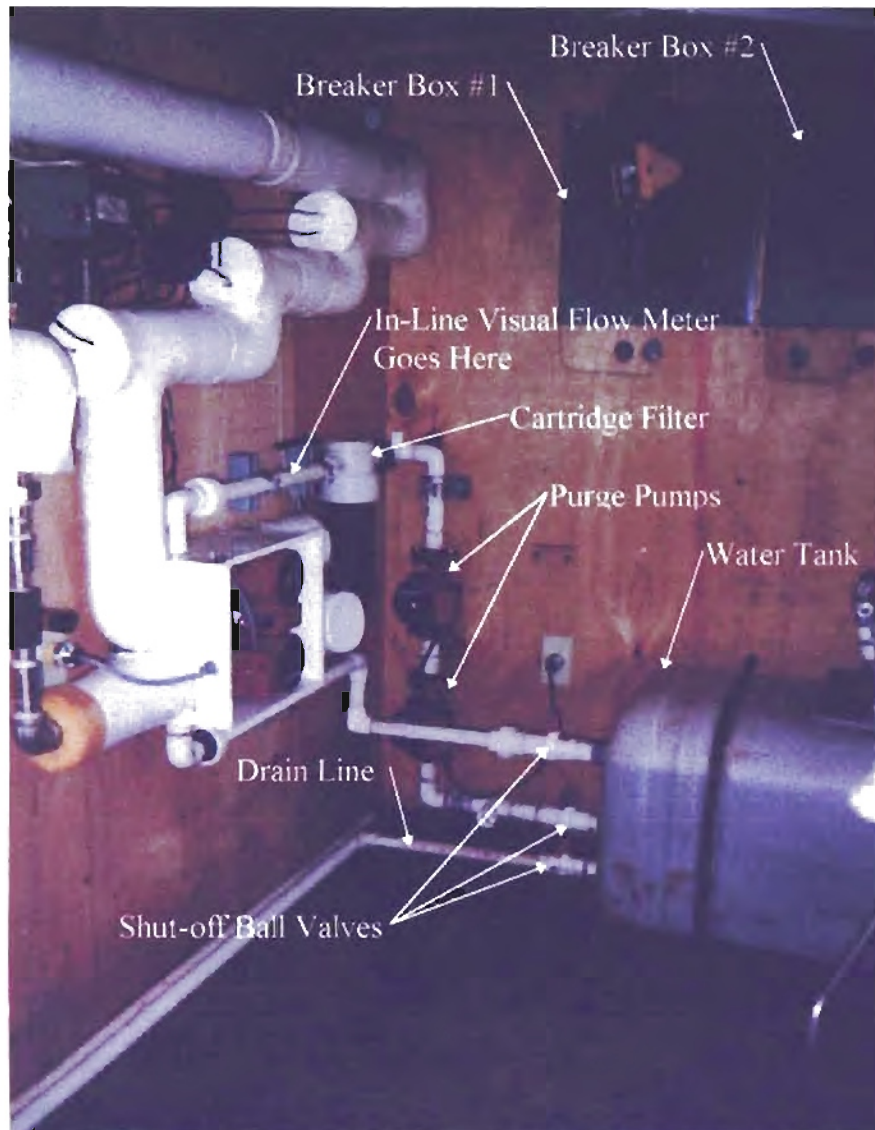
Figure 2-7 View of Front Wall Depicting the Water Supply/Purging Equipment

2.3.5. *Water Circulating Pumps*

The fifth component of the water supply system is the circulating pump system.

The circulating pump system is composed of two pumps placed just after the water filter

as seen in Figure 2-8. These pump are also Grundfos UP26-99F series pumps. They are

230Volt/1.07Amp pumps. The design of the plumbing makes use of the pumps physical characteristic ability to mount in-line. The advantages of using the in-line pumps as opposed to other pumps are simple mounting, easy installation, and minimal maintenance time. The circulating pumps aid in purging the U-bend and pressurizing the system line. When the purge pump and the two circulating pumps purge the U-bend, they produce 9-10 gpm flow for a 250 ft deep borehole using ¾" nominal pipe.
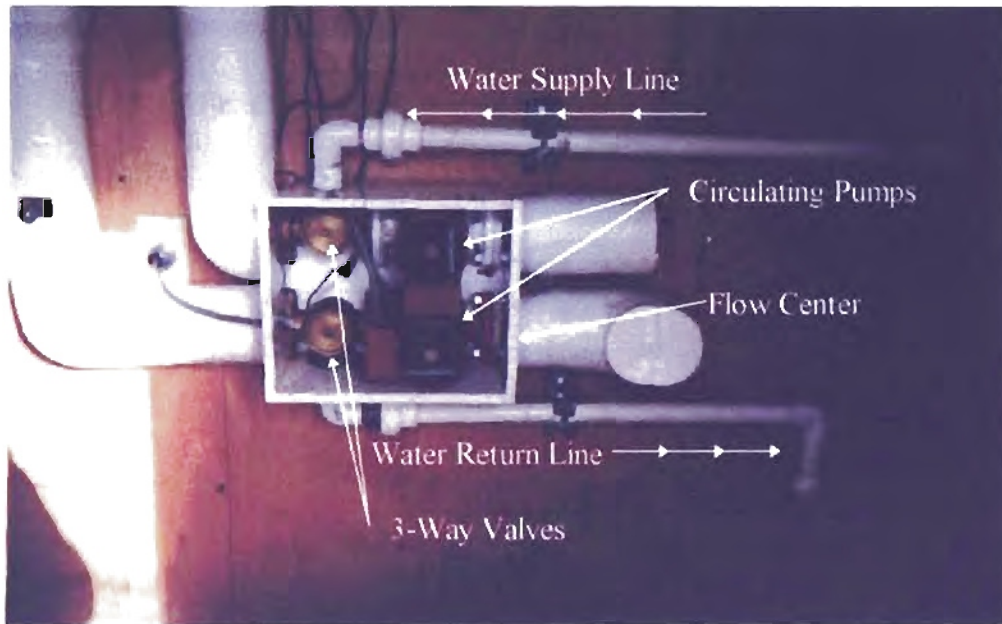
Figure 2-8. Left Side Wall View of Water Circulation Pumps and Flow Control Valves

2.3.6. Water Valve Control

The sixth component of the water supply system is the flow direction control valve system shown in Figure 2-8. The valves can direct water in a number of different flow patterns. These valves are very small and easily turned. The different flow patterns used during purging and experimental testing can be seen in Figure 2-9. During the purging operation of a test. flow pattern A is set first to purge the borehole line only, for

approximately 15-20 minutes. The purge time is set to IGSHPA standard I.E.7. of the

Design and Installation Standards (IGSHPA, 1991). Flow pattern A creates an open

loop with the water supply tank and flushes the line at approximately 8 gpm. After

purging the borehole line, flow pattern B is set to purge the stainless steel plumbing

inside the trailer for about 15-20 minutes. This flow pattern also creates an open loop

with the water supply tank and flushes the plumbing at approximately 5 gpm. Next, flow

pattern C is set to purge both the borehole loop and the stainless steel plumbing for an

additional 10 minutes. Finally, flow pattern D is set to close the system off from the

water supply tank. This creates a closed loop system, circulating the fluid continuously.

| Flow Direction | Flow Direction | Flow Direction | Flow Direction |
| A | B | C | D |
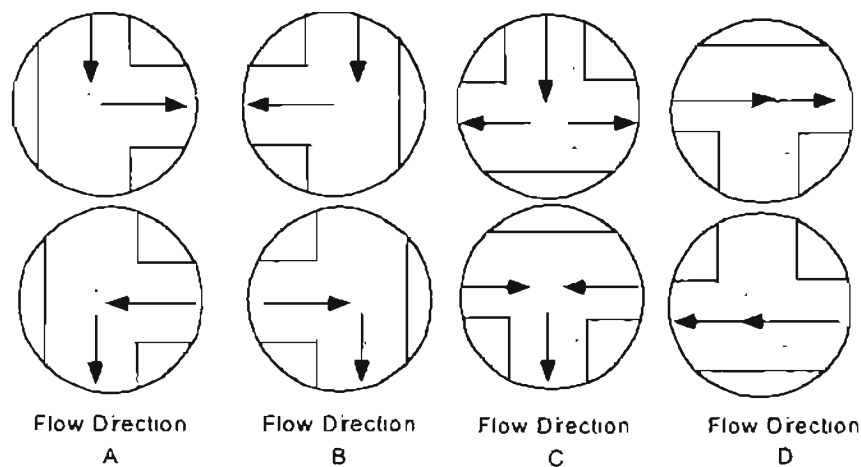
Figure 2-9. Flow Pattern of Flow Control Valves

2.4. Power Supply

The power supply for the experimental test consists of two Devillbiss gasoline

generators. Each generator is capable of supplying 7000 Watts. They are supplied with

wheel kits, allowing the generators to move in and out of the trailer on ramps. Included

in this subsystem is all wiring and wiring accessories the electrical system.

31

The generators are configured and placed outside of the trailer toward the front left side of the trailer, when possible. Each generator is set to deliver 240 volts. Two power lines, one from each generator, are routed from the generators to outside receptacles located in the front trailer wall. The main breaker boxes are located on the same front wall inside of the trailer, shown in Figure 2-7. Separate generator powers each breaker box. The breaker box #1 handles the power requirements for the water heater elements and the two circulating pumps. The breaker box #2 supplies power to the rest of the trailer. The second breaker box contains the purge pump breaker, the A/C breaker, and two plug in receptacle breakers. The computer/data logger, instrumentation, and any other standard 115V power item in the trailer use the outlet receptacles.

2.5. Water Heating Method

The circulating water inside the closed loop system is heated with (up to) three in-line water heaters. The water heaters are ordinary water heating elements used in residential water heaters. Each water heater element has a screw-in mount for 1" NPT connections and is screwed into a tee joint, as shown in Figure 2-10.
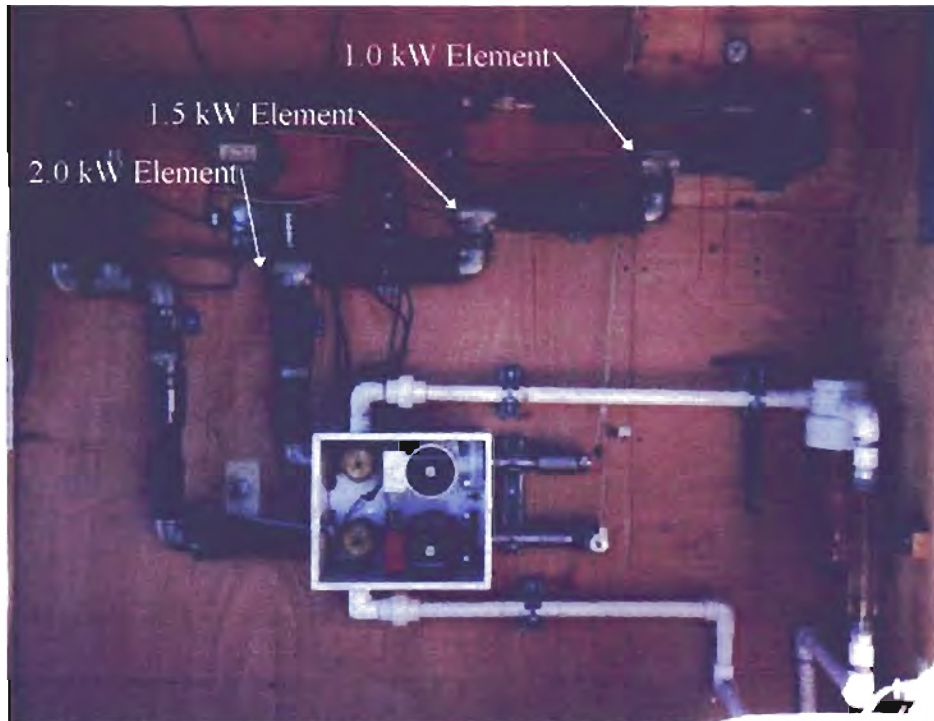
Figure 2-10. Heat Element Locations in Stainless Steel Plumbing Layout

The heater element #1 is rated at 1.0 kW, heater element #2 is rated at 1.5 kW, and heater element #3 is rated at 2.0 kW @ 240 volts. The design of the heater system allows the in situ system to vary the range of heat input between 0.0 kW and 4.5 kW. The 2.0 kW heater is connected to a Silicon Controlled Rectifier power controller, which can vary the power between 0 kW and 2.0 kW. By varying the power to this element and switching the other two elements on or off, the entire range of 0.0 - 4.5 kW can be achieved. The power controller for the 2.0 kW heating element is a SCR power controller with a manual potentiometer for varying the full output as a percentage. The location of the SCR power controller is shown in Figure 2-11. The manual potentiometer is mounted next to the LED digital display for the power input. It can be seen in Figure 2-18.

As the water flows clockwise within the plumbing in Figure 2-10, it flows across each water heater element. The direct contact with the flowing fluid in a counter flow fashion optimizes the amount of heat transferred from the heater elements to the fluid. This further reduces transient heat transfer effects, as compared to using the same heater elements in a tank* (an early design concept). Also, the power measurement is used to determine the heat flux in the borehole, and a tank adds an undesirable time lag between the power measurement and the heat transfer to the borehole.
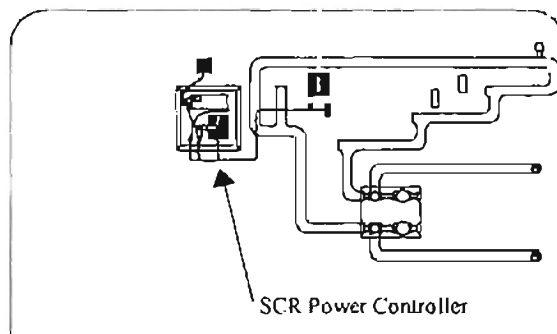
Figure 2-11. SCR Power Controller Location

Total energy input to the circulating fluid is measured by a watt transducer. The total energy is the energy from the heater elements and the energy from the circulating pumps. Early tests indicated that the circulating pumps are a significant source of heat input, on the order of approximately 300 to 400 watts.

---

* Another trailer, built by a commercial firm, utilized a water tank. The tank was subject to sudden changes in exiting water temperature when (apparently) the water in the tank was experiencing buoyancy-induced instability.

34

2.6. Pipe Insulation

The stainless steel plumbing is insulated to aid in reducing heat loss. All piping contained within the trailer is insulated using a fiber glass material called Micro-Lok insulation shown in Figure 2-12.
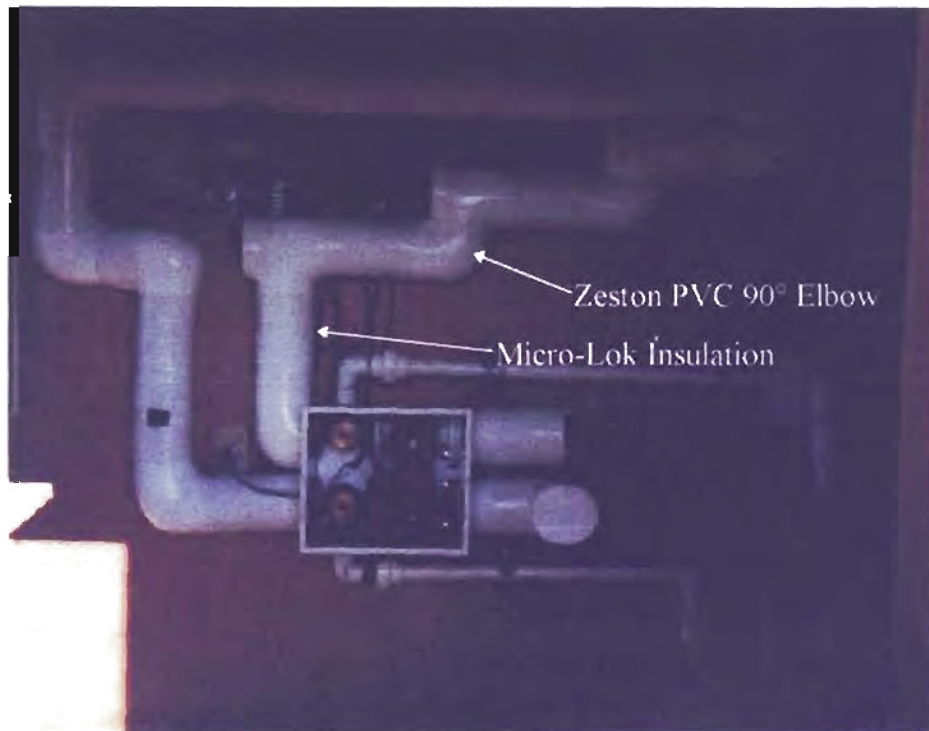
Figure 2-12. Inside Pipe Insulation

In Figure 2-10, the stainless steel pipe was not yet covered. Figure 2-12 depicts all plumbing components insulated with the exception of the flow center. The Micro-Lok pipe insulation is 1 ½" inches thick with an R-value of approximately 5.5 (hr-ft^2-°F/Btu). Micro-Lok is chosen due to its "hinged" siding to easily wrap around each pipe length and formidable compressed fiberglass structure for custom fitting at awkward pipe joint locations. Zeston PVC fittings are also used to cover and insulate special joint locations such as each tee joint with the water heater elements.

It is also necessary to insulate the exterior exposed pipe leads from the U-bend. Figures 2-13, 2-14, and 2-15 depict the insulation of the exterior pipe. Early tests revealed considerable heat loss through the exterior pipes if they were not well insulated. The heat loss is due to the distance from the ground surface to the trailer hook-up connectors that can vary from just a few feet to as much as 20 or 30 feet. Some insulation was in use, but a larger R-value improved the overall heat balance difference.
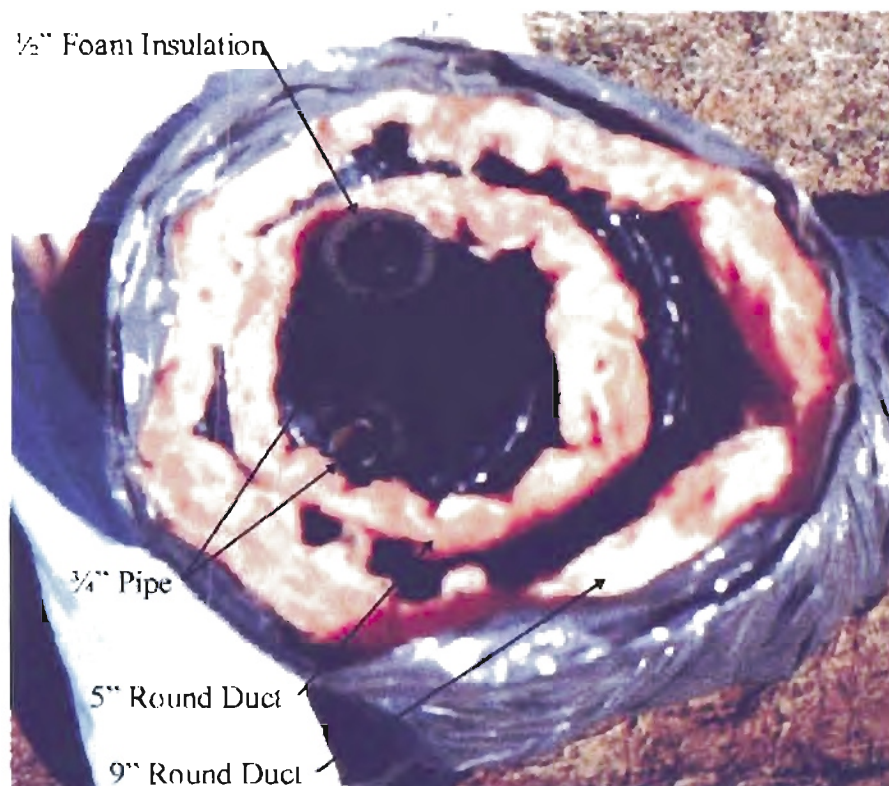
Figure 2-13. Insulation of the Exterior Pipe Leads from a U-bend

First, 1/2" foam insulation is placed around the exterior pipe leads as shown in Figure 2-13. Next, the 5" round duct insulation is pulled around the foam insulation. Finally, the 9" round duct insulation is pulled on top of the 5" round duct insulation. The R-value of each round duct section is 6 (hr-ft-°F/Btu). Combining the insulation

thermal resistances, the foam insulation. and estimating the air gap. the total R-value of thermal resistance is approximately 18.75 (hr-ft-°F/Btu)[*].

Figure 2-14. Exterior Insulation Connecting to the Trailer

After the exterior pipe leads are insulated. they are connected to the exterior barb connections of the trailer. shown in the left-hand picture of Figure 2-14. Once the connections to the barbs are complete. the remaining round duct insulation is pulled over the exterior barb fittings and taped to the side wall of the trailer as seen in the right hand picture of Figure 2-14. The round duct insulation is then adjusted to ensure it covers all of the exterior pipe leads exposed out of the ground displayed in Figure 2-15.

---

[*] All of the tests performed before January 1, 1997 were *not* insulated as described in this section. Only the ½ inch foam insulation and crude wrapping of fiberglass batt insulation was used during the previous tests. Effects of changes in the weather are clearly visible in the test data. See, for example, in Appendix C. the test data of Site A #5 on 11/25/96, which shows a cold front coming through. The effect of the cold front can be seen in Figure 5-5.

Figure 2-15. Round Duct Insulation Covering Pipe

2.7. *Temperature Measurement*

The water temperature is measured at the inlet and outlet to the trailer. as shown in Figure 2-16. The sensors for the two temperature measurements are 4 ½" stainless steel Omega ON-410-PP series thermistor probes with 1/8" NPT fitting. The probes have an accuracy of ±0.18°F for $2252\Omega@25°C$. The probes are immersed in the circulating fluid.
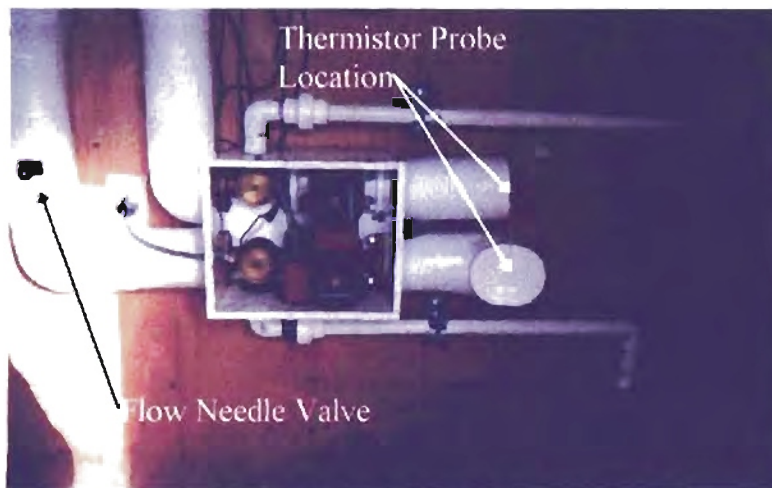
Figure 2-16. Temperature Probe Location on the Inner Trailer Wall

A digital display meter receives the signal from a probe. The two digital display meters are Omega DP25-TH-A series digital display meters with analog output boards. The

accuracy of the meters is ±0.3°F. The meters can sense a temperature from -112 to 302 °F. The analog output is pre-set by the manufacturer to be 0-10Vdc for the user specified temperature range. For this experiment 0-10Vdc represents a temperature range of 50-150°F. The data logger can retrieve the analog signal.

In addition, several temperature measurements are taken using type-T thermocouples manufactured by Omega. The outside air temperature and inside air temperature are both measured. Each thermocouple as well as the other temperature sensing instrumentation is calibrated. The calibration procedure is detailed in chapter 3.

2.8. Flow Sensing/Control Equipment

Precise monitoring of the circulation flow rate is essential to compute an accurate heat balance. The flow sensing equipment consists of three basic elements. These elements are the flow sensor, flow display meter, and the flow control valve.

2.8.1. Flow Sensor

The flow sensor has two ¼" NPT ports. With the ¾" ports, the flow meter mounts directly into the plumbing without any special modifications to the pipe system. The location of the flow sensor with respect to the rest of the system is shown in Figure 2-17. Since the flow meter adapts so well to the existing plumbing layout, the connection ports of the flow meter serve as union disconnection joints for our plumbing system should any work or maintenance to the plumbing be required. This allows us to maintain the plumbing in sections. The flow sensor is an Omega FTB4607 model. It has

a range of 0.22 gpm to 20 gpm. The flow sensor features a high frequency pulse output from a spinning paddle that rotates about a vertical axis. The claimed accuracy is ±1.5% of the flow rate at 20 gpm and ±2.0% of the flow rate at 0.8 gpm. The flow sensor has an operating range of 32°F to 190°F. The flow meter is designed for a uni-directional flow system. An arrow on the flow meter specifies the flow direction. It requires at least 15 pipe diameters distance upstream and 5 pipe diameters downstream to create a uniform flow.

2.8.2. *Flow Indicator*

The flow indicator display is compatible with the flow sensor. It is an Omega DPF401-A with TTL Level Inputs. It can readily accept the output pulses from the flow sensor for frequency ranges of 0.2Hz to 20kHz. It does require user specified flow units, and frequency conversion rate (i.e. the flow sensor is set for 75 pulses/gal of flow measured, so the meter must be set too using the operating manual). It has an analog output accessory that sends a voltage reading to the data logger for data collection. The analog signal is set using the correct conversion units for flow. The procedure is similar to that of the thermistor probes and should be followed in the user manual of the flow indicator display. The indicator has preset calibration numbers determined by the manufacturer. Checks are made routinely to assure the numbers are correct.
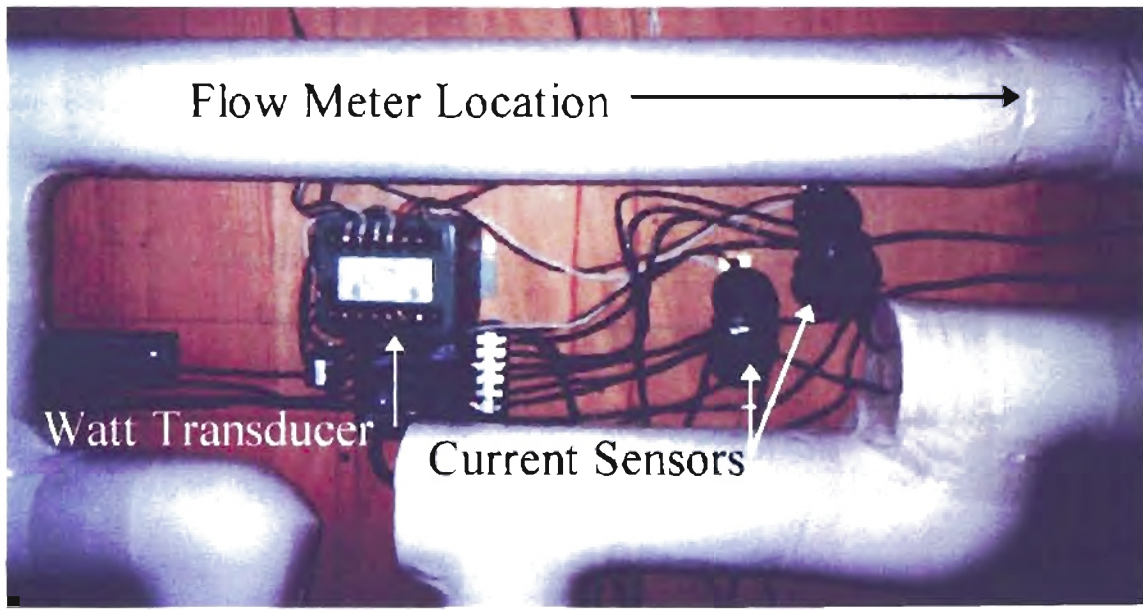
Figure 2-17. Close-up View of Watt Transducer

2.8.3. Flow Control Equipment

A thermoplastic needle valve controls the flow rate. The location of the needle valve can be seen in Figure 2-16. The valve has a very sensitive micro-turn adjustment knob. The knob allows a test to run at a very constant flow rate. This piece of equipment was chosen to reduce fluid oscillations that sometimes occur with other more robust and conventional flow valves such as a gate or globe valve.

2.9. Watt Transducer

A watt transducer is put in place to measure power input to the water heater elements and the circulating pumps. The watt transducer is built and calibrated by Ohio Semitronics, Inc. The model depicted in Figure 2-17 is PC5-061DY24. One leg of the line is connected to the watt transducer terminal strip so the transducer can measure the

voltage. Two current sensing doughnuts determine the actual current flowing to the water heater elements and circulating pumps. One leg of each wire set is sent through one doughnut and the other leg of each wire set is sent through the other doughnut. The watt transducer has a sensing range of 0 to 20 kW with an accuracy of ±0.5% of full scale reading. In order to receive better accuracy for our range of 0-2.0 kW, the electrical wires are wrapped around each doughnut 4 times to reduce the full scale reading to 5 kW. The watt transducer has an analog output signal of 0-10 volts of full-scale reading. The signal is sent to the Fluke Data Logger and a green LED digital display. The display can be seen in Figure 2-18. The display configured to have a readout of power with the units of Watts. If the 2.0 kW water heater is in use, the display assists in precise power adjustment using the manual potentiometer that is located next to the display.

2.10. Data Acquisition and Logging

The watt transducer and digital displays' analog outputs are measured by a Fluke Hydra Data Logger. Each of the digital displays' voltage signal is a DC voltage signal configured on an output scale of 0-10volts for each measurement. The signals sent to the data logger from the digital displays are:

1. Temperature of water leaving the trailer (Vdc)
2. Temperature of water returning to the trailer (Vdc)
3. Flow Rate (Vdc)

In addition, several other measurements are made directly:

1. Watt Transducer (Vdc)
2. Temperature Inside the Trailer (thermocouple)
3. Temperature Outside the Trailer (thermocouple)

As each signal is retrieved, it is stored in two places. The first place the data is stored is inside the data logger's own memory. The data is then down loaded at a later time without losing any measurements. If a computer, via remote or RS-232 connection controls the data logger, then the data is also stored in a data file setup by the manufacture's software program. Figure 2-18 is a picture of the data acquisition system.

The software program allows configuration of the data logger for an experimental test. The software allows real time plots every time the data input channels are scanned. Once the data is retrieved by any of the afore mentioned methods, it is stored in an ASCII data file and can be read by other programs
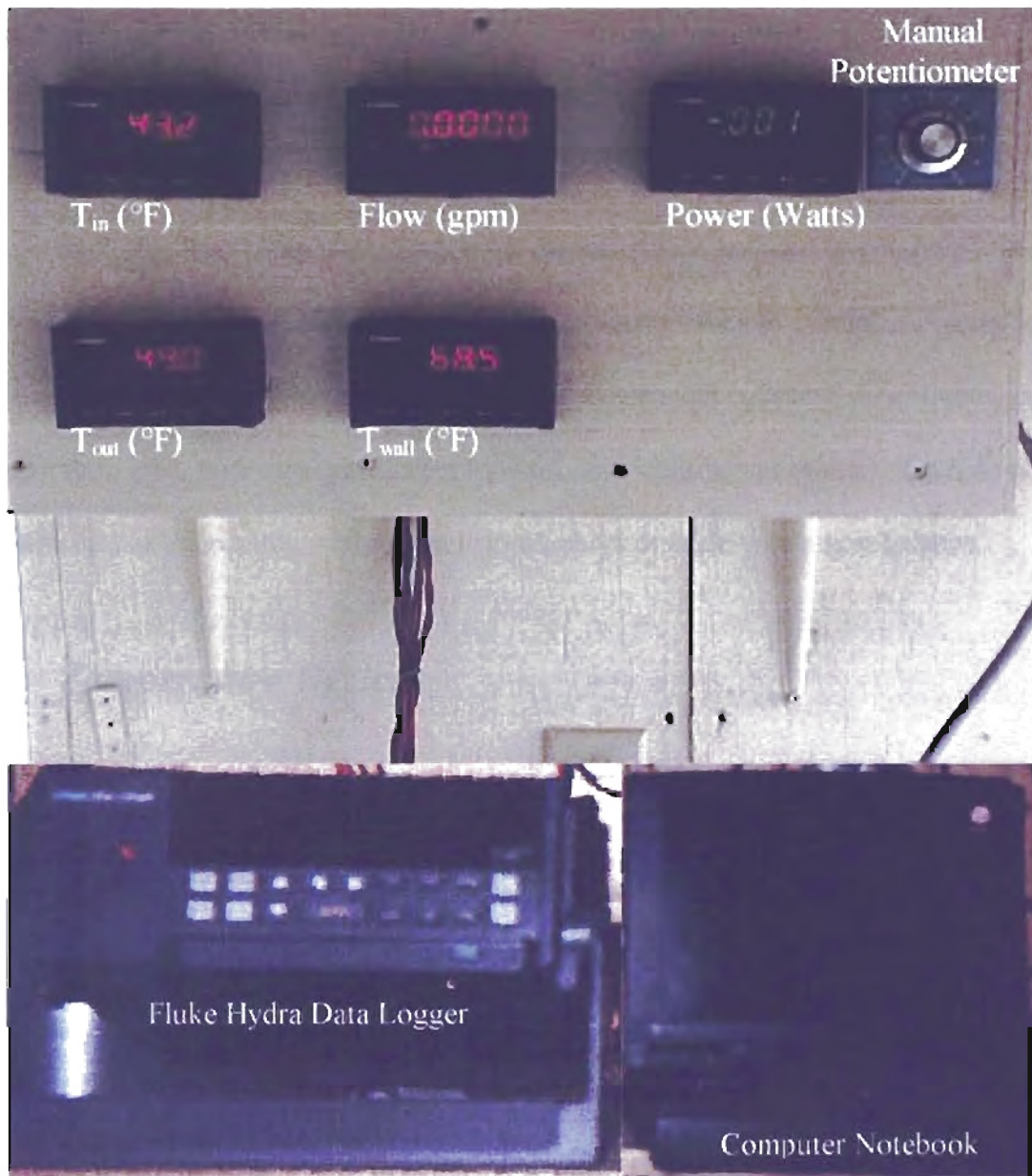
Figure 2-18. Typical Data Acquisition System

3. Calibration of Experimental Devices

With any experimental apparatus, some uncertainty exists for each measurement. These errors are then compounded when the measurements are used to compute other parameters. Therefore, it is desirable to minimize uncertainties by careful calibration of the sensors and data acquisition equipment. The experiment collects data of three types, temperature (°F), flow rate (gallons per minute), and input power (watts). Each device is calibrated independently, and then an overall check is made with a heat balance.

3.1. Temperature Devices

There are three thermistor probes, two thermocouple probes, and one exposed thermocouple used to measure temperature. Each device serves a separate and specific purpose. Two of the thermistor probes are used to determine the fluid temperatures leaving and returning into the trailer. The thermocouple probes measure the ground and outside air temperatures. The thermocouple measures the inside room temperature. Some of the devices require extreme accuracy while some can be used with an acceptable uncertainty of ± 1.0 °F.

3.1.1. Thermocouple Probe and Exposed Junction Thermocouple

The exposed junction thermocouple is a type-T thermocouple, which measures the inside air temperature for the duration of each experimental test. The uncertainty is

about ±0.56°F (0.3°C) of the reading as stated by the manufacture. The thermocouple was not calibrated because the error associated with the reading was acceptable.

The thermocouple probe is used to measure the outside air temperature for each test. This thermocouple probe uses type-T wire and is 6" in length. The connection of the two wires is an ungrounded junction. A stainless steel casing that creates the probe portion of the sensing device surrounds the ungrounded junction. Since the temperature probe is a type-T thermocouple, it has the same temperature sensing range of -454°F to 752°F (-270-400°C). The error is about ±0.56°F (0.3°C) of the reading. Since it was used to measure the outside air temperature, the thermocouple probe was also determined to have a reasonable error that did not need to be taken into account for the overall heat balance equation used as heat loss or heat gain through the wall to the pipe inside of the trailer. The probe was calibrated in the same manner as discussed in the next section with the thermistor probes.

3.1.2. Thermistor Probes

The experimental apparatus uses three thermistor probes. The probes measure the temperature of the water as it leaves the trailer (T_{out}) and as it enters the trailer (T_{in}). The probes are 4 ½" in length with a 1/8" NPT screw thread. The first and second probes are mounted to a drilled and tapped hex head bolt. The hex head bolt is mounted to one of three ports of a pipe Tee joint. The third thermistor probe is retained as a backup for the first two probes, but currently measures the temperature between the wall

the pipe is mounted against and the insulation around the stainless steel pipe (T_{wall}). The thermistors are accurate to ±0.2°F (±0.1°C).

Each thermistor probe is wired to an LED temperature display that in turn has an analog output signal to be received by the Fluke Data Logger. The error associated with the LED display is ±0.3°F (0.2°C).

3.2. Temperature Calibration Procedure

Calibrating the temperature devices began by selecting a known source of constant or near constant temperature. An environmental chamber was selected to create the constant temperature surrounding. This chamber uses both heating and cooling to maintain a set temperature. The user can set the temperature of the chamber. For the calibration, 10°F increments starting at 50°F are the set point temperatures until the final temperature of 120°F is achieved.

Another thermistor probe calibrated within two decimal places is used as one of the sources for the known temperature inside the environmental chamber. Two precision thermometers are also used inside the chamber to read the temperature inside the environmental chamber. One thermometer is accurate to ±0.1°F and a temperature reading range of 30°F to 80°F. The second thermometer is accurate to ±0.1°F and a temperature range of 75°F to 125°F.

Each temperature "system" is intact, as each probe is set inside the chamber, along with the calibrated probe. A temperature "system" consists of the following: thermistor probe, thermistor wire from probe to the LED display, LED display, analog

47

output wire from the LED display to the Fluke Data Logger, and the Fluke Data Logger. This calibration approach will lump each individual component error associated with each temperature measurement into one total error. Then the calibration coefficients can be determined for a linear correction. The linear correlation is the same procedure the manufacturer of the temperature sensing instrumentation uses.

In order to distinguish each temperature measurement separately they are assigned a color code. The color code key is as follows:

White = (T_{in}) The temperature measurement of the water coming into the trailer.

Red = (T_{wall}) Backup Device; The temperature measurement at the wall.

Green = (T_{out}) The temperature measurement of the water as it leaves the trailer.

The 6" thermocouple probe was also calibrated at this time. It maintained a wire length of approximately 12ft.

After the temperature of the environmental chamber was in equilibrium at 50°F, readings of the calibrated thermistor probe display were taken over a period of 10 seconds. Then an average value was calculated because the second digit past the decimal place fluctuated ±0.03 of the average value. Next, a reading was taken on the precision thermometer that has the applicable temperature range and recorded. Finally, the channels of each temperature device were scanned and recorded in the internal memory by the Fluke Data Logger over 10 seconds. The values of each temperature measurement read by the Data Logger were average in the same manner as the calibrated

thermistor probe. This step was repeated for each 10°F increment until 120°F was reached.

In order for the LED readout screen to display a temperature, a linear association between the raw voltage measured and the actual temperature must be manually scaled to read temperature values. For temperature measurement a conversion must be determined for the display to calculate for a given input voltage. Equation 3-1 is the relationship between the temperature and raw voltage. Equation 3-1 takes on the y = mx + b linear equation.

$$T(^\circ F) = \frac{(150^\circ F - 50^\circ F)}{10 - 0Volts}(Raw\_Volts) + 50^\circ F \qquad (3\text{-}1)$$

Table 3-1 shows each reading taken by the Fluke with average values in bold print. Once the individual values are tabulated, each LED display reading is reduced to the raw voltage reading. Once the raw voltage is obtained, a statistical regression is conducted on the values. The regression is linear with residuals set at 2% or approximately 0.01°F using the Excel 95 data analysis function. The linear regression follows the same form used in equation 3-1 except new coefficients for the raw voltage and values for the constant are calculated. Table 3-2 shows every temperature reading taken in the environmental chamber. All of the temperatures are within ±0.1°F. Therefore, the thermistor temperature measurement uncertainties are estimated as ±0.1°F.

	White	Red	Green	TC-Probe
Reading 1	49.9	50.6	50.5	50.7
Reading 2	50.0	50.5	50.5	50.7
Reading 3	50.1	50.5	50.5	50.7
Reading 4	50.1	50.6	50.5	50.7
Reading 5	50.1	50.6	50.5	50.7
Average	*50.0*	*50.6*	*50.5*	*50.7*
Reading 1	60.0	59.0	59.0	58.9
Reading 2	60.0	58.9	59.0	58.9
Reading 3	60.1	59.0	59.0	59.0
Reading 4	60.2	58.9	59.0	59.0
Reading 5	60.3	58.9	59.0	59.0
Reading 6	60.3	59.0	59.0	59.0
Average	*60.1*	*59.0*	*59.0*	*59.0*
Reading 1	69.8	70.6	70.6	70.5
Reading 2	69.9	70.6	70.6	70.5
Reading 3	70.0	70.6	70.7	70.6
Reading 4	70.0	70.6	70.7	70.5
Reading 5	70.0	70.6	70.7	70.6
Average	*69.9*	*70.6*	*70.6*	*70.6*
Reading 1	80.4	79.5	79.6	79.6
Reading 2	80.4	79.5	79.6	79.6
Reading 3	80.4	79.5	79.6	79.6
Reading 4	80.4	79.5	79.6	79.6
Reading 5	80.4	79.5	79.6	79.6
Average	*80.4*	*79.5*	*79.6*	*79.6*
Reading 1	91.3	89.7	89.7	89.7
Reading 2	91.3	89.7	89.8	89.7
Reading 3	91.3	89.7	89.8	89.7
Reading 4	91.3	89.7	89.8	89.7
Reading 5	91.3	89.7	89.8	89.7
Reading 6	91.2	89.7	89.7	89.7
Average	*91.3*	*89.7*	*89.8*	*89.7*
Reading 1	97.7	97.7	97.7	97.6
Reading 2	97.7	97.7	97.7	97.6
Reading 3	97.8	97.7	97.7	97.6
Reading 4	97.7	97.7	97.7	97.6
Reading 5	97.7	97.7	97.7	97.6
Reading 6	97.7	97.7	97.7	97.6
Average	*97.7*	*97.7*	*97.7*	*97.6*
Reading 1	109.6	109.6	109.6	109.5
Reading 2	109.6	109.6	109.6	109.4
Reading 3	109.6	109.6	109.6	109.5
Reading 4	109.6	109.6	109.6	109.5
Average	*109.6*	*109.6*	*109.6*	*109.5*
Reading 1	118.8	118.8	118.8	118.6
Reading 2	118.8	118.8	118.8	118.6
Reading 3	118.8	118.8	118.8	118.6
Reading 4	118.8	118.8	118.8	118.6
Reading 5	118.6	118.8	118.8	118.6
Average	*118.8*	*118.8*	*118.8*	*118.6*

Table 3-1. Recorded Temperature Measurements for Calibration Test

Table 3-2. Non-Calibrated Temperature Measurements

Calibrated Thermistor	Thermometer	White	Red	Green	TC-Probe
50.6	50.6	50.0	50.6	50.5	50.7
59.0	59.0	60.1	59.0	59.0	59.0
70.5	70.5	69.9	70.6	70.6	70.6
79.4	79.4	80.4	79.5	79.6	79.6
89.6	89.6	91.3	89.7	89.8	89.7
97.6	97.6	97.7	97.7	97.7	97.6
109.5	109.5	109.6	109.6	109.6	109.5
118.5	118.5	118.8	118.8	118.8	118.6

After each regression of the raw voltage, the new calculated coefficient (m) and the constant (b) can be applied back into equation 3.1 and a new set of temperatures are determined. The new temperatures are tabulated in Table 3-3.

Table 3-3. Calibrated Temperature Measurements

Calibrated Thermistor	Thermometer	White	Red	Green	TC-Probe
50.6	50.6	50.6	50.6	50.5	50.6
59.0	59.0	59.0	59.0	59.0	58.9
70.5	70.5	70.5	70.5	70.6	70.5
79.4	79.4	79.5	79.4	79.5	79.5
89.6	89.6	89.6	89.6	89.6	89.6
97.6	97.6	97.7	97.6	97.5	97.6
109.5	109.5	109.4	109.4	109.4	109.4
118.5	118.5	118.5	118.6	118.5	118.5

Table 3-4 gives the coefficients and constants for each temperature device. Since the Fluke Hydra data logger directly monitors the thermocouple probe, it should take on a near one to one linear relation as seen in Table 3-4.

Table 3-4. New Coefficients for Equation 3.1

Temperature Device	Coefficient (m)	Constant (b)
White	10.00188	50.0775
Red	9.956861	50.06037
Green	9.95378	50.05189
Thermocouple Probe(6")	1.000241379	-0.07051528

3.3. Flow Meter Calibration

The flow meter is calibrated by utilizing a stopwatch and bucket. Three people work together to collect all of the necessary measurements and readings to calibrate the flow meter. One person controls the stopwatch and records the actual start and stop time. Another person runs the Fluke that in turn scans the channel to which flow meter signal is connected. The last person fills the bucket to a predetermined line and weighs the bucket of water on a scale. The bucket is marked so that it contains approximately 5 gallons of water. This procedure is performed for several different flow rates controlled by the needle valve of the pipe system. The calibration occurs at the two exterior flow ports of the trailer.

Each flow rate requires the following information: Weighing of the bucket (grams), zeroing out the weight of the bucket by itself, marking time to fill bucket to approximately 5 gallons, recording actual time began and finished filling the bucket, scanning the channel for the duration of the time to fill bucket. Once all information is collected, it is necessary to make use of the conversion of grams to lb_m. Once the conversions are made, the actual flow rate can be determined by the following equation:

$$Q(gal/min) = \frac{Mass_{Water\_in\_Bucket}(lbm)}{Time_{Stop\_Watch}(min)} * \frac{1}{\rho_{Water}(ft^3/lbm)} * 7.483(gal/ft^3) \qquad (3\text{-}2)$$

This actual flow rate is compared to the flow rate measured by the flow meter. The flow meter signal is sent to an LED display box that contains an analog signal output. The analog signal is read by the Fluke. In order to reduce the uncertainty in the resistance

52

change in the wires and readings of the LED display and data logger, a linear regression statistical calibration is applied to the raw voltage of the signal of the flow meter using an Excel spreadsheet using the regression statistical function. This regression was set to fit the data within a 2% residual. The residual is the statistical function's ability to find the coefficients within a percentage of accuracy. The preliminary results indicated the flow meter was not correctly set.

The new calibrated equation for the flow meter is:

$$Flow\_Rate(gpm) = 2.04851529 * Raw\_Voltage_{flow\_Meter} - 0.03807149 \qquad \textbf{(3-3)}$$

The results from the calibration test are given in table 3-5. The original flow meter signal was misreading the flow rate by a factor of approximately two.

Table 3-5. Results from Flow Meter Calibration Procedure

Actual Flow (gpm)	Measured Flow (gpm)	Calibrated Flow (gpm)	Error (%)
0.875995	0.432813	0.848553	3.2
1.943090	0.978517	1.966436	1.2
2.839573	1.422996	2.876957	1.3
3.943883	1.927575	3.910595	0.9

3.4. Watt Transducer

The watt transducer measures the amount of power (electricity) transferred to the water via resistive water heater elements and the circulating pumps. The watt transducer is calibrated by the manufacturer and has a seal of warranty on the casing ensuring calibration. The transducer is accurate to ±1% of the reading and ±0.5% of the full scale reading. The transducer is rated for 20kW, but by looping the wire through the current sensors four times, the rating is changed to 5kW. The decrease in range

increases the accuracy of the readings four fold. The watt transducer has an analog

output signal preset by the manufacturer as 0-10V for the range measured. For our case

it would be 0-10V for 0-5kW. This analog signal is sent to an LED display that in turn

has another analog signal also setup as 0-10V. Those readings are sent to the data

logger.

3.5. Heat Balance

In order to verify the experimental measurements are reasonably, a justifiable

means of validation is required. The approach is to use a heat balance. The simplest

expression of the heat balance equation is:

$$q_{in} = \frac{62.4(lbm \, / \, ft^3) * 60(min/ \, hr)}{3.414(Btu \, / \, hr - Watt) * 7.483(gal \, / \, ft^3)} * \dot{V}c_p(T_{out} - T_{in}) \tag{3-4}$$

Where, q_{in} (watts) is the measured heat input to the water heater elements and

    pumps

  $\dot{V}$ (gpm) is flow rate

  c_p (Btu/lbm-°F) is the specific heat of water, equal to 1.0(Btu/lbm-°R)

  T_{in} and T_{out} (°F) are measured from the thermistor probes

After applying all of the calibration equations to the measurement devices, the

heat transfer rate predicted by the right hand side of equation 3-4 can be compared to the

measured power input (left hand side of equation 3.4). The numbers summarized in

Table 3-6 are the average values over the length of each test and they are used to

compare the instrumentation uncertainties and total heat input error.

Table 3-6. Heat Balance Check

Location and Date	Watt Transducer Reading (Watts)	Average $Vc_p(\Delta T)$ (Watts)	Difference (Watts)	% of Total Average Power
Site A #1 1-6-97	2458.7	2556.8	98.1	3.98
Site A #2 1-9-97	2457.9	2601.6	143.7	5.85
Site A #3 2-27-97	2482.6	2617.3	134.7	5.43
Site A #4 3-5-97	2479.4	2618.0	138.5	5.59
Site A #5 4-21-97	2513.1	2597.8	84.7	3.37
Site A VI 4-29-97	3497.3	3637.6	140.3	4.01
Site A #2 5-28-97	3199.0	3202.5	3.5	0.66
Site A #1 6-2-97	3181.2	3212.2	31.1	1.04

The uncertainties in the temperature measurement are ±0.1°F for the probes and ±0.3°F for the signal conditioner of the digital displays with the analog signal. Adding the errors in quadrature gives the total uncertainty for the temperature measurements given in equation 3-5.

$$\Delta T \text{ uncertainty} = \sqrt{\sqrt{(\pm 0.1)_{in}^2 + (\pm 0.3)_{in}^2} + \sqrt{(\pm 0.1)_{out}^2 + (\pm 0.3)_{out}^2}} \approx \pm 0.45° F \qquad (3\text{-}5)$$

Taking into account that the ΔT for each test is approximately 6°F, the uncertainty due to the temperature measurements becomes:

$$error = \cdot\frac{\pm 0.49° F}{6° F} \approx \pm 7.45\% \qquad (3\text{-}6)$$

Using the highest error for the flow meter taken from Table 3-5 of ±3.2%, the total uncertainty in the heat balance equation is:

$$\text{Total error} = \sqrt{(\pm 0.0745)^2 + (\pm 0.032)^2} \approx \pm 8.11\% \qquad (3\text{-}7)$$

The error for the watt transducer measurement is ±1% of the reading plus ±0.5% of the full scale reading, which is equal to ±1% ±25 Watts. The greatest discrepancy between the LHS and RHS of the heat balance equation in Table 3-6 was 5.85% of the total heat input. This discrepancy is well within the bounds of the known uncertainties, and so there are no inexplicable errors.

4. Development of Numerical Model using Parameter Estimation

Several different approaches have been used to estimate the ground thermal properties (e.g. Mogensen, 1983, Kavanaugh, 1991). A different approach to the solution, parameter estimation coupled with a numerical model, is presented here. Parameter estimation involves minimizing the differences between an experiment and an analytical or numerical model by adjusting inputs to the model. In this case, a numerical model of the borehole and surrounding ground is used to compare to the experimental results. Some inputs to the model, such as power as a function of time, are fixed and other inputs, such as the thermal conductivity of the ground and the thermal conductivity of the grout are allowed to vary. By systematically varying the thermal conductivity of the ground and the thermal conductivity of the grout so that the minimum difference between the experimental results and the numerical model is found, a best estimate of the thermal conductivities may be found.

The numerical model used is described in section 4.1. It accepts as input:

- power in 5 minute intervals (obtained from experimental data)
- undisturbed ground temperature (measured at beginning of test)
  geometrical information:
  (pipe size, wall thickness, borehole diameter, pipe spacing, depth)
- ground thermal properties (conductivity and volumetric specific heat)
- grout thermal properties (conductivity and volumetric specific heat)
- fluid properties (conductivity, volumetric specific heat, flow rate and viscosity)

Most of the inputs will be determined based on knowledge of the borehole installation. A few, however, will be treated as independent variables in an optimization. The optimization is performed with a non-linear optimization technique, e.g. Nelder-Mead Simplex, although other methods such as exhaustive search or steepest descent might be the error. The objective function for the optimization is the sum of the squares of the errors between the numerical model solution and the experimental results, specifically:

$$Error = \sum_{n=1}^{N}(T_{experimental} - T_{numerical\ model})^2 \tag{4-1}$$

Where, N = The total number of Data Points

$T_{experimental}$ = Average of input and output temperature at nth data point

$T_{numerical\_model}$ = Average fluid temperature at nth data point

Once the error in equation 4-1 is determined, then a mean error per estimated temperature data point can be determined. The mean error can range as high as 1.0 °F to as low as 0.05 °F. Figure 4-1 shows how well a high and low mean error parameter estimation compares to the experimental temperature. In one case, the mean error is 0.35 °F per estimated data point. In the other case, the mean error is 0.08 °F per estimated data point.
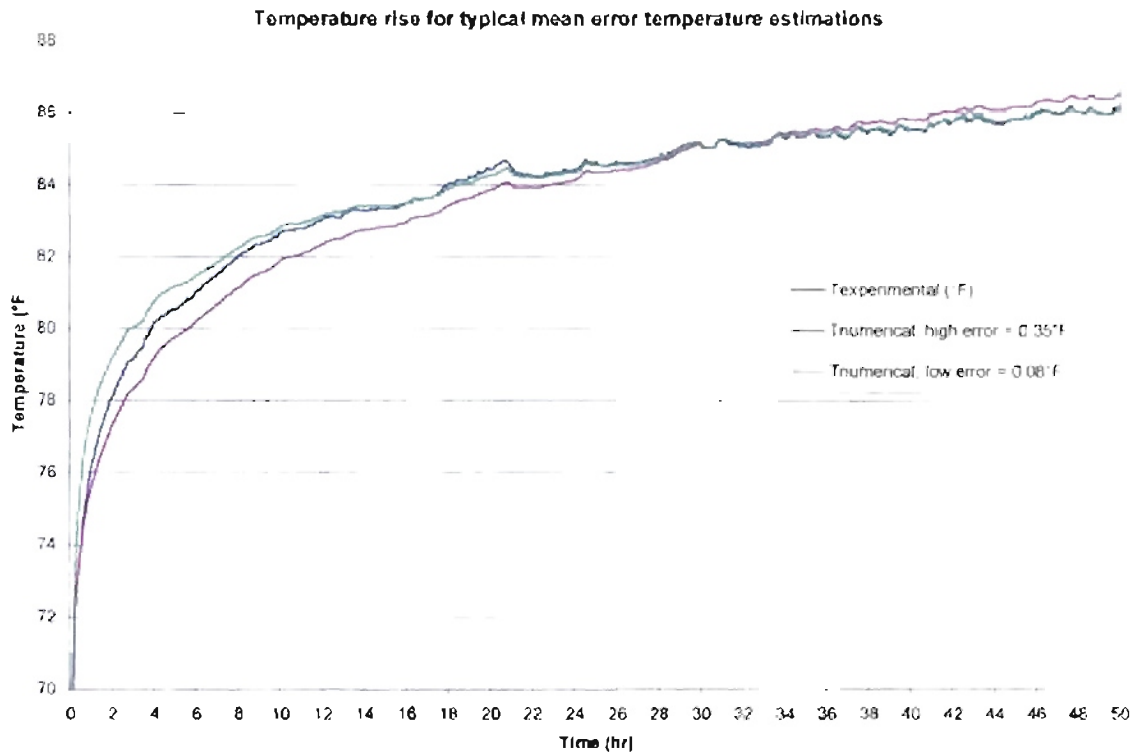
Figure 4-1. Typical Temperature Rises for Different Mean Error Temperature Estimations

The independent variables for the optimization may be almost any of the inputs, although the obvious choices include the ground thermal properties, the grout thermal properties and the pipe spacing. One possible set of independent variables includes just the ground thermal conductivity and the grout thermal conductivity. The optimization domain for a specific test with this combination is shown in Figure 4-2. In this case, the minimum lies in a turning valley, inferring that there may be a range of combinations that give similar values for similar, near minimum sum of the squares of the errors. The optimization procedure used here is described in section 4.3.
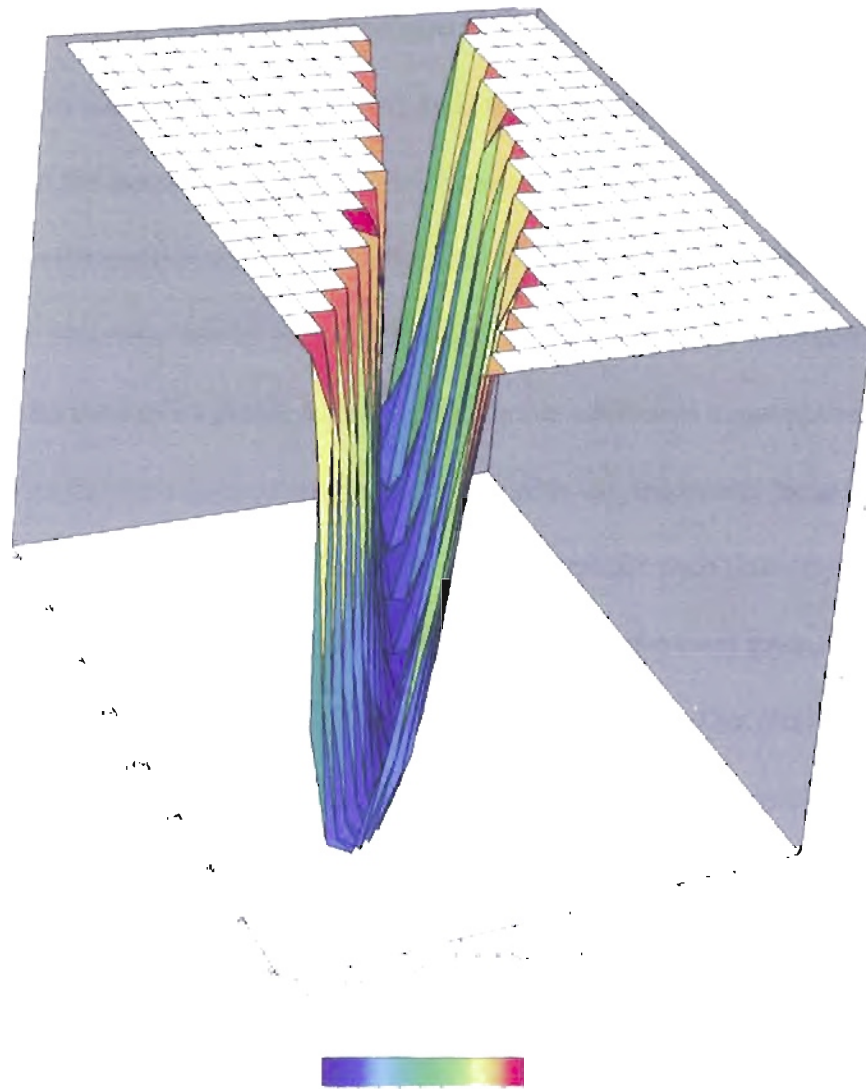
Figure 4-2. Minimization Domain Using the Exhaustive Search Method

4.1. Numerical Model Methodology

Both the line source and cylinder source models attempt to represent the ground

loop heat exchanger as a simple geometrical object, an infinite line source and an infinite

cylinder source respectively. The numerical model can more accurately model the ground

loop heat exchanger by representing each component of a ground loop heat exchanger

(U-tube, grout-filled borehole, and the surrounding ground). This section will detail the steps taken to adequately model the borehole using a numerical modeling technique. The validation of the numerical model will be discussed in section 4.3. The numerical model described in this section was developed primarily by Yavuzturk (1996).

The numerical model requires less approximation than the analytical models. However, because of its detail, it does require some additional assumptions. The numerical model does attempt to handle the possible varying power input (heat pulse), but assigns each pipe a percentage of the total power input for each time step. The pipe with the downward flow is assumed to dissipate 2/3 of the total power input, while the pipe with the upward flow dissipates 1/3 of the total power input. This distribution is assumed to be representative of the entire borehole. Yavuzturk (1996) has modified Patankar's (1991) CONDUCT program and developed a working 2-D model to simulate a single borehole. The modified program used for this project is described below. The modifications involved specifying the borehole geometry and allowing for heat generation to also vary with time (variable power input).

This approach begins with the general 2nd order differential equation in cylindrical coordinates for conduction heat transfer as:

$$\frac{1}{\alpha}\left(\frac{\partial T}{\partial t^2}\right) = \frac{\partial^2 T}{\partial r^2} + \frac{1}{r}\left(\frac{\partial T}{\partial r}\right) + \frac{1}{r^2}\frac{\partial^2 T}{\partial \theta^2} \tag{4-2}$$

This, of course, is a simplification of the 3-dimensional geometry to a two-dimensional geometry in the r- and θ-direction and assuming a unit depth in the z-direction. The equation will be solved using Patankar's (1991) finite volume approach. The boundary condition is adiabatic at the outer radius. However, a check is made to

61

insure that the solution domain is large enough that the outer boundary condition has no effect on the solution. The initial condition is that all temperatures are at the far-field temperature. Since a symmetry exists on the $\theta = 0°/\theta = 180°$ plane, only one half of the entire domain will be solved. Energy balance equations are set up for each finite volume for the heat flux through a particular control volume based upon the boundary and initial conditions of the solution domain.

The model uses a five-minute implicit time step. The time step is chosen to be the same as the measurement interval in the experimental data acquisition system. The power over the five-minute period is assumed to be the average between the measurement at the beginning of the interval and the measurement at the end of the interval. The power is represented in the model by heat generation in the "fluid" cells. The "fluid" cells are given a high thermal conductivity and a low volumetric specific heat. This has the effect of dissipating the energy without introducing any thermal resistance inside the fluid. These approximations are necessary because of the 2-dimensional approximation.

The actual number of control volumes in each direction is dependent upon the actual size of the borehole and the actual size of the HDPE pipe used within the borehole. Typically, the solution domain grid size is set to have approximately $50(\theta) \times 100(r)$ finite control volumes. The numerical model grid is coded so that the grid spacing gradually increases the control volume size in the r-direction as r increases. This algorithm allows a fine grid in the immediate area of the borehole and a coarse grid in the area surrounding the borehole. Figure 4-3 is a representation of the grid generation within the borehole. Figure 4-4 is a view of the entire solution domain scaled to size. It is important to note

that the intersection of the "grid" lines represent the nodes, or centers of the control volumes.
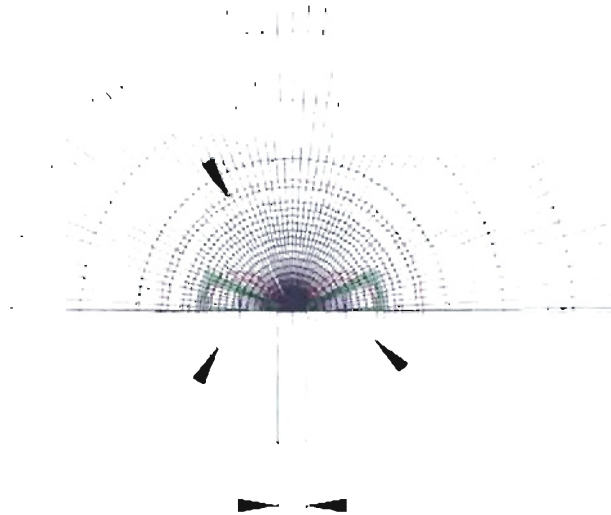
Figure 4-3. Scaled Drawing of Borehole with Pipe, Pie Sector, and Grid Node Points Indicated by the Legend

The model uses a 5-minute implicit time step. The time step is chosen to be the same as the interval of the experimental data collection.
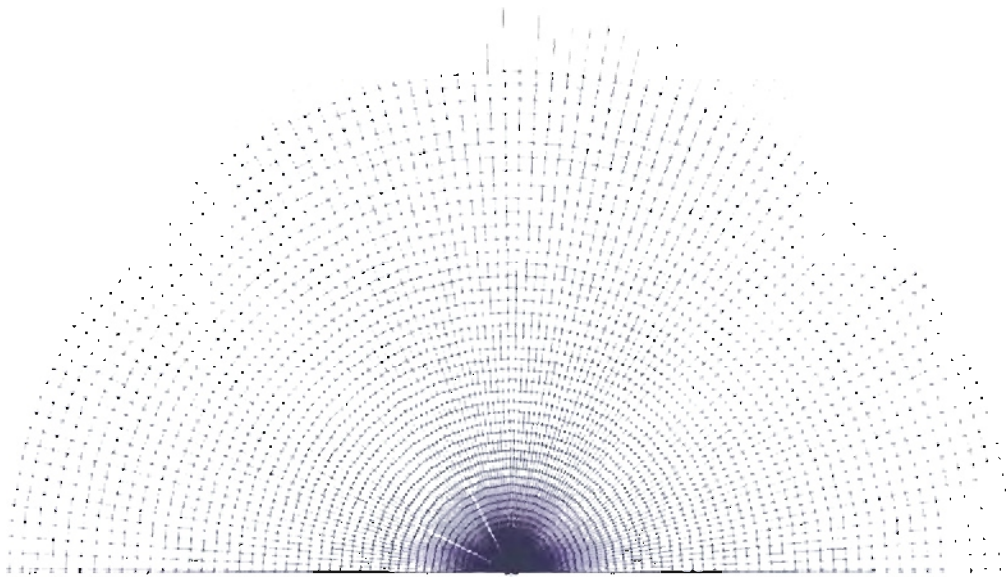
Figure 4-4. Solution Domain for Numerical Model

Modeling the borehole is simple with the type of coordinate system used, but to stay with the coordinate system the modeling of the pipe segments is a challenge. Figure 4-5 is a detailed layout of the "pie" approximation to the pipe, remembering that only the top half is modeled due to symmetry.

Figure 4-6 shows the pie sector approximation to the two pipes. The nodal points, where the temperature at each location is numerically solved, are shown in Figure 4-6 as the intersection of the black lines. The control volumes, which represent the pipe wall, are drawn in green. The assumption is made that the pie-shaped sector represents a half HDPE pipe. The odd shape of the pie sector approximation compared to the half cylinder shape of the pipe can be attributed to two factors.
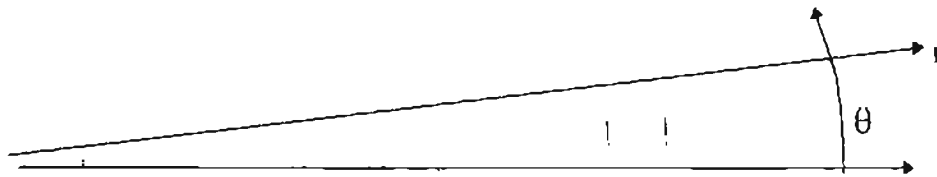
Figure 4-5. Pie Sector Approximation of ½ the Pipe

The wall thickness of the HDPE directly affects the wall thickness of the pie sector. The code was written to assign the number of control volumes in the r-direction to an incremental distance matching the wall thickness of the pipe as can be seen in Figure 4-5. The flow area of the pipe is the second factor in the shape of the pie sector. The numerical model matches the inside perimeter of three sides of the pie sector to the inside perimeter of the half pipe.

As shown in Figure 4-6, there is one control volume inside each pie-shaped sector's control volumes that attempts to represent the HDPE pipe. Within each of those particular control volumes the thermal conductivity is calculated from a thermal resistance circuit. The thermal conductivity of the HDPE pipe over the thickness of the HDPE pipe is, obviously, one of the lumped resistances. The other resistance is convection due to the fluid flow inside of the HDPE pipe. The two resistances are added up in series and the thermal conductivity of the numerical model control volumes that represent the HDPE pipe is set so that the cell's resistance (normal to the pipe wall) matches the calculated resistance. Hence, the assigned thermal conductivity is actually an effective thermal conductivity. Due to the odd shape of the pie sector approximation, different thermal conductivity values must be assigned to the pipe represented control volumes. The left hand and right control volumes are set to be the same value calculated from the lumped resistance. However, the top control volumes must be modified because they change in thickness as r. In order to account for the changing thickness, each control volume on the topside of the pie sector is scaled. Since the control volumes increase in thickness (θ direction) as r increases, the effective thermal conductivity must be decreased to maintain a constant thermal resistance, as r increases.
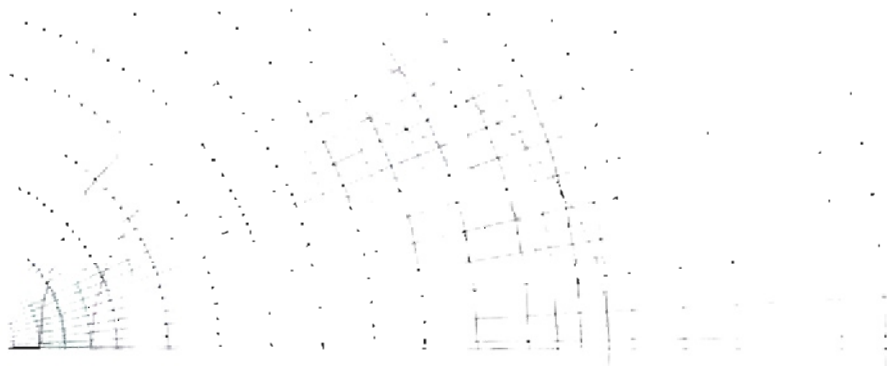
Figure 4-6. Pie Sector Approximation with Nodal Points at the Intersection of Each Grid Line (black)

The numerical model requires three input files, one of which gives parameters such as the fluid properties, borehole depth, far-field temperature, etc. The other two files give the power and temperature at 5-minute intervals. The model requires the experimental average temperature, determined by averaging the inlet and outlet temperatures in degrees Fahrenheit, and the experimental power input measured by the watt transducer in Watts. The input of the experimental power will eliminate problems that could occur or be associated with typical power fluctuations introduced with the use of portable power generators or utility power supply lines. Figure 4-7 is a typical input file required by the numerical model to run a simulation to estimate the ground thermal properties optimizing two variables.

```
INPUT DATA FILE FOR NELDER-MEAD SIMPLEX MINIMIZATION
                (FLOATING K_SOIL,K_GROUT)
     ─────────────────────────────────────

     *Full path and file name of the variable power data*
C:\MSDEV\PROJECTS\2D_MODEL\POWER_SiteA1-01-06-97.DAT
  *Full path and file name of the experimental temperature data*
 C:\MSDEV\PROJECTS\2D_MODEL\TEXP_SiteA1-01-06-97.DAT
              *Number of data points minus (1)*
                           866
                  *Borehole depth [ft.]*
                           244
                 *Far field temperature [F]*
                          63.1
           *Soil Storage term-lambda- [Btu/hr-F-ft]*
                          0.43
             *Pipe conductivity [Btu/hr-F-ft]*
                         0.226
             *Fluid conductivity [Btu/hr-F-ft]*
                         10000
            *Fluid dynamic viscosity [lbm/ft-hrs]*
                          2.39
                 *Fluid density [lbm/ft^3]*
                         62.32
              *Fluid volumetric flow rate [gpm]*
                          3.00
         *Grout storage term-lambda- [Btu/ft^3-F]*
                         52.00
          *Pipe storage term-lambda- [Btu/ft^3-F]*
                         30.00
         *Fluid storage term-lambda- [Btu/ft^3-F]*
                        0.0001
                  *Borehole radius [ft.]*
                      0.145833333
                *Pipe outer diameter [ft.]*
                         .0875
           *Distance between U-tube legs [ft.]*
                        0.0233
                 *Pipe wall thickness [ft.]*
                      0.00791667
                    *Time step [hr.]*
                        0.0833
```

Figure 4-7. Typical Input File for Numerical Model to
Estimate Ground Thermal Properties for Estimating Two Variables.

4.2. Numerical Model Validation of Methodology

Unfortunately, there is no analytical solution for two pipes in a grout-filled borehole surrounded by an infinite medium with a different thermal conductivity. So, the model was simplified for comparison to an analytical solution. This was done by removing one leg of the U-tube; setting the pipe conductivity, grout conductivity, and ground conductivity to all be equal; and using a constant power. This allows us to compare the numerical model's pie-slice-shaped pipe to the cylinder source solution. Any deviations between the numerical model and the analytical solution are then assumed to be caused by either the shape approximation, or possibly other numerical errors.

Figure 4-8. Pie Sector and Cylinder Source Temperature Plot and Error Comparison. 4.5" Diameter Borehole with a 0.75" Diameter Pipe. Sector Approximation of the Pipe with Perimeter Matching. k=1.5, L=250 ft, Tff=63°F

A constant heat input value is set at 3500 Watts. The cylinder source integral was solved analytically using a computer software program called Mathamatica. *Figures 4-8, 4-9, 4-10, 4-11, and 4-12 compare the cylinder source solution with the numerical model solution for different borehole diameters, soil thermal conductivities, borehole depths,*

and far-field temperatures. The % error is based on the temperature and is calculated

using equation 4-3.

$$\%\,Error = \left| \frac{T_{numerical\ model} - T_{cylinder\ source}}{T_{cylinder\ source} - T_{far\ field}} \right| * 100 \qquad (4\text{-}3)$$

Table 4-1. Comparison of Different Geometries of Numerical Solution

Figure:	$D_{borehole}$(in)	D_{pipe} (in)	$L_{borehole}$ (ft)	T_{ff} (°F)	k_{soil} (Btu/hr-ft-°F)	% Error at 192 hour
4-8	4.5	0.75	250	63	1.5	0 5
4-9	4.5	0.75	150	48	1	2
4-10	3.5	0.75	250	63	1.5	3
4-11	3.5	0.75	150	48	1	1
4-12	4.5	1.25	150	48	1	5

Table 4-1 compares the different configurations used to verify the numerical

method is adequate. The % errors in Table 4-1 are at the 192nd hour. It seems likely that

the approximation of the cylinder shape causes a more significant error early on in the test.

In every case the average temperature calculated by the model lags behind the cylinder

source average temperature values.
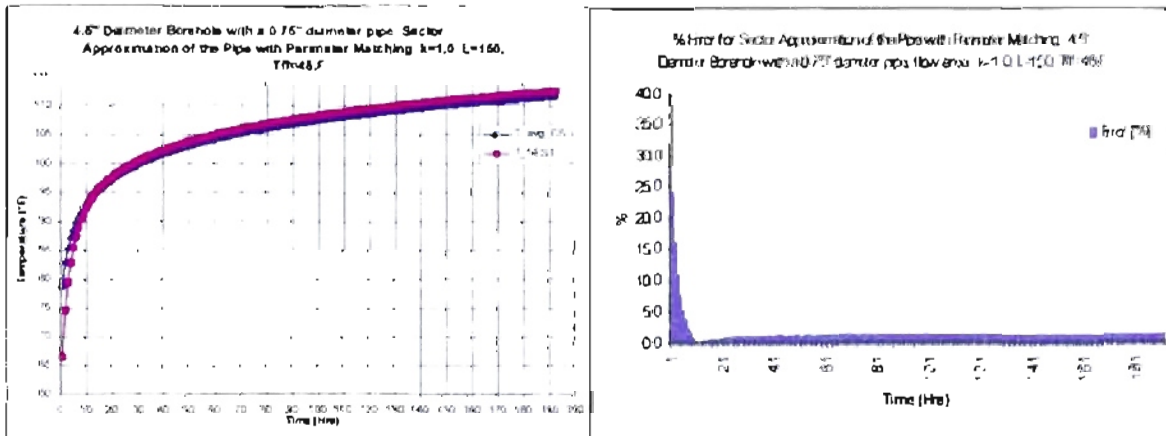
Figure 4-9. Pie Sector and Cylinder Source Temperature Plot and Error Comparison.
4.5" Diameter Borehole with a 0.75" Diameter Pipe. Sector Approximation
of the Pipe with Perimeter Matching. k=1.0, L=150 ft, Tff=48°.F

The high initial error could imply that it is necessary to ignore some initial portion of the data when matching for parameter estimation. In Table 4-1, the average error for solving a particular case is only about 2% after 192 hours of simulation. The worst case is occurs when a 1 ¼" pipe is used, yielding a 5% error. In reality it will be very unlikely that this particular size of pipe will be used to perform an in situ test. Based upon these results, the numerical model is performing within a reasonable threshold of error. It might be useful to note here that representing the pipe as being flattened into a pie shape causes this error. Other than that, the model is faithful in representing the location of the pipes and the borehole shape. Other models such as the line source or cylinder source, when applied to the standard two-pipes-in-borehole configuration, are even grosser representations. Therefore, we would not expect them to perform better, and would expect an even longer time before effects of the local borehole geometry are washed out.
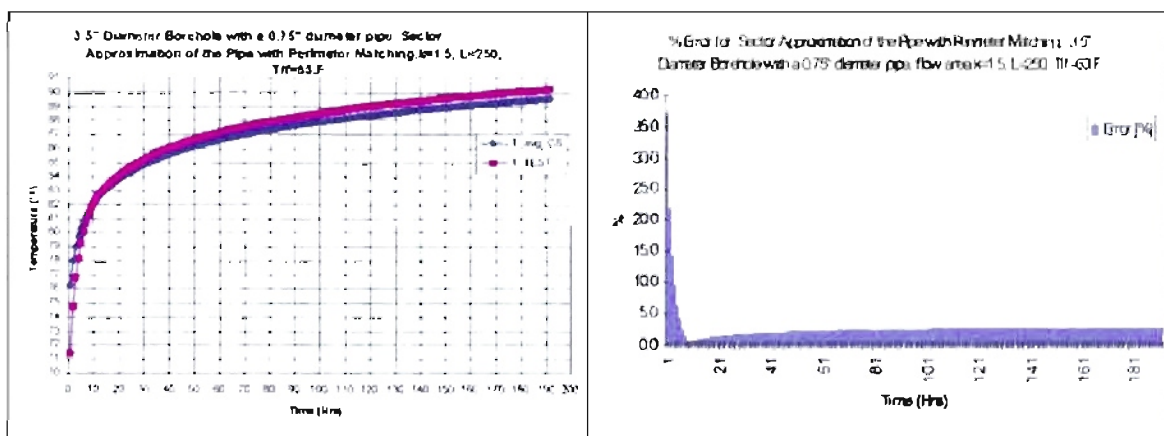
Figure 4-10. Pie Sector and Cylinder Source Temperature Plot and Error Comparison. 3.5" Diameter Borehole with a 0.75" Diameter Pipe. Sector Approximation of the Pipe with Perimeter Matching. k = 1.5, L=250 ft, Tff=63°F
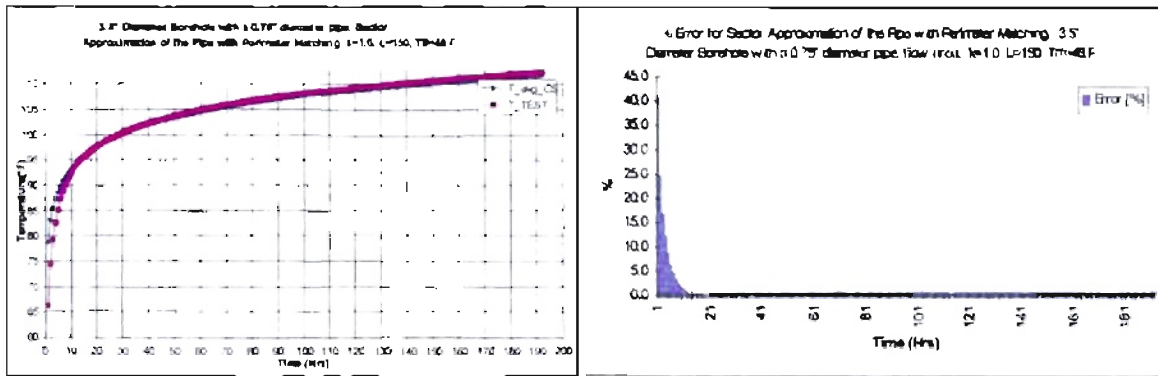
Figure 4-11. Pie Sector and Cylinder Source Temperature Plot and Error Comparison. 3.5" Diameter Borehole with a 0.75" Diameter Pipe. Sector Approximation of the Pipe with Perimeter Matching. k=1.0, L=150 ft, TIF=48°F
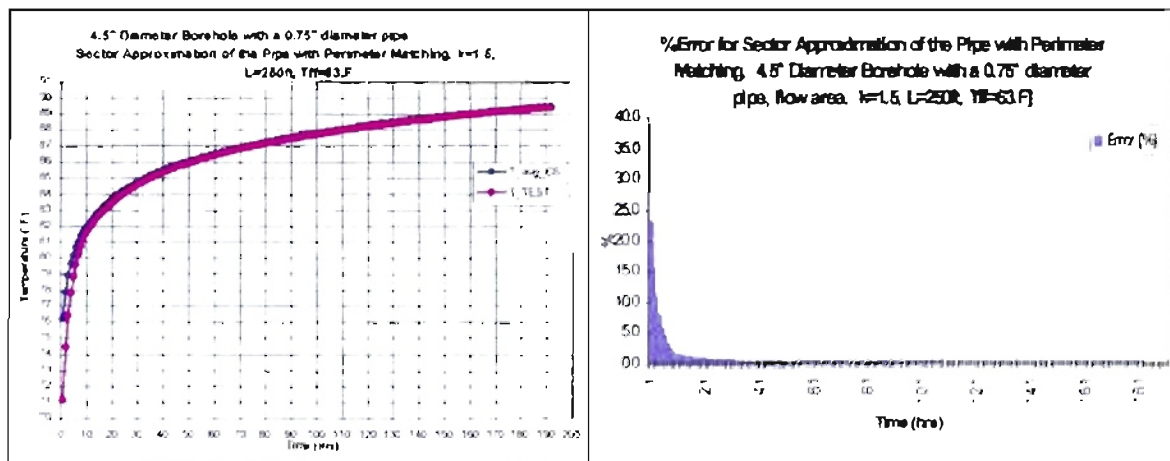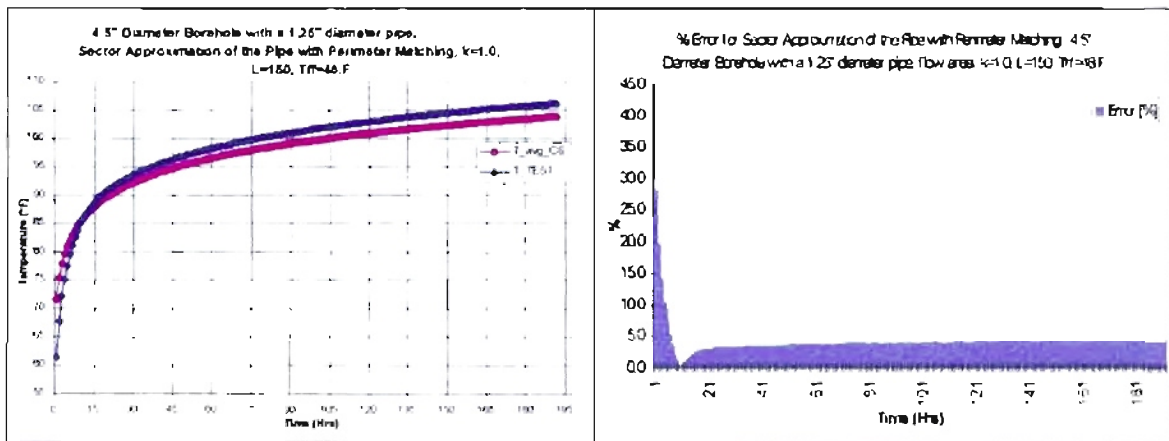

Figure 4-12. Pie Sector and Cylinder Source Temperature Plot and Error Comparison. 4.5" Diameter Borehole with a 1.25" Diameter Pipe. Sector Approximation of the Pipe with Perimeter Matching. k=1.0, L=150 ft, TIF=48°F

The next step was to actually model the HDPE pipe thermal conductivity and fluid convection. So, the model and analytical solution under the previous procedure was modified. The thermal conductivity of numerical model was changed by setting the pie-shaped control volumes that represent the HDPE pipe conductivity to a different value, as described in the previous section, rather than being equal in value to all other properties. At the same time, the model retained the grout conductivity, and ground conductivity to all be equal; and still used a constant power.
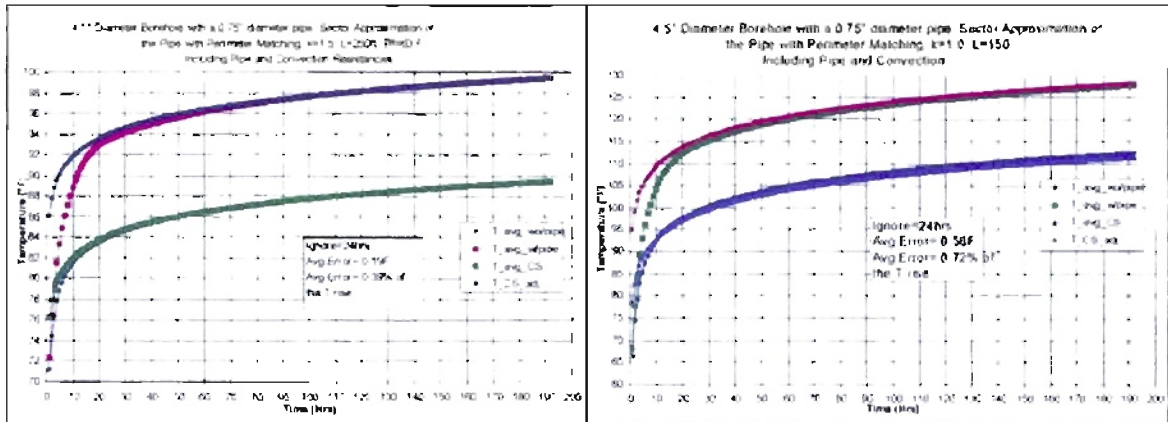
Figure 4-13. Pie Sector and Cylinder Source Temperature Plot with and without the Pipe
Thickness that includes the Thermal Resistance Estimate for 4.5" Diameter
Borehole with a 0.75" Diameter Pipe, L= 250 ft and 150 ft, and Tff = 63°F
and 48°F. Sector Approximation of the Pipe with Perimeter Matching for
k =1.5 and k =1.0 including Pipe and Convection Resistances

The cylinder source solution should also account for the pipe. There is not an

exact analytical solution for the cylinder source that includes the pipe, but there is an

approximate analytical solution. This involves treating the pipe as an infinitesimally thin

thermal resistance. The cylinder source modified solution is referred to as cylinder source

adjusted (cs_adjusted) in Figures 4-13, 4-14, 4-15, and 4-16.
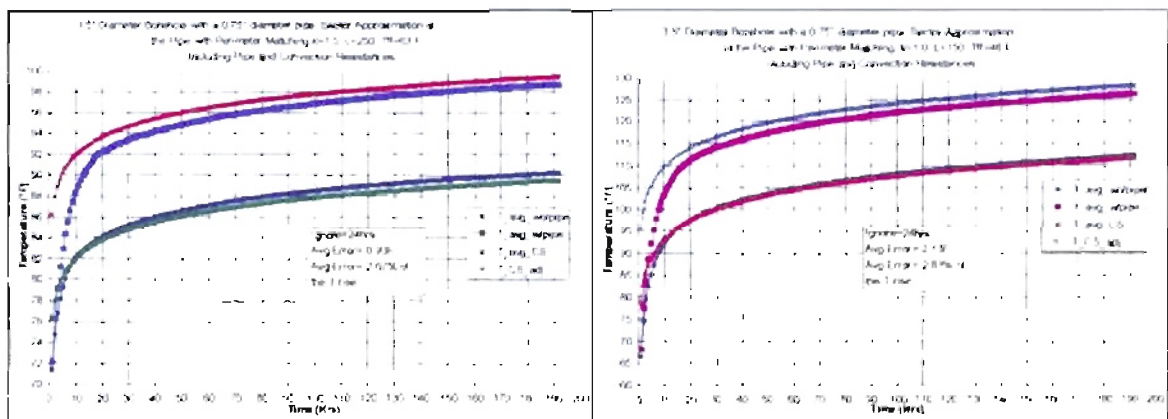
Figure 4-14. Pie Sector and Cylinder Source Temperature Plot with and without the Pipe
Thickness that includes the Thermal Resistance Estimate for 3.5" Diameter
Borehole with a 0.75" Diameter Pipe, L= 250 ft and 150 ft, and Tff = 63°F
and 48°F. Sector Approximation of the Pipe with Perimeter Matching for
k =1.5 and k =1.0 including Pipe and Convection Resistances

72
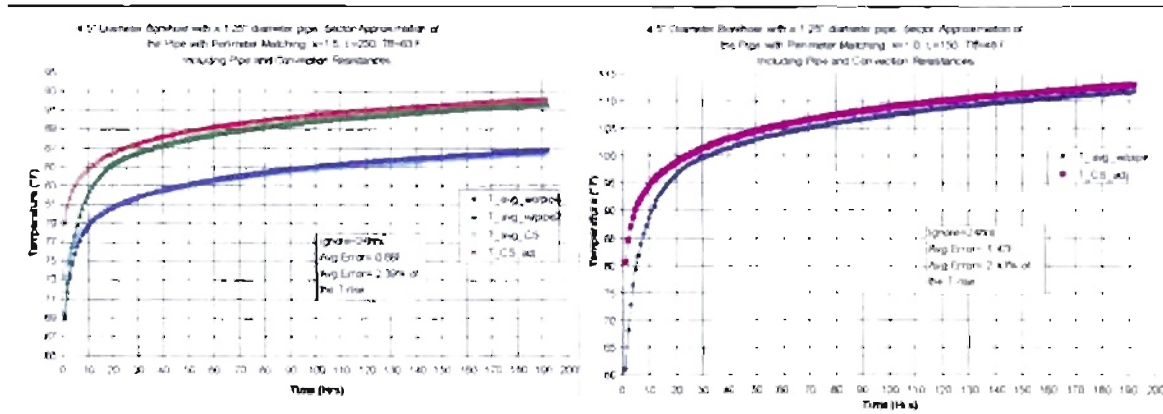
Figure 4-15. Pie Sector and Cylinder Source Temperature Plot with and without the Pipe
Thickness that includes the Thermal Resistance Estimate for 4.5'' Diameter
Borehole with a 1.25'' Diameter Pipe, L = 250 ft and 150 ft. and Tff = 63°F
and 48°F. Sector Approximation of the Pipe with Perimeter Matching for
k = 1.5 and k = 1.0 including Pipe and Convection Resistances

In each figure, it can clearly be seen that the numerical and cylinder source

solutions differ more when the solutions include the pipe. The average error listed in each

plot is determined by using equation 4-1, but instead of using the experimental average

temperature, it is replaced with the adjusted cylinder source average temperature. The

average % error is calculated by using equation 4-3, then averaging the % over the length

of the simulation and ignoring the % error for the first 24 hours of the average numerical

and cylinder source temperatures. In all of the cases shown in Figures 4-13, 4-14, 4-15,

and 4-16, the numerical average temperatures are lagging behind the adjusted cylinder

source solutions even worse than before.
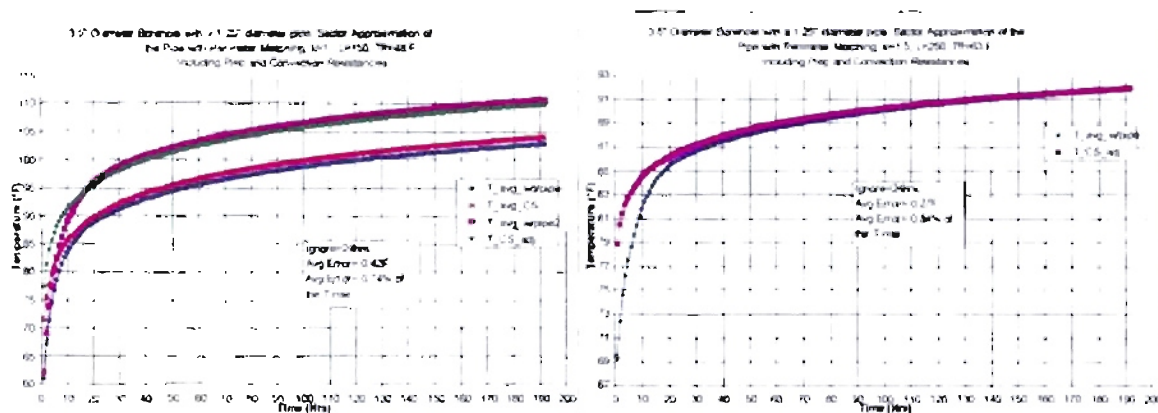
Figure 4-16. Pie Sector and Cylinder Source Temperature Plot with and without the Pipe Thickness that includes the Thermal Resistance Estimate for 4.5" Diameter Borehole with a 1.25" Diameter Pipe, L= 250 ft and 150 ft, and TIT = 63°F and 48°F. Sector Approximation of the Pipe with Perimeter Matching for k =1.5 and k =1.0 including Pipe and Convection Resistances

The difference between the two solutions is largest near the beginning; this is, unfortunately, the most important time. It is not certain what is the cause of the difference, whether the numerical model approximation or the approximate analytical cylinder source is causing the % error to be higher in the start up. A possible answer is that the finite pipe thickness in the numerical model is more important, and the cylinder source's infinitesimally thin representation of the pipe causes some error. With the errors being relatively small, it is safe to presume the numerical model is a good representation. Further investigation of the differences would be useful.

Another check performed on nearly all of the validation solutions described previously was related to the temperature at the other boundary. The boundary condition at the last radial location is adiabatic. If the model has a large enough solution domain, then the temperature at those locations should remain constant. If the temperature at those locations is gradually increasing, the temperature of the fluid will be adversely affected. Figure 4-17 shows the temperature as a function of location after a simulation of 192 hours, showing that beyond about 10 feet, the heating has had no effect. As

74

shown in Figure 4-17, the boundary temperature is 63.0 °F after 192 hours of simulation. This alleviates the question of heating up the outer boundary after time. Note that the outer boundary will eventually heat up if the problem is not set up correctly; if the time were to have been 250 hours, then there would have been an increase in that temperature at the boundary. For this reason, the domain boundary is set at 20 feet in the numerical model and a check on the temperature at the outer boundary is made.
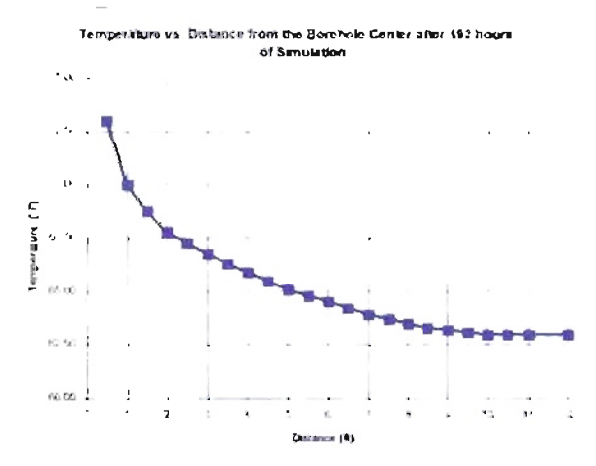
Figure 4-17. Temperature as a function of distance from the center of the domain.

By using $100r \times 50\theta$ cells, the numerical model adequately compares to an analytical solution within 2%-3% of the temperature rise. The error is very reasonable since the biggest factor in the error is the point of modeling a half-cylindrical ring by a "pie" shaped sector ring that matches only the perimeter. In the θ-direction, there is no convenient way to change the discretization, because it is set so the perimeter of the pie-shaped sector can match the perimeter of the half pipe.

It is difficult or impossible to exhaustively and comprehensively validate a numerical model. However, where checked the numerical model has proven to be reasonably valid. Also, this seems to be the best available approach, when compared to representing the U-tube as either a line source or a cylinder source.

4.3. Nelder-Mead Simplex Search Algorithm

The parameter estimation technique utilizes a search method called the Nelder-Mead Simplex search algorithm. This algorithm is sometimes referred to as the AMOEBA algorithm. The optimization subroutine was obtained from Numerical Recipes (Press, et al., 1986). It is written explicitly for functions of several variables, known as multidimensional minimization. The simplex algorithm is simple to implement because it does not involve any derivatives, requiring only function evaluations.

This algorithm creates a geometrical figure in N-dimensions of N+1 points and interconnecting lines or surfaces, where N is the number of independent variables. This figure is known as a simplex. In two dimensions it is a triangle, in three dimensions it is a tetrahedron. In order to start the procedure, there must be some initial simplex, which consists of user "guesses". The vertices of the simplex are changed in a series of steps. Each step is chosen by taking the highest function evaluation point and reflecting it through the opposite face of the simplex to some (hopefully) lower point. Depending on the outcome the simplex may then be expanded or contracted. This motion resembles amoeba-like movement; thus the name "amoeba".

Typically, the algorithm is terminated when a fractional tolerance is met with respect to the function evaluation. It should be noted that the simplex algorithm should be restarted after the fractional tolerance is achieved because it may have found local minima. For a case where the independent variables are k_{soil} and k_{grout} the simplex is a 2-D geometric object with three vertices in the same plane as shown in Figure 4-18.
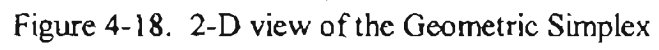
Figure 4-18. 2-D view of the Geometric Simplex

5. Results and Discussion

5.1. Experimental Tests

The Line Source model, the Cylinder Source model, and the numerical model will each be evaluated for selected experimental tests. There were 22 experimental tests performed in different geographical locations. Some locations had multiple boreholes to test with different ground loop heat exchanger parameters such as different depths, diameters, and grout material. A summary of every test performed can be found in Appendix A. Seven tests were selected to investigate the three methods for analyzing the experimental data. The dimensions of each borehole at Site A are detailed in Figure 5-1. Table 5-1 describes each set of the seven tests selected. Table 5-2 reviews a list of secondary test(s) used to demonstrate some of the results, but not used for detailed analysis due to the short data length. Appendix B contains the experimental data plots of temperature, power, and flow rate.

Site A Stillwater, OK   Test Location
Borehole Configurations for In Situ Thermal Conductivity Tests

Vertical Well #1
Grout- Benseal
Depth- 250'

Well #6
Incomplete Grout
Level— NOT Tested

3.5 m

Well #1
Grout- 30% Bentonite
Depth- 244'

Well #3
Grout- Thermal Grout 85
Depth- 252'

Well #5
Grout- E-Z Mud
Depth- 252'

3.5 m

3.5 m

3.5 m

3.5 m

4.5 m

3.5 m

Vertical Well #2
Grout- Benseal
Depth- 250'

Well #2
Grout- Thermal Grout 85
Depth- 252'

4.5 m

Test Well for
IGSHPA 3-Day May 21, 1997
Technical Demonstration

Well #4
Grout- 30% Bentonite
Depth- 250'

Drawing Not to Scale

Figure 5-1. Borehole Location Relative to Site A Stillwater, OK

Table 5-1. Summary of Experimental Tests Used for Detailed Analysis

Date	Location	Description	Duration(hr)
1-6-97	Stillwater, OK Site A	#1- 3 ½" borehole, 244' deep, grouted with 30% solids Bentonite. Powered by electric utility.	72
1-9-97	Stillwater, OK Site A	#2- 3 ½" borehole, 252' deep, grouted with Thermal Grout 85. Powered by electric line.	170
2-27-97	Stillwater, OK Site A	#3- 4 ½" borehole, 252' deep, grouted with Thermal Grout 85. Powered by electric line.	120
3-5-97	Stillwater, OK Site A	#4- 4 ½" borehole, 250' deep, grouted with 30% solids Bentonite. Powered by electric line.	73
5-28-97	Stillwater, OK Site A	#2- 3 ½" borehole, 252' deep, grouted with Thermal Grout 85. Powered by electric line.	170
6-2-97	Stillwater, OK Site A	#1- 3 ½" borehole, 244' deep, grouted with 30% solids Bentonite. Powered by electric line.	93
9-26-97	Chickasha, OK	Test Well for Smart Bridge Project- 3 ½" borehole, 250' deep grouted with 30% solids Bentonite, Power by Electric Generators	99

Table 5-2. Summary of Project Locations and Secondary Experimental Tests

Date	Location	Description	Duration(hr)
6-5-96	Richardson, TX	4 ½" borehole, 200' deep, grouted with Thermal Grout 85	11
6-6-97	Richardson, TX	4 ½" borehole, 200' deep, grouted with Ben-seal	10
8-8-96	Brookings, SD	#4- 6 " borehole, 200' deep, grouted with Thermal Grout 85. Power Supply from Building hookup.	12
11-6-96	Stillwater, OK Site A	#2- 3 ½" borehole, 252' deep, grouted with Thermal Grout 85. Powered by electric line.	75
11-12-96	Stillwater, OK Site A	#1- 3 ½" borehole, 244' deep, grouted with 30% solids Bentonite. Powered by electric line.	71
11-17-96	Stillwater, OK Site A	#3- 4 ½" borehole, 252' deep, grouted with Thermal Grout 85. Powered by electric line.	73
11-21-96	Stillwater, OK Site A	#4- 4 ½" borehole, 250' deep, grouted with 30% solids Bentonite. Powered by electric line.	73
11-25-96	Stillwater, OK Site A	#5- 3 ½" borehole, 252' deep, grouted with Benseal. Powered by electric line.	76
4-21-97	Stillwater, OK Site A	#5- 3 ½" borehole, 252' deep, grouted with Benseal. Powered by electric line.	93

5.2. Sensitivity of Line Source Model

The line source model for determining the thermal conductivity is easily

implemented using a spreadsheet. As discussed in section 1.2.5, the soil conductivity can

be estimated from the slope of the temperature vs ln(time) line:

$$Slope = \frac{\dot{Q}}{4\pi k_{soil}}$$

(5-1)

where,

Q = Average power Input per unit length (Btu/hr-ft)

The line source model has apparent problems with estimating the soil thermal conductivity because it is very sensitive to the temperature fluctuations that can sometimes occur during an experimental test. This is demonstrated in Figure 5-2.

Thermal conductivity using 3 hour time period
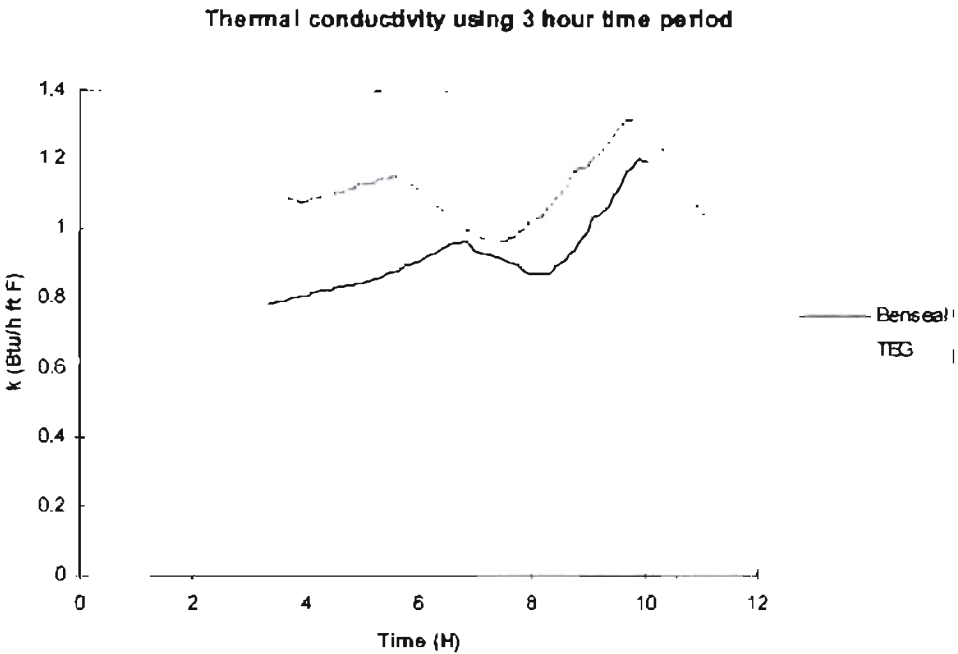
Figure 5-2. Sensitivity of the Thermal Conductivity Value to Minor Perturbations such as Power Fluctuations of Approximately 100 Watts

Using the data from Richardson, TX on 6-6-96, the thermal conductivity was systematically calculated for a floating 3-hour period. So, the thermal conductivity value at 3 hours in Figure 5-2 is calculated using the experimental data from 0 to 3 hours and the value at 6 hours is determined from the experimental data from 3 to 6 hours. Depending on where one chose to determine the slope of the line based on the time interval, different thermal conductivities result. In fact, the values of k_{soil} oscillate. This was not the only data set found to display these characteristics; in fact, most data sets show the same trend. Figure 5-3 also displays the same trend. Further investigation has revealed that any minor perturbation in the system will lead to the same problem. The

perturbations can arise from power changes, strong weather fronts, and changes in the flow rate. Longer tests also displayed oscillatory behavior: it did not settle out with time. Every test performed exhibits some form of changing conductivity.
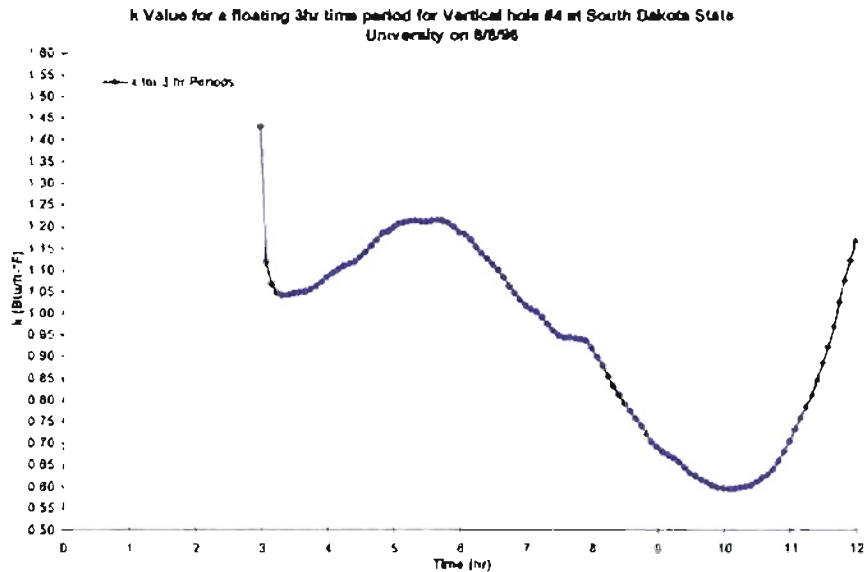
Figure 5-3. Sensitivity of the Thermal Conductivity Value to Minor Perturbations

5.3. *Experimental Results for Line Source Model*

Figure 5-4 shows the temperature versus the ln(time) for a 114-hour test. The data shown in figure 5-4 are susceptible to many different interpretations depending on where the slopes are taken. The calculated thermal conductivity values ranges between 1.13 Btu/hr-ft-°F and 1.73 Btu/hr-ft-°F for the different slopes shown. The conductivity resulting from the different slopes are quantified in Table 5-3. Again, this is from a number of factors.

The Average Fluid Temperature of Site A #2 in Stillwater, OK on 1-9-97 versus the Natural Log of Time. This plot is used to determine the slope of the data for the Line Source Model.
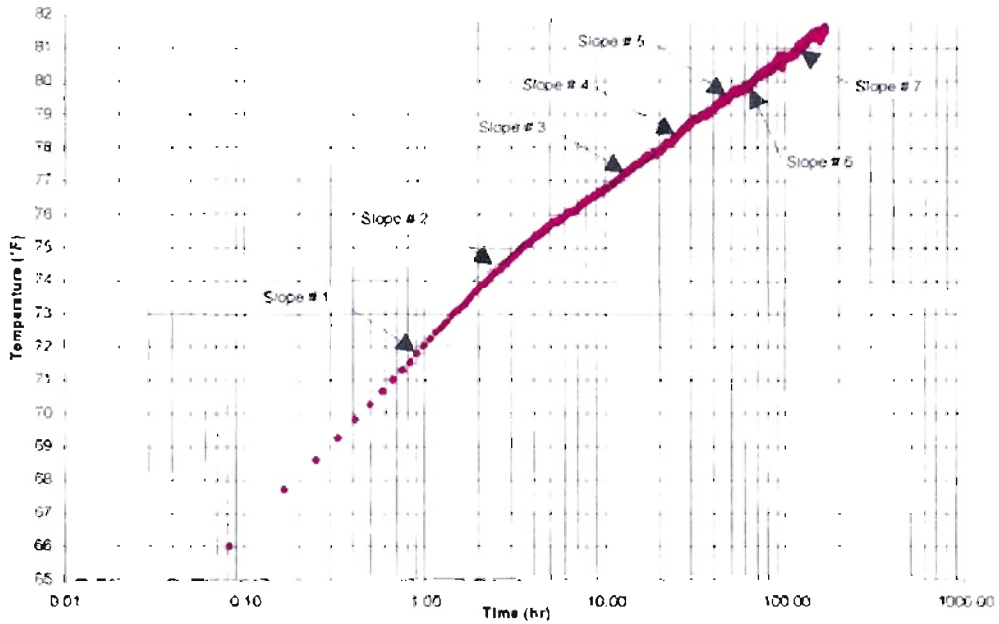
Figure 5-4. Experimental Test of Sensitivity of Slope to Perturbations

Another example of the wide range of the possible predictions is from Site A #5 tested on 11-25-96. The Line Source results can be seen in Figure 5-5. Again, depending on where the slopes are taken (time interval) the calculated thermal conductivity values ranges between 0.66 Btu/hr-ft-°F and 3.60 Btu/hr-ft-°F shown in Table 5-3.

Table 5-3. Thermal Conductivity Estimations for Site A #2 and #5, respectively

Average Period (hr)	Average Power (Btu/hr)	Slope	K_{soil} (Btu/hr-ft-°F)
Site A #2			
1-3	8449.6	2.352	1.13
4-11	8388.6	1.600	1.66
11-19	8395.8	1.749	1.52
20-30	8389.5	2.172	1.22
40-60	8408.2	1.534	1.73
60-90	8395.1	1.816	1.46
100-150	8374.8	2.138	1.24
Site A #5			
1-2	8749.8	4.239	0.66
2-6	8706.3	3.173	0.87
4-15	8673.7	2.349	1.18
25-50	8640.1	0.764	3.60

The Average Fluid Temperature for Site A # 5 in Stillwater, OK on 11-25-98 versus the Natural Log of Time. This plot is used to determine the slope of the data for the Line Source Model
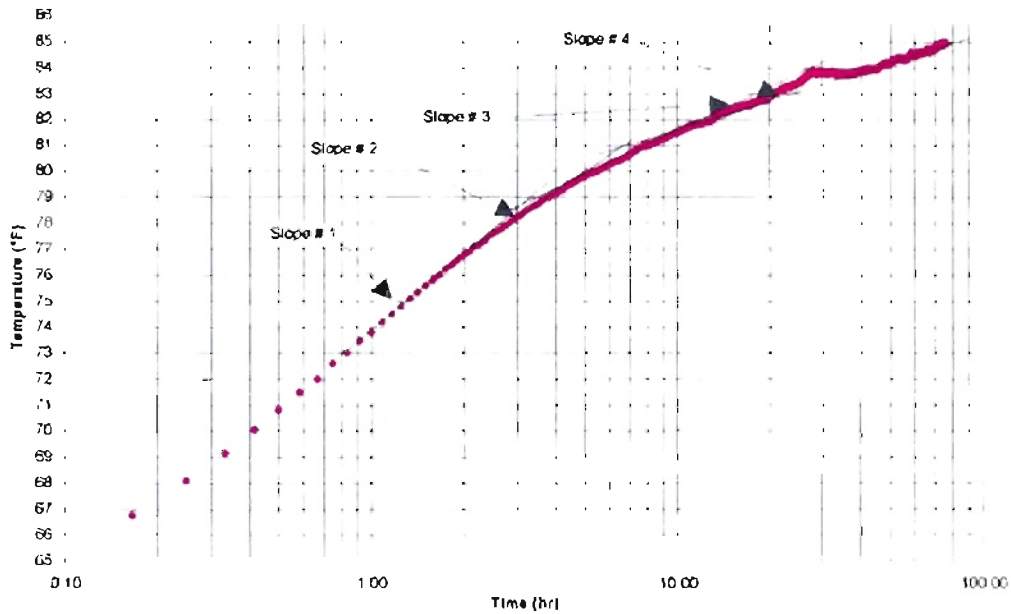
Figure 5-5. Experimental Test of Sensitivity of Slope to Perturbations

It is difficult to make any comparison between Site A # 2 and # 5. Both tests should yield the same ground thermal conductivity because the soil composition is the same, yet neither case gives reasonable results. This trend manifests itself in almost every experimental data set. This has led us to reject this approach for analyzing the in situ test data.

5.4. Experimental Results for Cylinder Source Model

Two data sets were used to estimate the thermal conductivity of the ground using the cylinder source method. As described in Chapter 1, the step by step procedure of the cylinder source solution involves many equations and calculations. A recent publication by ASHRAE has listed the same procedure in condensed form with tables and figures in place of the equations. This procedure is described by Kavanaugh and Rafferty in Ground Source Heat Pumps- Design of Geothermal Systems for Commercial and Institutional Buildings, Chapter 3- Fundamentals of Vertical Ground Heat Exchanger Design, Section 3.5- Field Tests for Determining Soil Properties (Kavanaugh and Rafferty, 1997) (Referred to in this section as "the handbook"). This procedure was this section.

To begin this procedure some general information about the borehole and borehole drill must be known. Some of the general information includes:

- HDPE pipe used for the test

- Borehole backfill material

- General knowledge about the cuttings from the bore (i.e. type of soil/rock, moisture content, etc.)

Next, an effective thermal resistance of the ground by a daily pulse using equation 5-2 is calculated.

$$R_{gJ} = \left[\frac{L_c \left(t_g - \frac{t_{wi} + t_{wo}}{2} \right)}{-3.41 W_c} - R_b \right] \frac{1}{F_{sc}}$$

(5-2)

Where, t_g is the undisturbed ground temperature (°F)

t_{wo} is the outlet water temperature (°F) at the last timed point

t_{wi} is the inlet water temperature (°F) at the last timed point

L_c is the borehole length (ft)

F_{sc} is the short circuiting heat loss factor taken from the Figure 3.3 of the handbook.

R_b is the borehole resistance (hr-ft-°F/Btu) taken from Table 3.2 of the handbook.

W_c is the power input for cooling (Watts)

Once this information is known, the thermal resistance can be calculated using equation 5-2. Then, the ground thermal conductivity (k_g) and thermal diffusivity (α_g) are "guessed" from Table 3.4, based on the knowledge of the geological conditions from the drill cuttings. Next, the Fourier number (F_o) is calculated from equation 5-3.

$$Fo = \frac{4\alpha_g \tau}{d^2}$$

(5-3)

Where, τ is the time interval of the test in days

d is the equivalent diameter of the pipe used (taken from Table 3.2 of handbook)

From the Fourier number that was calculated is used to estimate a G-Factor using Figure 3.2 of the handbook. Once the G-Factor is estimated, the thermal resistance of the ground is calculated using equation 5-4.

$$R_g = \frac{G}{k_g}$$

(5-4)

Once the thermal resistance of equation 5-4 is calculated, it is compared to the thermal resistance value determined from equation 5-2. After that, the ground thermal

conductivity and thermal diffusivity are adjusted until the thermal resistance of the ground calculated in equation 5-4 matches the value from equation 5-2.

After looking up the table values for the soil conditions at Site A, a simple spreadsheet was set up to update the values as different guesses were used for different data sets. Table 5-4 shows a typical spreadsheet configuration for the data sets evaluated.

Site A #5 on 11-25-96								
tg	63	Table 3.4	k	1	1.1	1.1	1	1.1
twi	81.9	Table 3.4	alpha	0.8	1	1.2	0.7	0.9
two	87.9							
Ic	250							
Rb	0.09							
Fsc	1.04							
Wc	2526							
Rgd	0.525							
d	0.15	Table 3.2						
		Days	t =72 hour	3	3	3	3	3
		Equation 3.4	Fo	426.7	533.3	640 0	373.3	480 0
		Figure 3 2	G	0 55	0 56	0 588	0 54	0 56
			Rg	0.550	0.509	0.535	0.540	0.509

Table 5-4. Typical Spreadsheet for Cylinder Source Method

Data from Site A #1 on 6-2-97 and Site A #2 on 1-9-97 are shown in Table 5-5. The data are used in a spreadsheet similar to that in Table 5-4 to estimate the soil properties at different times for each data set. The soil thermal conductivity estimated over the test period is shown in Figure 5-6. The thermal conductivity appears to be approaching a near constant value. Unfortunately, the two separate tests do not estimate the same soil thermal conductivity. This is due inherently to the different grout material used in each borehole. Site A # 1 is grouted with Bentonite (k_{grout} = 0.85 Btu/hr-ft-°F); Site A # 2 is grouted with thermally enhanced grout (k_{grout} = 0.43 Btu/hr-ft-°F).

Table 5-5. Experimental Values used in the Cylinder Source Solution for Site A #1 on 6-2-97 and Site A # 2 on 1-9-97

Site A # 2 on 1-9-97					
TIME	time(hr)	T_{in} from Gnd (°F)	T_{out} to Gnd (°F)	Flow (gpm)	Power(Watt)
1/9/97 18:02	1.00	69.1	75.0	3.014	2472.5
1/10/97 3:02	10.00	73.8	79.7	3.063	2454.2
1/10/97 13:02	20.00	74.9	80.8	3.065	2445.3
1/10/97 23:02	30.00	75.8	81.6	3.057	2449.9
1/11/97 9:02	40.00	76.2	82.1	3.001	2467.7
1/11/97 19:02	50.00	76.6	82.5	3.020	2467.6
1/12/97 5:02	60.00	76.9	82.7	2.982	2461.8
1/12/97 15:02	70.00	77.2	83.1	3.050	2459.6
1/13/97 1:02	80.00	77.3	83.2	3.015	2459.2
1/13/97 11:02	90.00	77.6	83.5	2.997	2452.9
1/13/97 21:02	100.00	77.8	83.6	3.068	2466.1
1/14/97 7:02	110.00	77.9	83.7	3.052	2466.5
1/14/97 17:02	120.00	78.2	84.0	3.108	2468.8
1/15/97 3:02	130.00	78.3	84.0	3.069	2446.8
1/15/97 13:02	140.00	78.4	84.3	2.985	2453.3
1/15/97 23:02	150.00	78.5	84.4	2.981	2452
1/16/97 9:02	160.00	78.4	84.3	3.047	2474.9
1/16/97 18:32	169.50	78.6	84.5	3.021	2439.9
Site A # 1 on 6-2-97					
TIME	Time(hr)	Tin from Gnd (°F)	Tout to Gnd (°F)	Flow (gpm)	Power(Watt)
6/2/97 13:40	1	75.1	82.4	3.07	3202.5
6/2/97 22:40	10	83.5	90.7	3.1	3166.5
6/3/97 8:40	20	85.3	92.5	3.06	3203.4
6/3/97 18:40	30	86.5	93.6	3.13	3179.3
6/4/97 4:40	40	86.9	94	3.1	3129.5
6/4/97 14:40	50	87.7	94.7	3.12	3153.7
6/5/97 0:40	60	87.9	95	3.02	3168.7
6/5/97 10:40	70	88.4	95.5	3.01	3135.9
6/5/97 20:40	80	89	96.4	3.03	3264.6
6/6/97 6:40	90	88.9	96.1	2.97	3208.6
6/6/97 15:10	98.5	89.4	96.5	3.01	3149

Results from Site A # 1 on 6-2-97 estimate a soil thermal conductivity of approximately 1.32 Btu/hr-ft-°F. The results from Site A # 2 on 1-9-97 have a significant variation with an estimated soil thermal conductivity of 1.65 Btu/hr-ft-°F. The two boreholes compare from 1.35 to 1.65 Btu/hr-ft-°F, which is a 22% increase from the lower value.
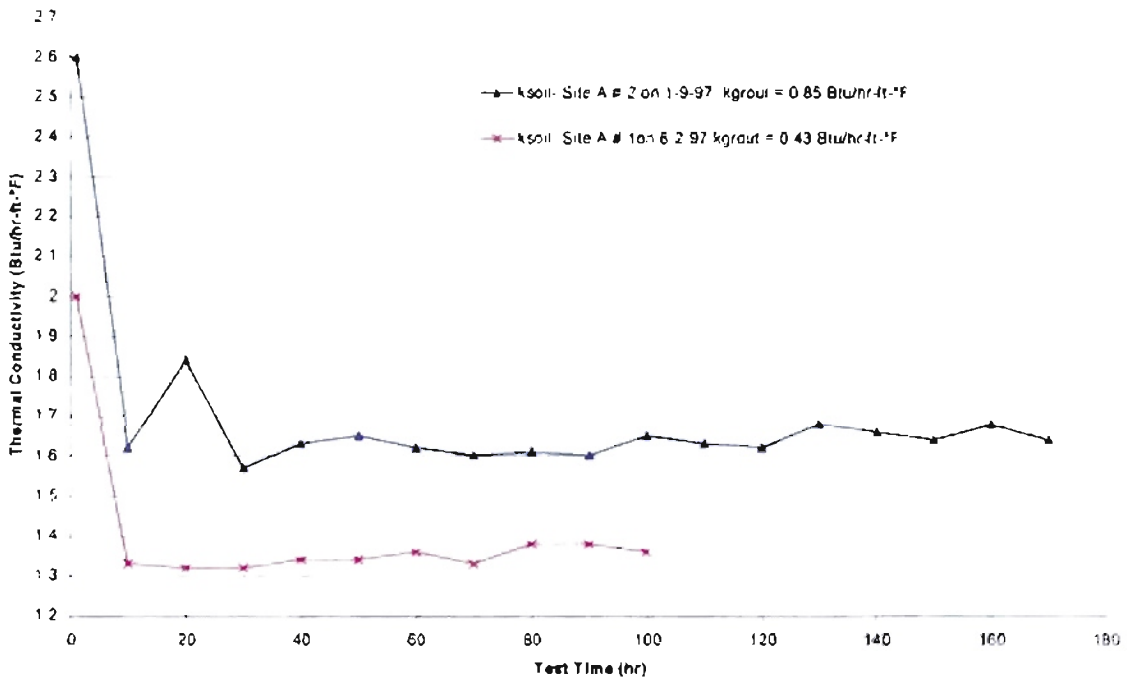
Figure 5-6. Cylinder Source Solution for Two Data Sets

Comparing the conductivity predictions between the two tests, the effect of grout thermal conductivity can be clearly seen even after adjusting the borehole thermal resistance according to Table 3.2 in the handbook. The borehole with thermally enhanced grout yields a significantly higher ground thermal conductivity. As shown in Figure 5-6, the estimations appear to be increasing slightly as time increases. Also, the value of ground conductivity predicted depends strongly on the length of the test. Kavanaugh and Rafferty (1997) do not suggest a minimum test time, although they give an example where a 12-hour test is used. For these boreholes, a 12-hour test would not predict the "converged value of the ground conductivity.

5.5. Overview of Parameter Estimation Results

As discussed in Chapter 4, there are a number of ways that the parameter estimation might be approached. Specifically, one, two, or more parameters might be estimated simultaneously. Although a number of approaches were tried, including estimating up to five parameters (soil conductivity, shank spacing, grout conductivity, soil volumetric specific heat, and grout volumetric specific heat) simultaneously, only the two most promising approaches will be presented in this thesis. The first is estimation of only the soil conductivity. This has the advantages of simplicity and speed, since only one parameter is varied. The disadvantage of using only one variable is that all of the other inputs must be "correct": shank spacing, grout conductivity, and grout volumetric specific heat.

The second approach, which is discussed in Section 5.7, involves simultaneous estimation of both soil conductivity and grout conductivity. This has the advantage of allowing for an approximate accounting for several borehole-related parameters: grout conductivity, shank spacing and even borehole diameter. (The borehole will not necessarily be exactly the diameter of the drill bit.) The estimated grout conductivity might be considered as an effective grout conductivity in this case.

Other approaches that involved estimation of additional parameters often gave very good fits to the experimental data. Unfortunately, some of the estimated parameters, especially the volumetric specific heats, were outside of what might be considered physically possible. Also, as more simultaneous parameters are estimated,

more computational time is required. With only considering simultaneous estimation of one or two parameters, the results presented in this chapter represent approximately 650 hours of CPU time on Pentium computers that ranged in clock speed from 90-233 MHz.

Furthermore, simultaneous estimation of both soil conductivity and soil volumetric specific heat is problematic. In a transient conduction heat transfer problem, the governing equation is often written with only the thermal diffusivity, the ratio of the thermal conductivity to the volumetric specific heat. From this, one might conclude that it is impossible to estimate conductivity and volumetric specific heat simultaneously, as there are an infinite number of values that represent the same value of diffusivity. However, one must keep in mind that the boundary condition at the wall of the pipe is effectively a fixed heat flux, and that therefore k dT/dx is fixed. This does allow simultaneous estimation of thermal conductivity and volumetric specific heat, even if the results are not always satisfactory.

Consequently, the value of volumetric specific heat has been estimated based on knowledge of the rock formation and treated as a known value. As it turns out, the results are not that sensitive to the assumed value of volumetric specific heat. This is demonstrated in Section 5.6.4.

Another important issue that should be discussed at the outset of the parameter estimation section is the issue of an "absolute truth model" for the thermal conductivity. The fundamental problem is that, to date, there is no location where an in situ test can be performed that the ground conductivity is already known. In other words, there is no completely independent method for determining the ground conductivity. As mentioned in Section 1.2.3, an effort is being made by Dr. Smith in the OSU Division of

Engineering Technology to measure the thermal conductivity samples taken from a cored borehole. If successful, this might provide an independent measurement of the thermal conductivity. Because there is no "absolute truth model", we are somewhat limited in the comparisons that can be made. For example, when attempting to answer the question of "how long does the test need to be?", we are limited to looking at different test lengths to find the length of test, beyond which the thermal conductivity will not change very much.

We can also look for other types of indirect confirmation that the method works correctly. For example, measurements of thermal conductivity taken at nearby boreholes with different grout types and pipe types should give approximately the same value.

5.6. Parameter Estimation with Single Independent Variable

In this section, results from parameter estimation with a single independent variable, soil conductivity, are presented. Section 5.6.1 focuses on the sensitivity of the results to the length of the test, and to the number of initial data hours that are ignored, if any. Sections 5.6.2-5.6.5 show the sensitivity of the results to other parameters with pre-estimated values – far field temperature grout conductivity, shank spacing and soil volumetric specific heat.

5.6.1. Determination of Initial Data Hours to Ignore and Length of Test

One of the most commonly asked questions about in situ testing is "How long does the test need to be?" At present, the best approach available for answering this question is to run long tests, and then use only portions of the data for estimating the thermal conductivity. As the portion of data used increases in length, there should be a point in time beyond which the estimated value of thermal conductivity does not change very much. Likewise, it might be useful to ignore some initial part of the data.

Analysis on the long data sets began with the assumption that a better parameter estimation may exist when a certain number of initial data points are ignored.

Solid 3-D bar Chart of the Estimated Thermal Conductivity using a specified length of hours
Data Set collected at Site A #2 on 1-9-97. The complete Data Set is approximately 170 hours
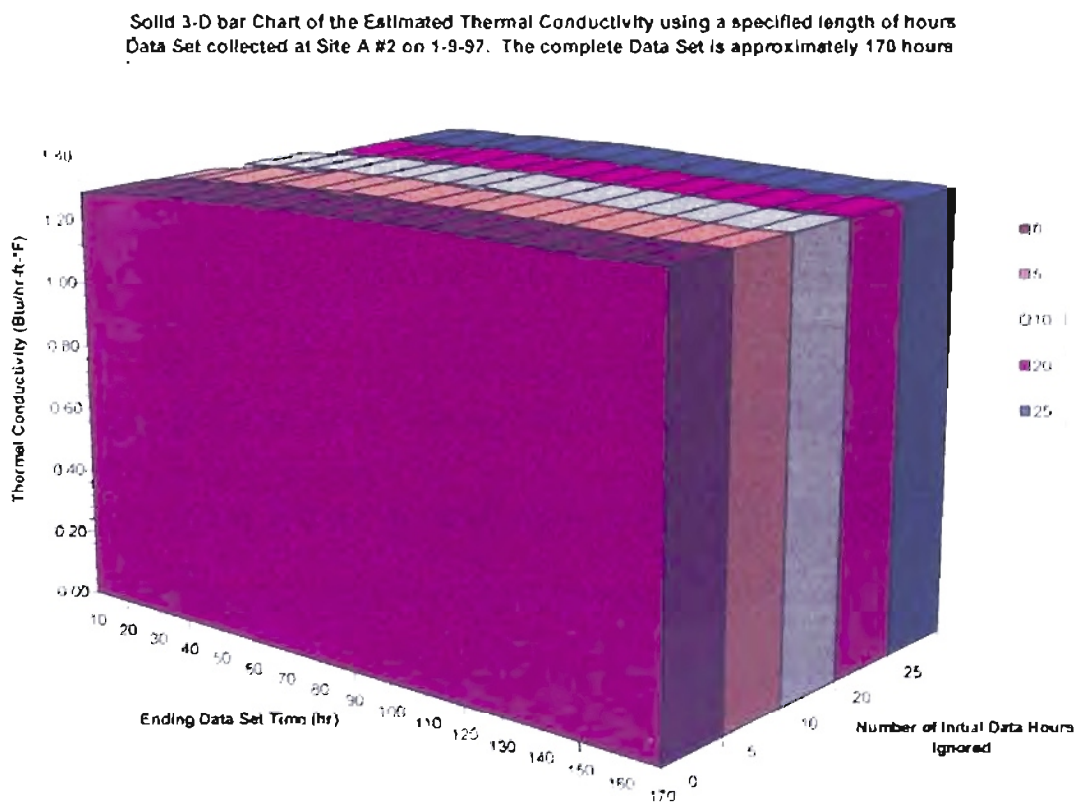

Figure 5-7. 3-D Bar Graph of an Experimental Test

Figure 5-7 is a 3-D view of a 170 hour long experimental data set. The predicted ground

thermal conductivities appear to be near constant for any number of initial data hours

ignored. All predicted values are approximately 1.3 Btu/hr-ft-°F. But, a better

representation is in Figure 5-8 that depicts a 2-D side view. With the scale for thermal

conductivity "zoomed" to 1.27-1.38, a small but steady increase in the estimated ground

thermal conductivity can be seen as additional data are used.
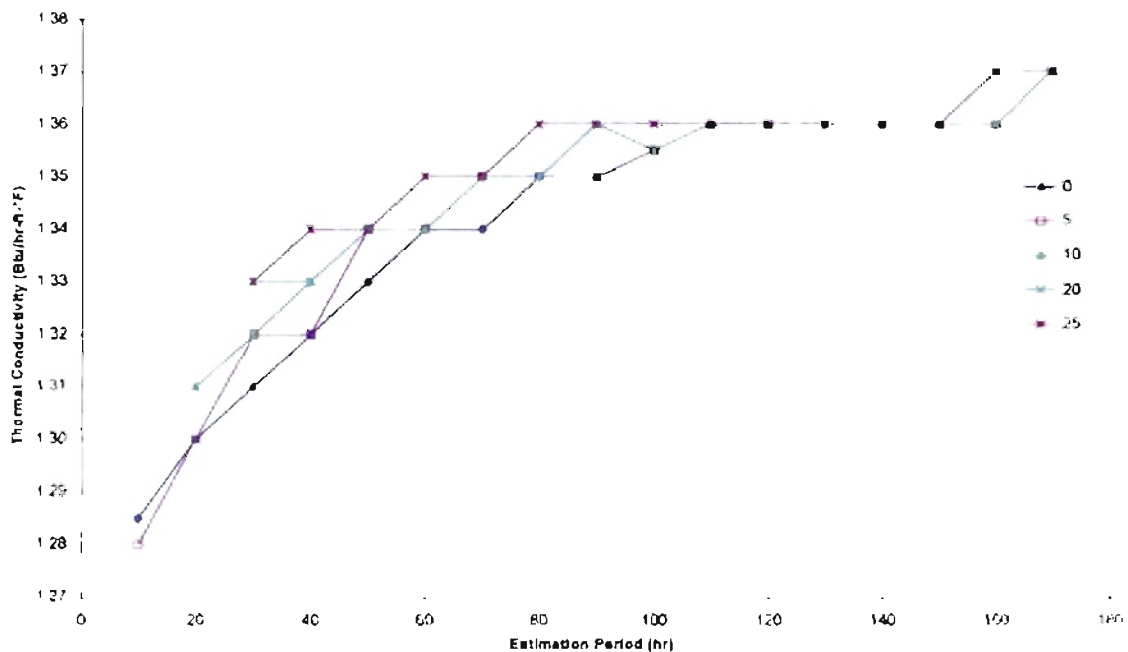

Figure 5-8. 2-D View of the Ground Thermal Conductivity for Site A #2 on 1-9-97

There are two trends* that can be seen in Figure 5-8. The first noticeable trend is the

asymptotic convergence to a ground thermal conductivity value of 1.36 Btu/hr-ft-°F as

the estimated period increases. The second trend of Figure 5-8 is that the more initial

data ignored, the more quickly the ground thermal conductivity predictions approach the

---

* A third "trend" might be the appearance of the plot. All values were only entered to the nearest
hundredth. Therefore, when we "zoom in" the values have clearly defined "steps".

asymptote line. This behavior of the ground thermal conductivity predictions can be

seen in several other data sets. Figure 5-9, 5-10, and 5-11 display the data sets that
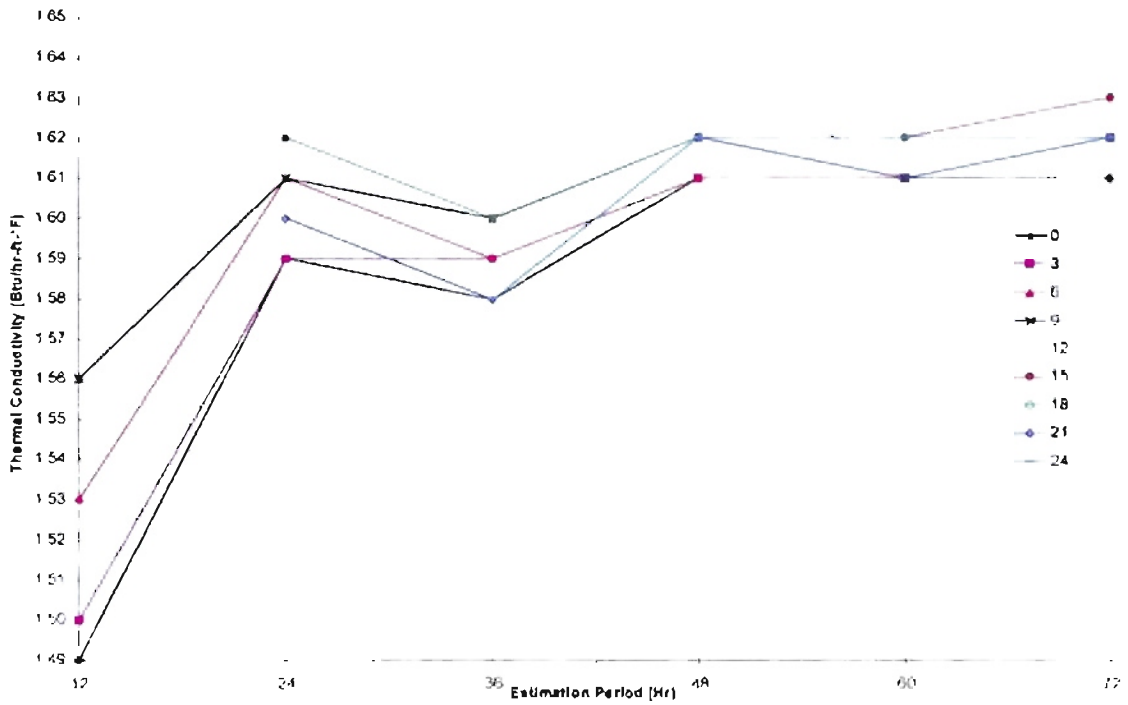
behave in similar manners as in Figure 5-8.

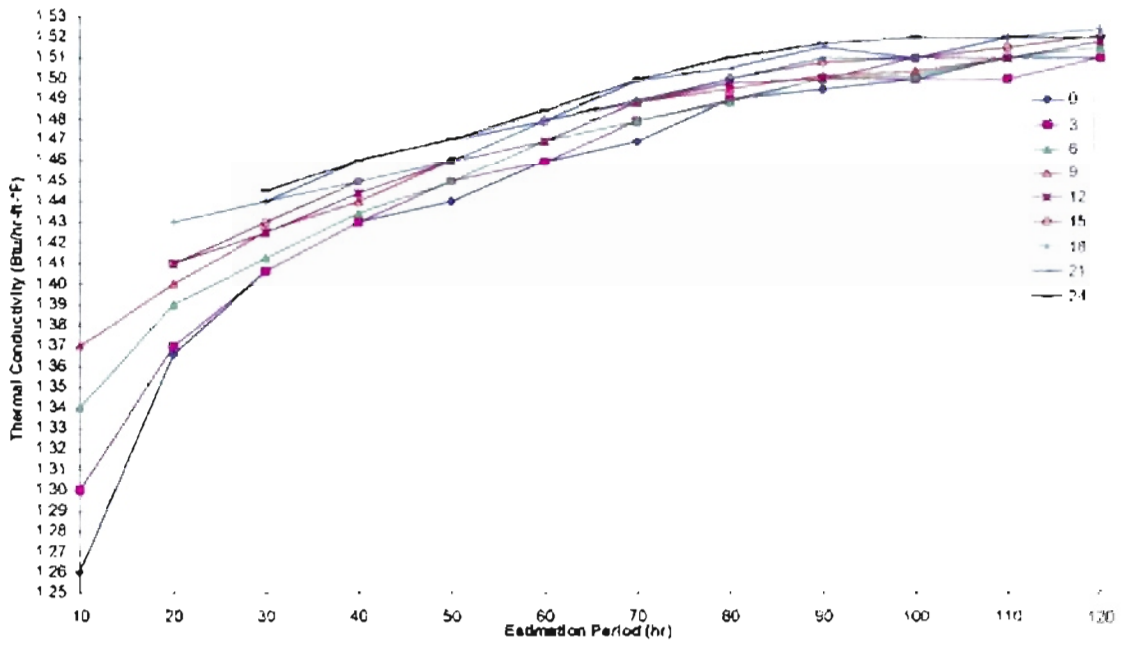Figure 5-9. 2-D View of the Ground Thermal Conductivity for Site A # 4 on 3-5-97

Figure 5-10. 2-D View of the Ground Thermal Conductivity for Site # 3 on 2-27-97
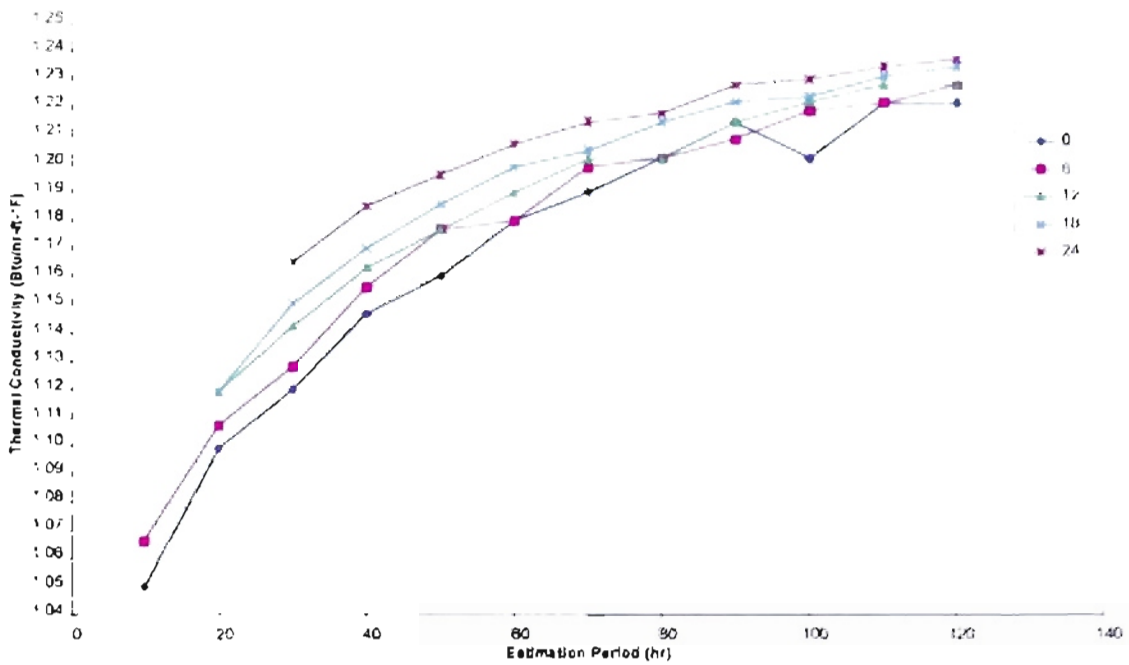

Figure 5-11. 2-D View of the Ground Thermal Conductivity for Site A # 2 on 5-28-97

96

In an attempt to determine the approximate number of initial data hours to ignore, 3-D surface plots of the average error per estimated data point are used. These plots can be seen in Figure 5-12, 5-13, 5-14, and 5-15. Figure 5-12 suggests some initial data should not be included in the parameter estimation optimization. Viewing Figure 5-12, one could interpret after about 6 hours of time, the error doesn't change significantly. Figures 5-13, 14, and 15 indicate that after 12 hours the error doesn't seem to significantly. By using the 3-D surface plots of the errors in conjunction the ground conductivity predictions plots, any estimation period ignoring at least the first 12 hours of estimation time appear to "approach" the "true" conductivity in less total estimation time. So, for one variable optimization, about 12 hours of initial data ignored would yield reasonable ground thermal conductivity predictions. This will aid in determining the length of test.

Surface plot of the Average Error per Estimated Data Point. Site A #4 on 3-5-97 for 72 hours.

Figure 5-12. 3-D Surface Error Plot of Different Ground Thermal Conductivity Predictions

Surface plot of the Average Error per Estimated Data Point. Site A #3 on 2-27-97 for 120 hours.

Figure 5-13. 3-D Surface Error Plot of Different Ground Thermal Conductivity Predictions

Surface plot of the Average Error per Estimated Data Point. Site A #2 on 5-28-97 for 120 hours
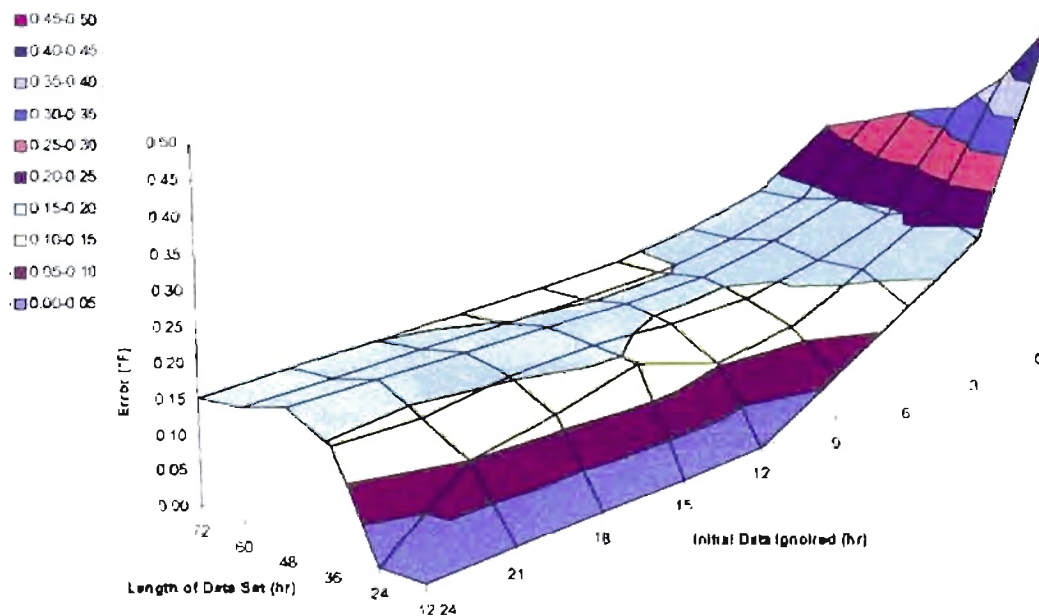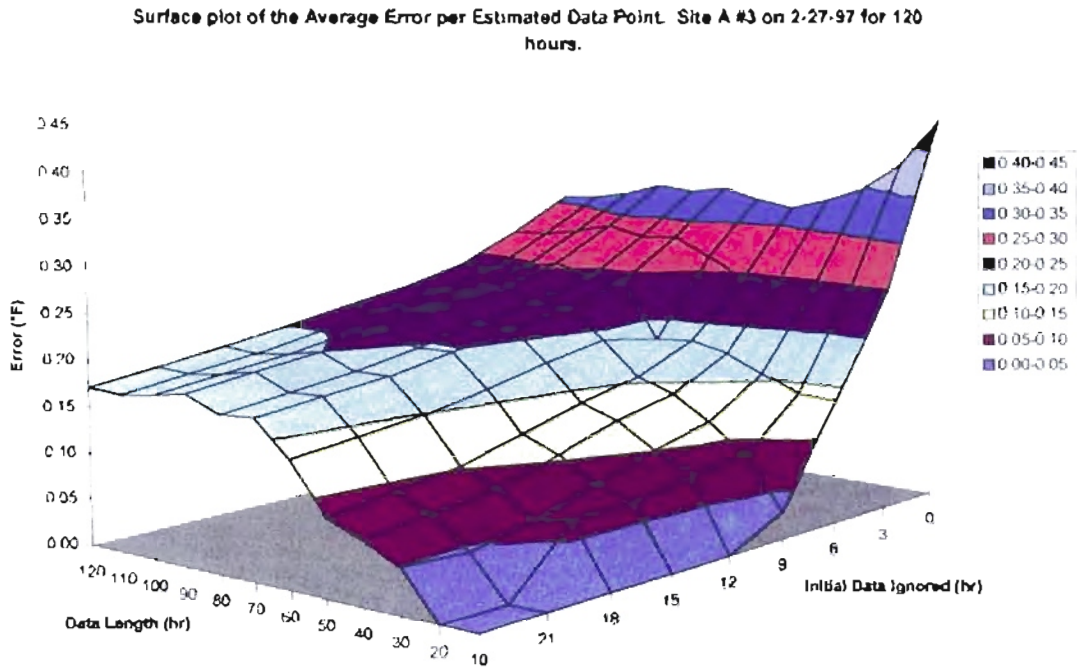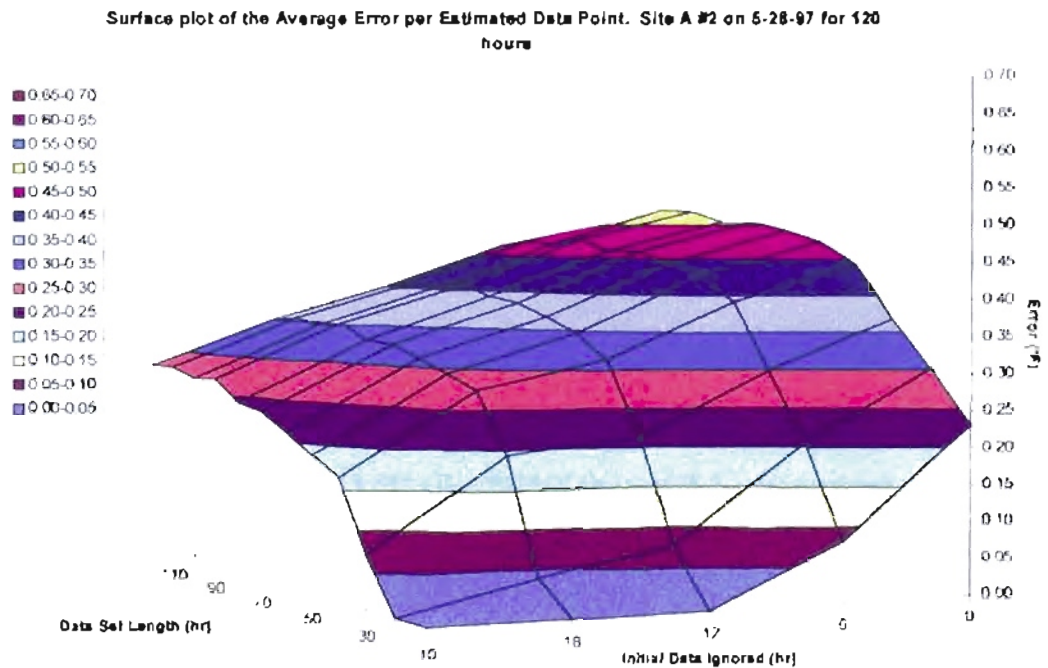

Figure 5-14. 3-D Surface Error Plot of Different Ground Thermal Conductivity Predictions

98
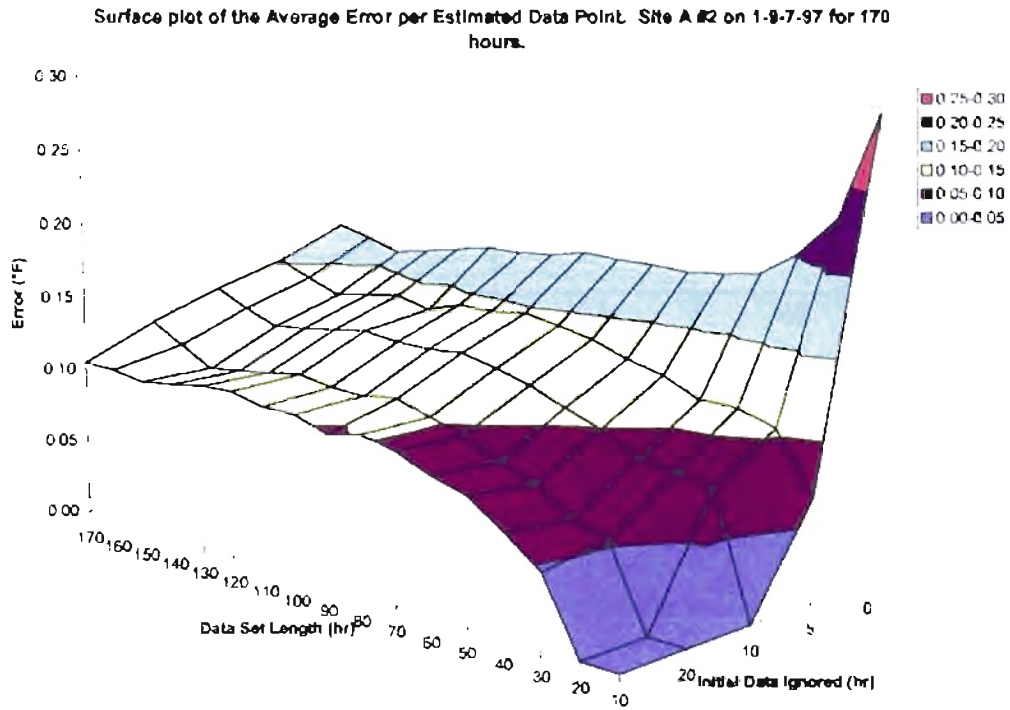
Figure 5-15. 3-D Surface Error Plot of Different Ground Thermal Conductivity Predictions

For cases shown in this section, the test length of the experiment will be estimated from the data sets that are at least 100 hours in total length. The sets are: Site A # 2 on 1-9-97 and 5-28-97 and Site A # 3 on 2-27-97. The final ground conductivity estimated for each data set will be averaged for 0 and 12 hours of initial data ignored. Then that average value will be treated as the most "true" value of the ground conductivity. Then, the length of test required to estimate the ground conductivity within 2% (the "98%" time) and 5% (the "95%" time) will be determined. These results are presented in Table 5-6.

Table 5-6. Estimation for Testing Length for the Estimation Period; Ignoring 12 Hours of Initial Data

Location and Date	"True" k_{soil} (Btu/hr-ft-°F)	98% Time (hours)	95% Time (hours)
Site A # 2 on 1-9-97	1.37	62	20
Site A # 3 on 2-27-97	1.52	73	42
Site A # 2 on 5-28-97	1.23	73	48

With the aid of Figures 5-8, 5-10, and 5-11, Table 5-6 can be explained in detail. By determining the final value for the each of the 100+ hour data sets, the estimation period for the length of test can be extrapolated depending on the number of data hours one would choose to ignore. Using the 12-hour-initial-data–hours- ignored estimation plot lines, the estimation time periods can be extrapolated from each figure. These results for the 2% and 5% are shown in columns 2 and 3 of Table 5-6. So, for the one variable estimation approach, the conductivity value and length of test can be 98% accurate with approximately 72 hours of data collection by ignoring the first 12 hours of the estimation period.

5.6.2. Sensitivity to Far-Field Temperature

The sensitivity of the numerical model to the assumed* ground far-field temperature can be seen in Figure 5-16. For one particular experimental data set, three different far-field temperatures were used as input parameters. One variable was estimated with spacing between the pipe legs set at 0.053 ft for all three cases. The

---

* The far-field temperature is estimated by reading the lowest temperature reading on the T_{in} display when the borehole is purged as described in Section 2.3.6.

numerical model is very sensitive to the ground far-field temperature. Even a 1.0°F difference yields significantly different thermal conductivity predictions.
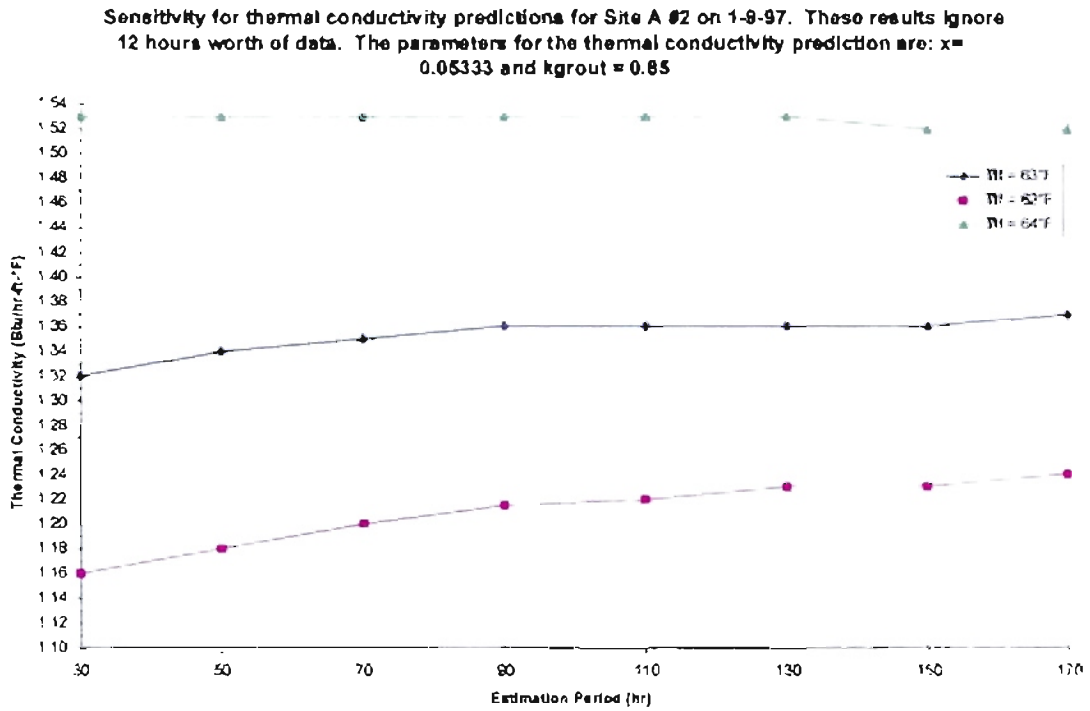

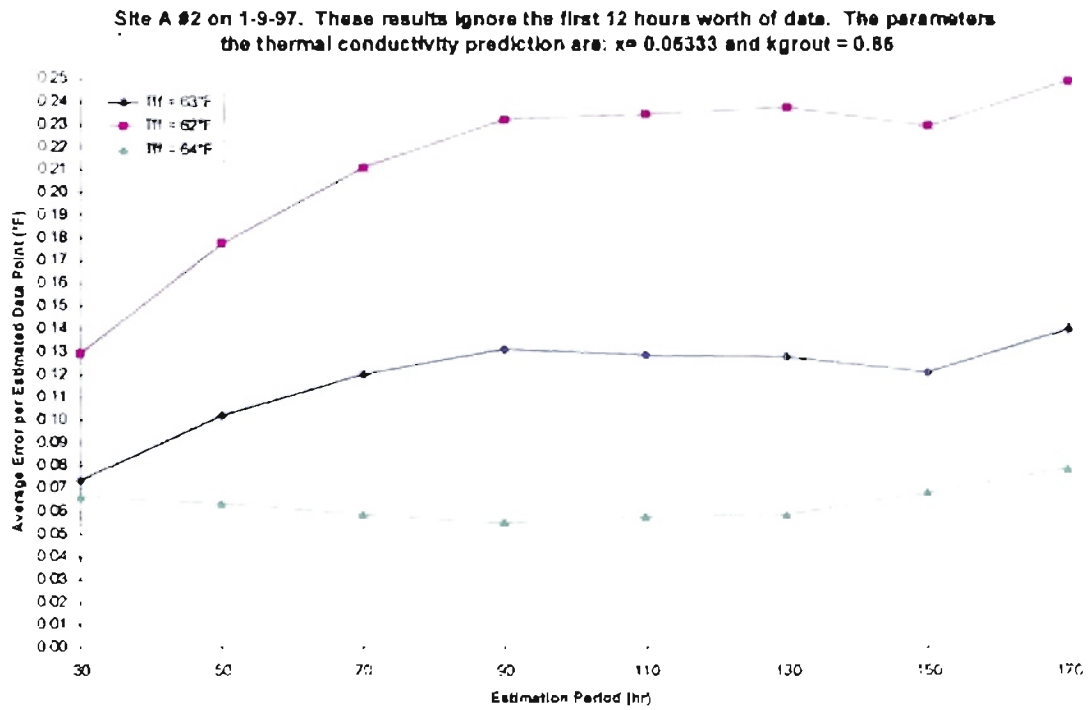Figure 5-16. Thermal Conductivity Estimations

Figure 5-17. Average Error Estimations

The errors between all three thermal conductivity predictions are also different and can be seen in Figure 5-17. These two figures indicate a very systematic and fairly accurate means of obtaining the ground far-field temperature is required.

5.6.3. Sensitivity to the Grout Thermal Conductivity

Another issue for estimation of a single parameter, ground conductivity, is the sensitivity of the prediction to the value of the grout conductivity. Using the same experimental data set of the previous section, three different values of grout conductivity were used. The resulting predictions for ground conductivities can be seen in Figure 5-18. The error associated with each grout thermal conductivity value can be seen in Figure 5-19. From the results shown in Figure 5-18, it can be seen that the model is sensitive to the grout thermal conductivity, but that the lowest error of Figure 5-19 is associated with the known grout used on that particular borehole. If a significantly wrong grout thermal conductivity value were to be used, the ground thermal conductivity could be quite wrong. (Note, that this would probably only happen if totally different grout types were used, e.g. thermally enhanced grout instead of Bentonite grout. Uncertainties in the value of thermal conductivity for a known grout type are likely to be comparatively small.)
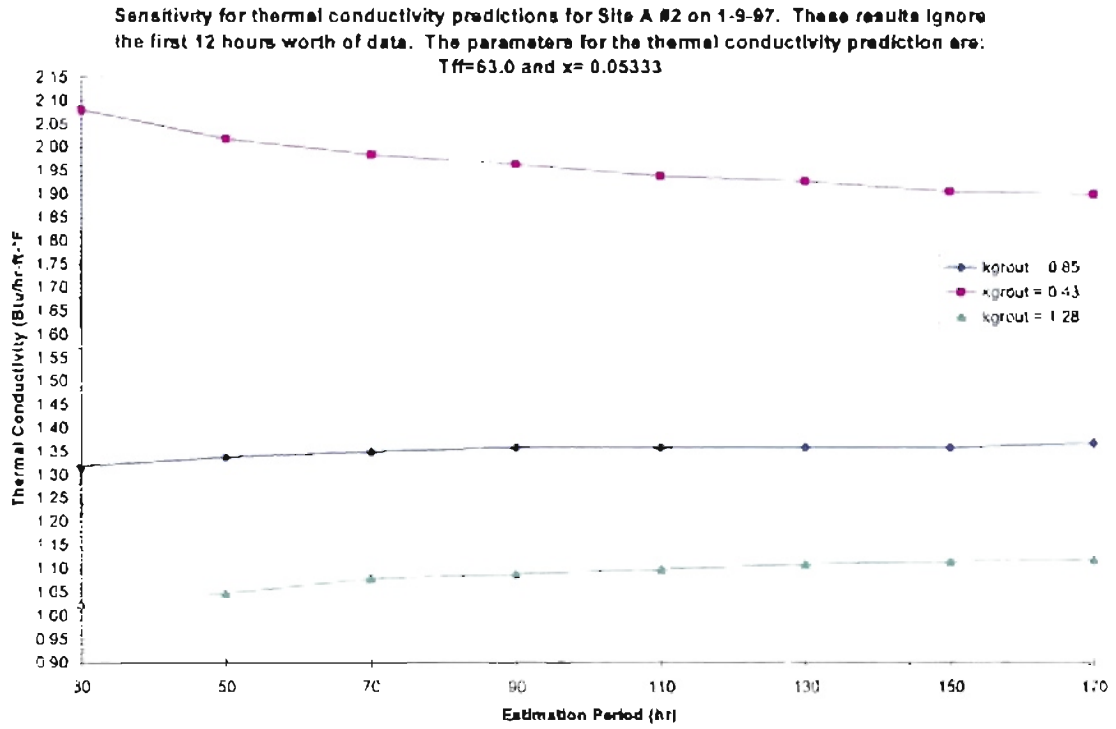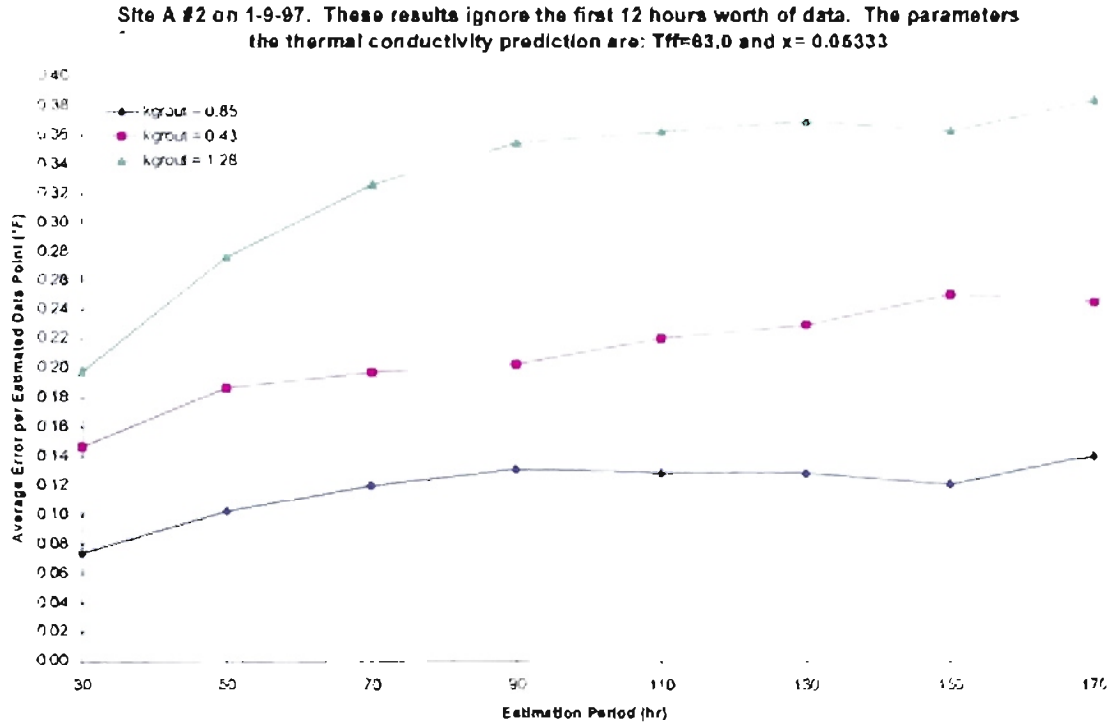
Figure 5-18. Thermal Conductivity Estimations

Figure 5-19. Average Error Estimations

5.6.4. Sensitivity to Volumetric Specific Heat

Since the thermal diffusivity is a ratio of the thermal conductivity and volumetric specific heat, it is difficult to estimate the parameters simultaneously because there are different numerator and denominator combinations that can result in the same diffusivity value. In order to illustrate the point, three separate volumetric specific heat values were varied with a single estimation variable (k_{soil}). Values of ρc_p reported in EPRI (1991) and GLHEPRO (Spitler. et al. 1996) for all soil and rock types range from about 18 to 40 Btu/ft³-°F. The results are shown in Figure 5-20. The different conductivity predictions are approximately 30% apart. The errors associated with the estimations also vary from approximately 0.17°F to 0.40°F, as seen in Figure 5-21. Because of the independence between k_{soil} and ρc_p, this difference in predicted soil conductivities is not as significant as it might seem.
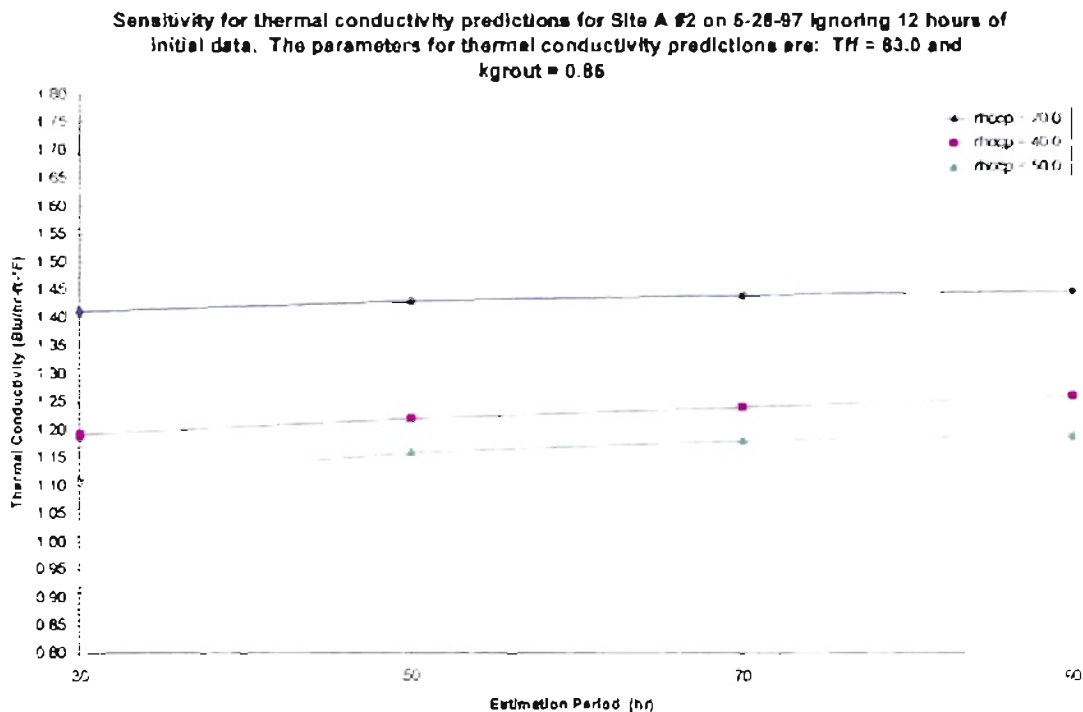
Figure 5-20. Conductivity Estimation for Different Volumetric Specific Heat Values

104

Figure 5-21. Average Error Estimations

Figure 5-22. GLHEPRO Main Input Screen

To illustrate the point, each ground conductivity and coupled volumetric specific heat were used as input values in GLHEPRO. The same daycare center used in Chapter 1 is used in this example. There are 12 boreholes spaced in a rectangle configuration. The

GLHEPRO input file can be seen in Figure 5-22 with the load-input file shown in Figure 5-23. Table 5-7 contains the results of the borehole sizing option of GLHEPRO.

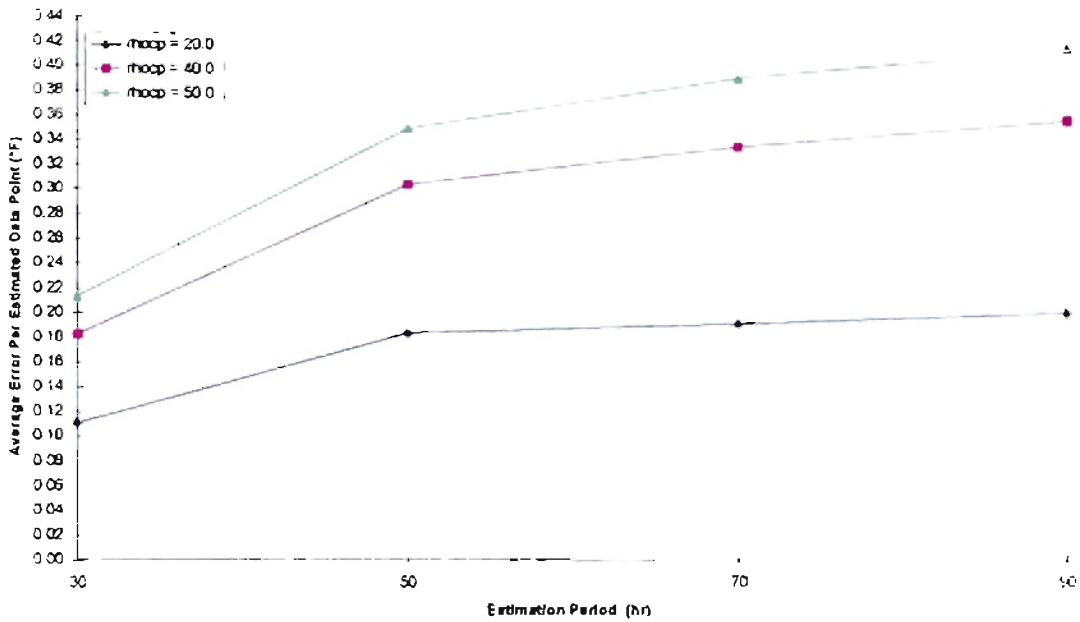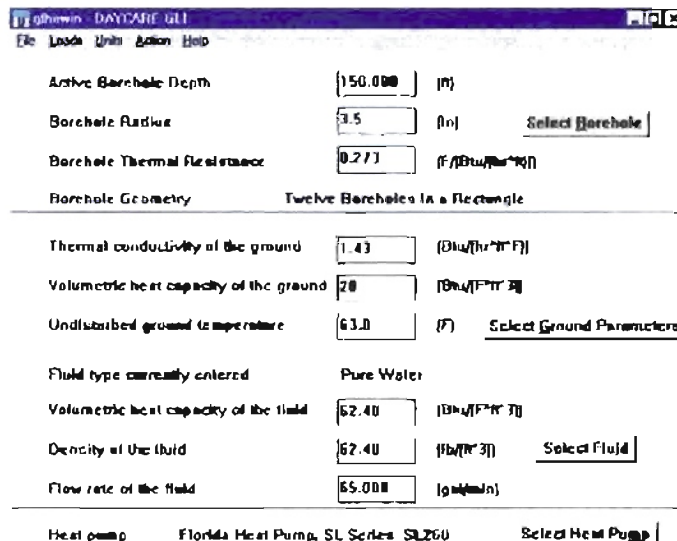| Month	Total Heating 1000 Btu	Total Cooling 1000 Btu	Peak Heating 1000 Btu/hr	Peak Cooling 1000 Btu/hr
January	29940.00	725.20	166.50	62.30
February	23910.00	358.60	166.70	49.59
March	17920.00	1769.00	138.70	106.50
April	8233.00	4617.00	81.37	176.30
May	1386.00	13990.00	40.33	267.10
June	364.50	29130.00	36.51	270.90
July	25.35	38870.00	19.43	299.80
August	11.14	42700.00	3.03	309.40
September	874.30	18570.00	37.60	268.50
October	5782.00	11080.00	78.30	227.30
November	19540.00	374.80	105.30	34.04
December	25250.00	495.40	152.20	72.19

Number of Peak Heating hours 8.00

Number of Peak Cooling hours 8.00

OK   Cancel

Figure 5-23. GLHEPRO Load Input File

Table 5-7. GLHEPRO Results for $k/\rho c_p$ Combinations

Volumetric Specific Heat (Btu/ft³-°F)	Averaged k_{soil} (Btu/hr-ft-°F)	Flow Rate (gpm)	Borehole Length (ft)
20	1.43	65	3369.56
40	1.23	65	3082.46
50	1.16	65	2964.00

The borehole lengths in Table 5-7 are within 9% of each other. It may have appeared that the differences in conductivity predictions were significant, but the impact on the ground loop heat exchanger design is relatively minor.

5.6.5. Sensitivity to Shank Spacing

The sensitivity of the ground thermal conductivity predictions to the shank spacing or the inside distance between the two pipes from pipe outer wall to pipe outer wall is presented in this section. Since it is difficult in practice to control the shank spacing, this parameter was varied to examine the sensitivity. This was due in part to the fact that once the U-tube is installed into the borehole, no one really knows what happens. It is possible that the U-tube twists and straightens the entire length, or the U-tube is not exactly in the middle of the borehole but located more on one side of the borehole than the other. For this reason, several experimental data sets were used to present the results of the numerical model sensitivity to the shank spacing.

Figure 5-24 is a ground thermal conductivity plot using two different shank spacing values ignoring 12 hours of initial data for Site A # 3 taken on 2-27-97. The figure displays about a 9% variation in the ground thermal conductivity predictions for two shank spacing values. The next step is to understand the errors associated with these predictions. The errors for each case can be seen in Figure 5-25.
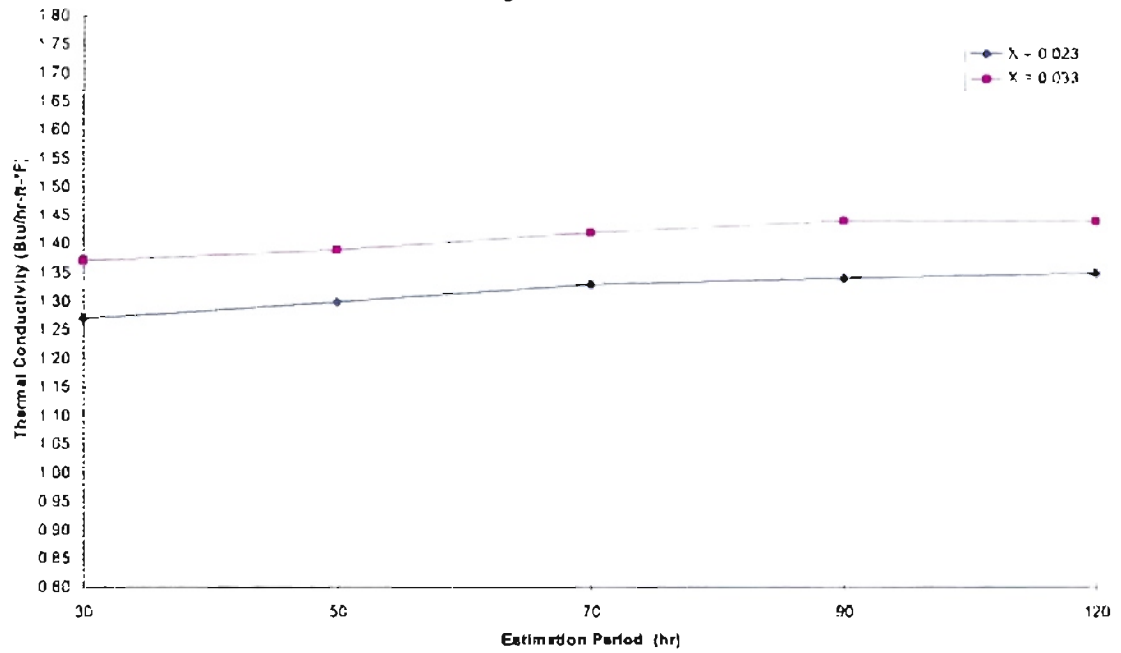
Figure 5-24. Thermal Conductivity Estimations

Figure 5-25 implies that the actual shank spacing for Site A # 3 on 2-27-97 is

closer to the x = 0.033 ft distance because the errors are much lower than those of a

shank spacing for x = 0.023.
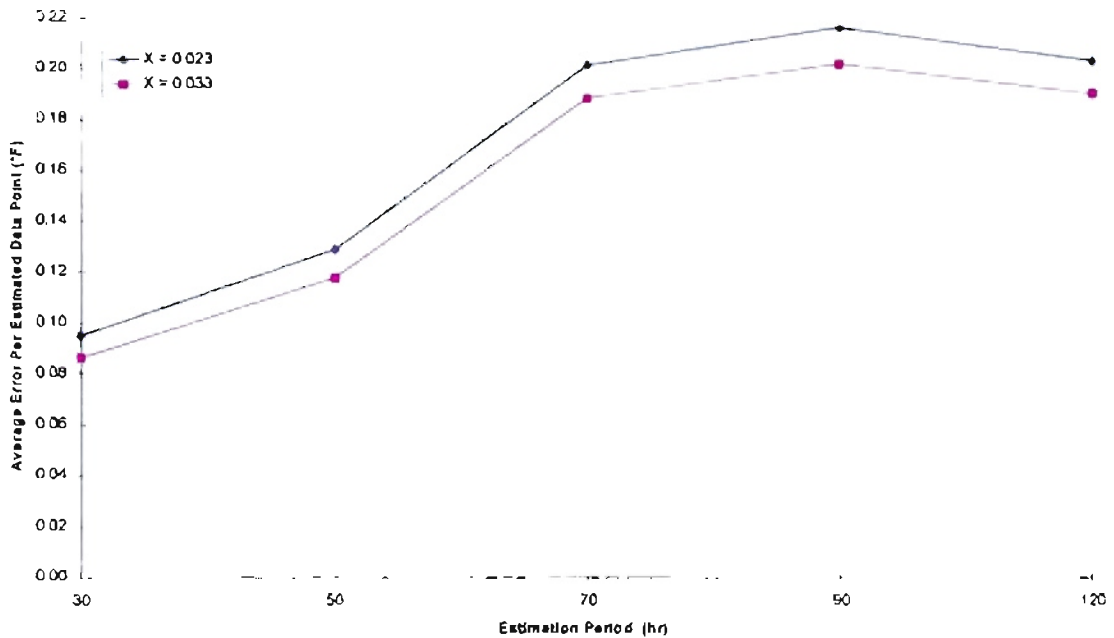
Figure 5-25. Average Error Estimations

Figure 5-26 and 5-27 are results from another data set collected at Site A #2 on 1-9-97.

In this case, three different shank spacing values were used. The different shank spacing

values estimated ground conductivity values ranging from 1.26 Btu/hr-ft-°F to 1.49

Btu/hr-ft-°F. The estimated ground conductivity values differ by 18%. The errors

associated with each shank spacing value's estimated ground conductivity can be seen in

Figure 5-26. As shown in Figure 5-27 the error for the largest shank spacing is

significantly different from the other two shank spacing estimations. Again it can be

stated that the small shank spacing predicts the best ground thermal conductivity based

on the estimation error, but it is clear the shank spacing sensitivity is important in the

parameter estimation method.
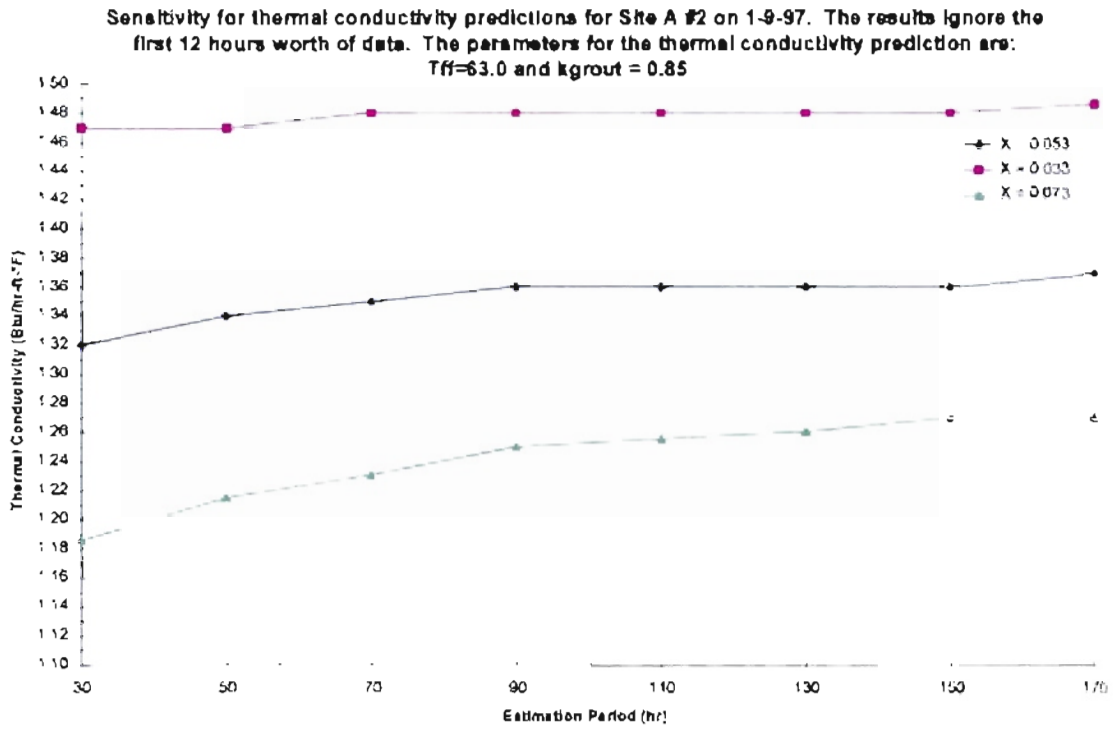
Figure 5-26 Thermal Conductivity Estimations

Figure 5-27. Average Error Estimations

110

In the results of Chickasha on 9-30-97, the same shank spacing sensitivity

characteristics described in the last paragraph are shown in Figures 5-28and 5-29. When

Figures 5-28 and 5-29 are viewed at the same time, it is interesting to note two

completely different ground thermal conductivity predictions yield approximately the
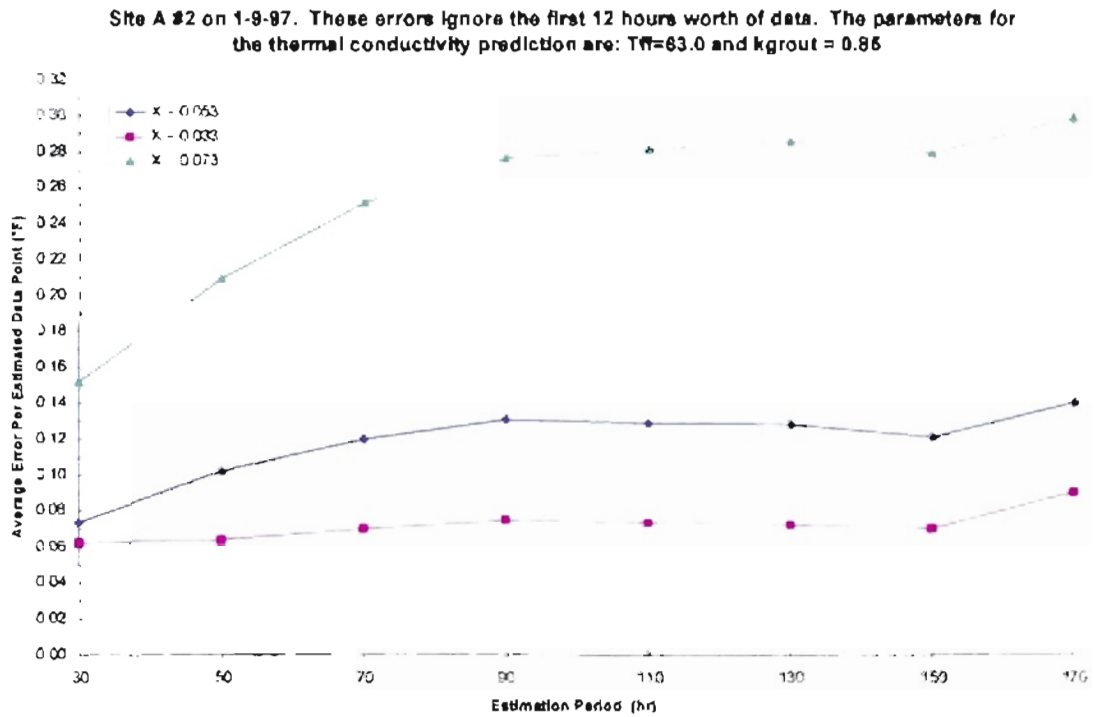
same error.
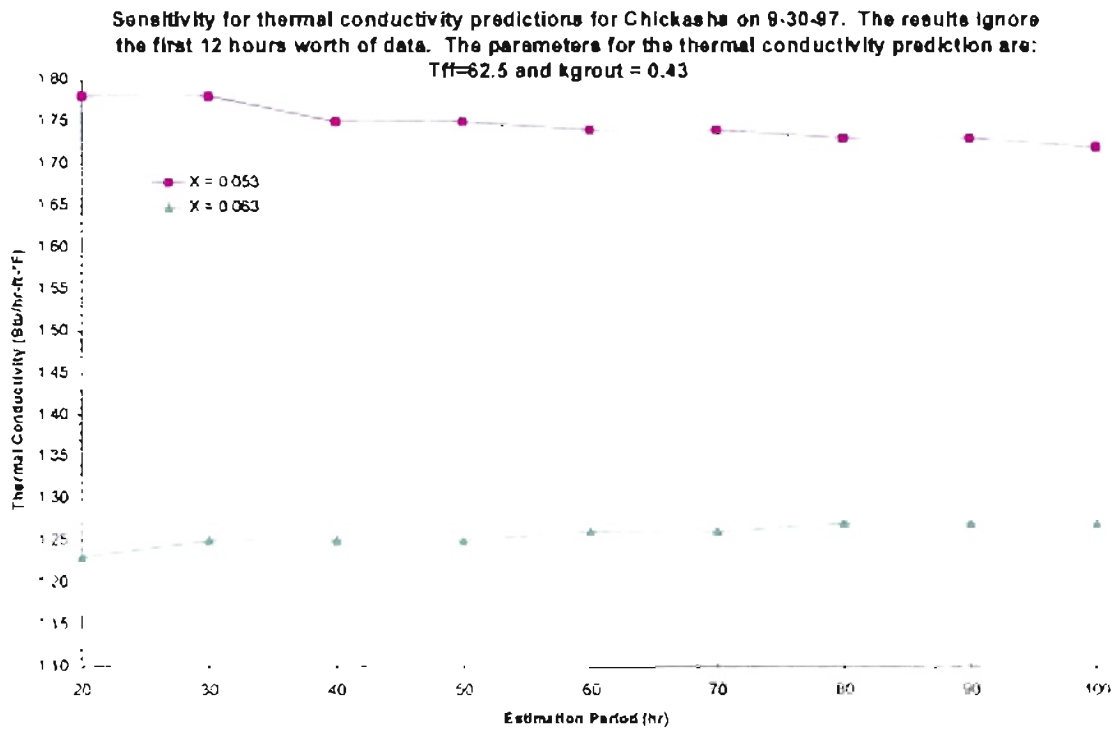
Figure 5-28. Thermal Conductivity Estimations
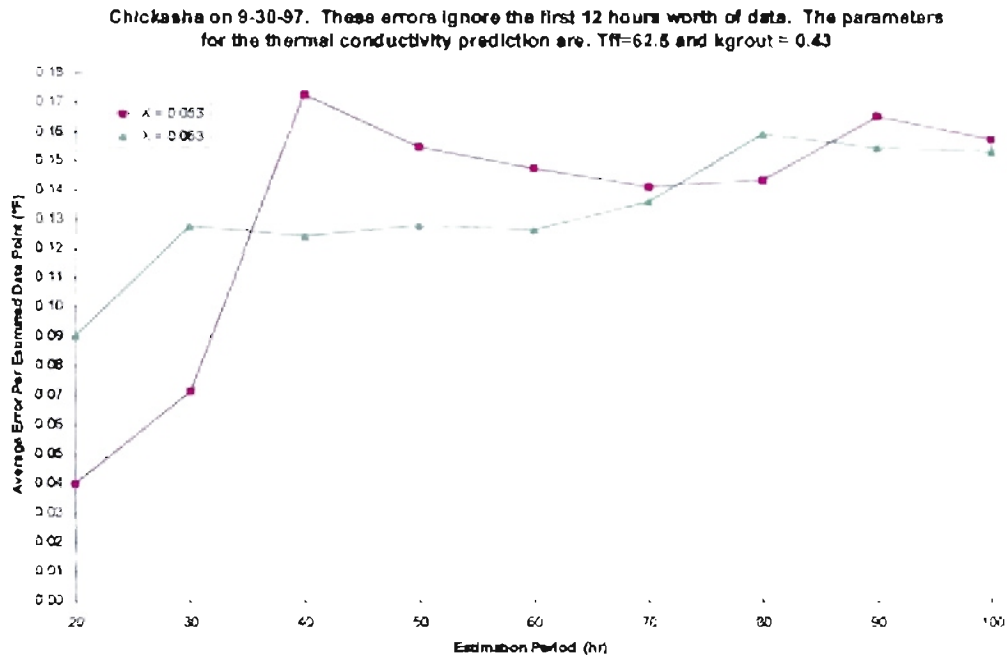
Figure 5-29. Average Error Estimations

It is evident as shown in these last four data sets, that the shank spacing is very
important to the estimation procedure and that any slight alteration could yield as much
as a 40% change in ground conductivity estimation for a single experimental test.
Looking again at Site A #1 and #2, these two boreholes should have nearly the same
actual ground thermal conductivity, but as stated earlier, a smaller ground conductivity
estimation is made for the same shank spacing in the previous data set. In the data set of
Site A #2 on 1-9-97, a k_{soil} value estimated was 1.49 Btu/hr-ft-°F, but in this data set a
k_{soil} value is estimated to be 1.25 Btu/hr-ft-°F. This discrepancy can be attributed to the
fact that these two boreholes use different grout types and the current single parameter
estimation in not enough to make proper adjustments for some the parameters that can
vary. One simple approach would be to estimate a second variable simultaneously that
could possibly account for things such as the shank spacing and the grout thermal
properties.

112

5.7.   *Parameter Estimation with Two Independent Variables*

As stated at the beginning of the chapter, estimation of only one variable cannot adequately account for uncertainties in the tube placement, grout conductivity, etc. A two variable parameter estimation will be presented in this section. The ground thermal conductivity will still be one of the estimated variables, but the second variable estimated will be the grout conductivity. The grout conductivity was chosen because it is believed that its estimation will account for both grout conductivity and the sensitive shank spacing.

5.7.1.   *Two Variable Optimization k_{soil} and k_{grout} using one shank spacing*

The results in this section begin with the Chickasha data set. The two variable estimation results can be seen in Figure 5-30. The ground thermal conductivity value estimated for this data set is about 1.60 Btu/hr-ft-°F ignoring the first 12 hours of data. The estimate value of k_{soil} is 5% less than that predicted with the single variable approach, but the estimated grout conductivity is significantly different from the known grout. The most likely explanation for this is that the estimated grout thermal conductivity has been adjusted by parameter estimation for the shank spacing (x = 0.033ft). In Figure 5-31, the error for this data set remains nearly steady at 0.1°F per data point. This is significantly lower than the error in the single variable estimation. Although the shank spacing and grout conductivity may be incorrect in value, the low

error indicates that both parameters can be reasonably accounted for by allowing the

grout conductivity to be varied.

Predicted Thermal Conductivity values for Chickasha on 9-26-97. These results are determined by estimating two parameters, ksoil and kgrout. This plot ignores 12 hrs worth initial data.
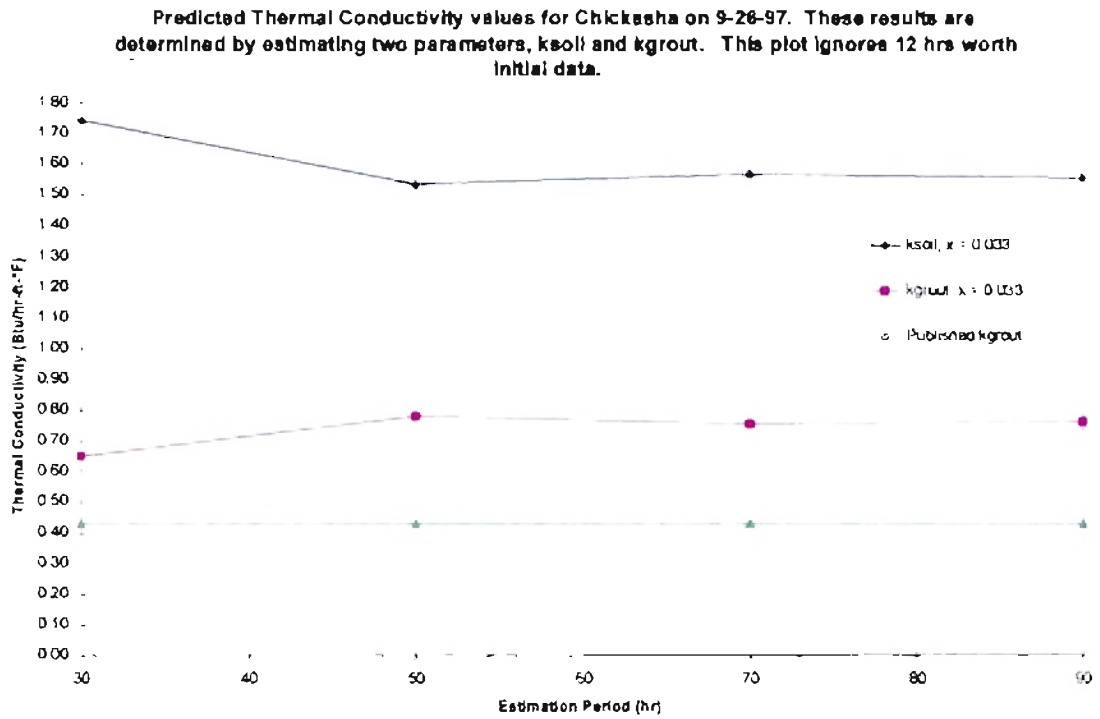
Figure 5-30. Thermal Conductivity Estimations
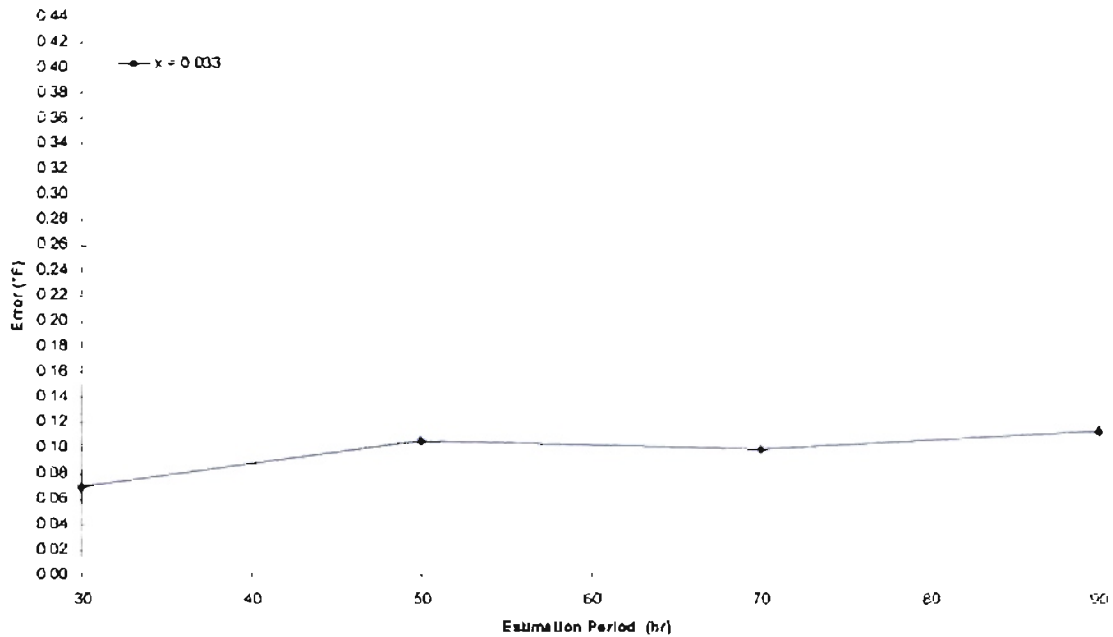
Figure 5-31. Average Error Estimations

Another data set is presented in Figure 5-32 from Site A #1 on 1-6-97. In this case a better estimate for the shank spacing was used. For this reason a better estimate for the grout conductivity is made. In fact after 50 hours of data, the grout conductivity is nearly at the published conductivity value. Again, we see the error for this estimation data set; the error is about 0.1°F per data point shown in Figure 5-33.

In the two cases shown so far, both parameter estimation values for the conductivities have had some initial time before the estimated value "leveled" off. The noticeable trend, seen in Figure 5-32 and 5-30, is possibly further indication the minimum time is not less than 45-48 hours of testing, even estimating two parameters simultaneously.

Figure 5-32. Thermal Conductivity Estimations

Error for Site A #1 on 1-6-97. These error ignore the first 12 hours worth of data.
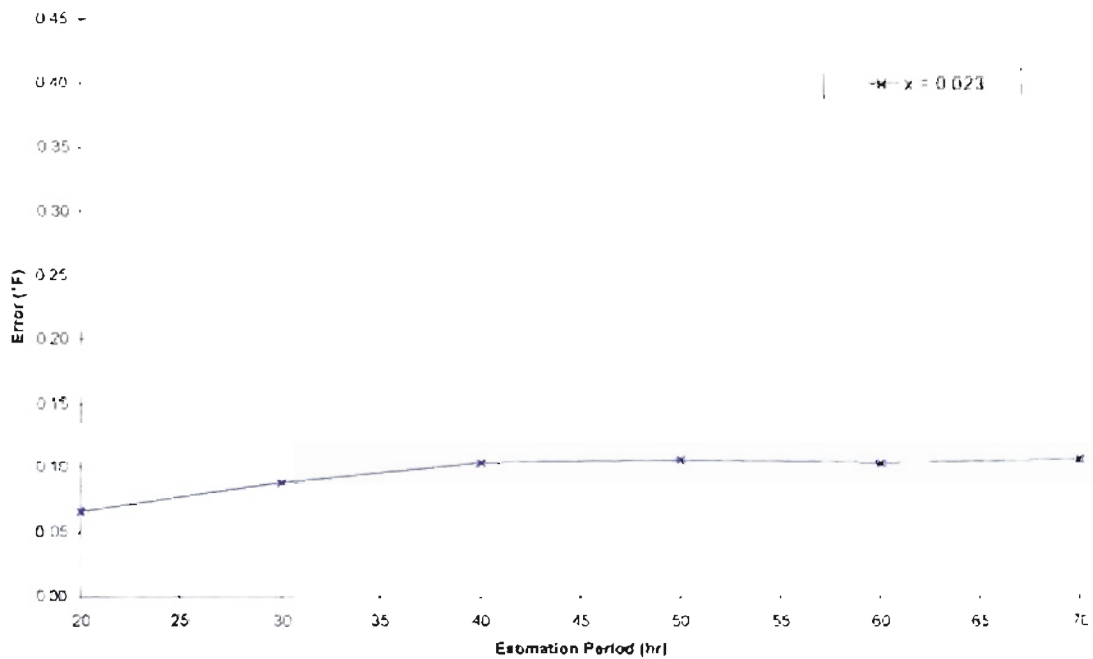
Figure 5-33. Average Error Estimations

116
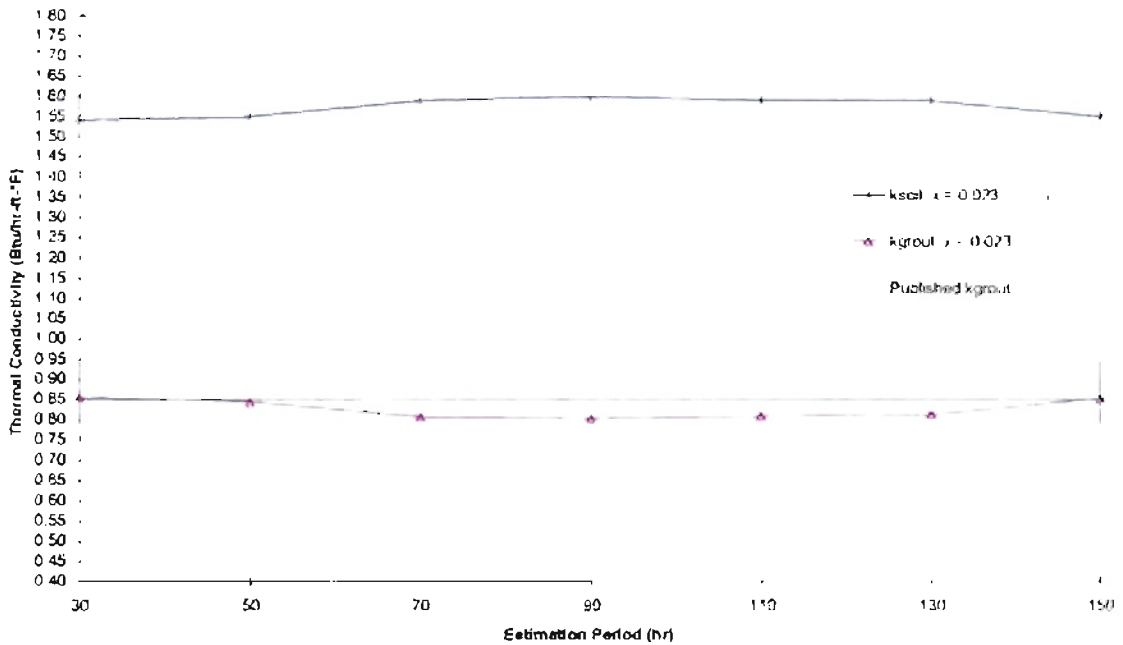
Figure 5-34. Thermal Conductivity Estimations

In our last case presented in this section, Site A #2 on 1-9-97 is the data set used.

The parameter estimation for this data set was able to predict nearly the same ground

conductivity and grout conductivity as that of Site A #1 on 1-6-97. Figure 5-34

indicates the same start up trend as the previous two data sets in this section, but it is

about 50 hours longer in estimation period. Although this data set was over 150 hours,

it provides the insight that after that period the estimated conductivity doesn't change

too much. The error for this plot can be seen in Figure 5-35. For this data set, the error

is about 0.06°F per data point.
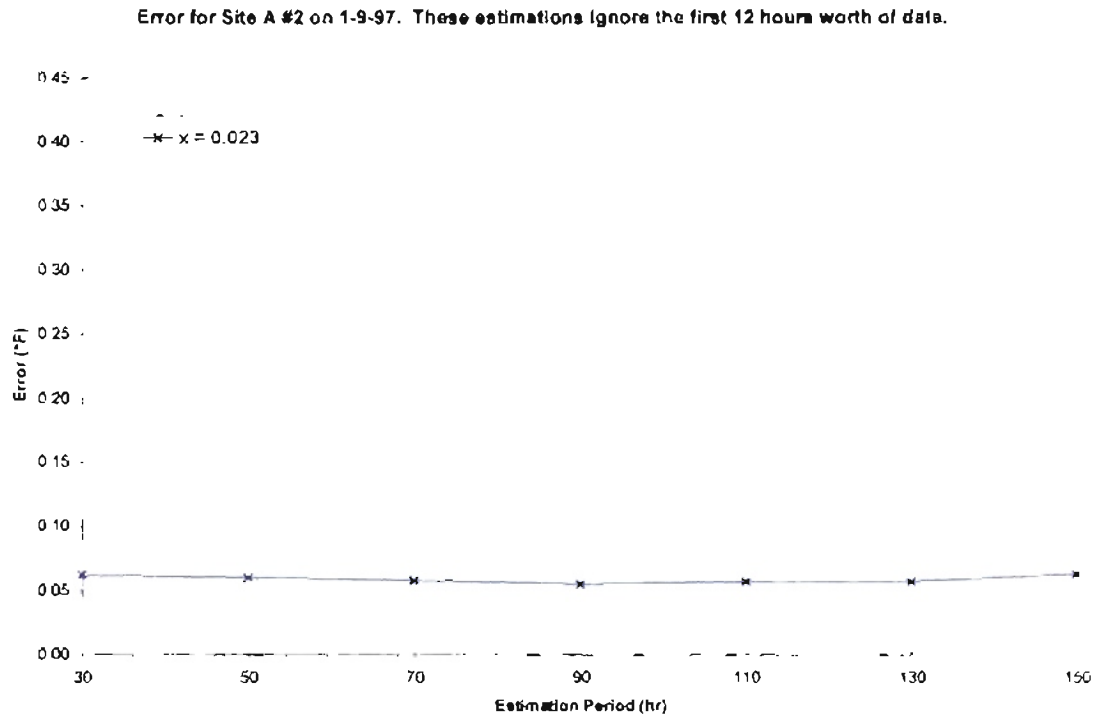
Figure 5-35. Average Error Estimations

5.7.2. Two Variable Optimization k_{soil} and k_{grout} comparing two or more shank spacing values

Now that the results from two variable optimization with one assumed shank spacing results have been presented, this section will present results using different shank spacing values for estimating two variables. In this section two cases are presented. The two cases presented in this section are Site A #1 on 6-2-97 and Site A #2 on 5-28-97.

The first results presented are from Site A #1 on 6-2-97 and are shown in Figure 5-36 and 5-37. Five different shank spacing values were used in the two variable estimation approach. All five shank spacing values estimated a ground thermal conductivity to be nearly the same value of 1.47 Btu/hr-ft-°F. The predicted grout conductivity, however, was different for each shank spacing value. The larger the shank spacing value, the worse the grout estimation compared to the known published value.

118
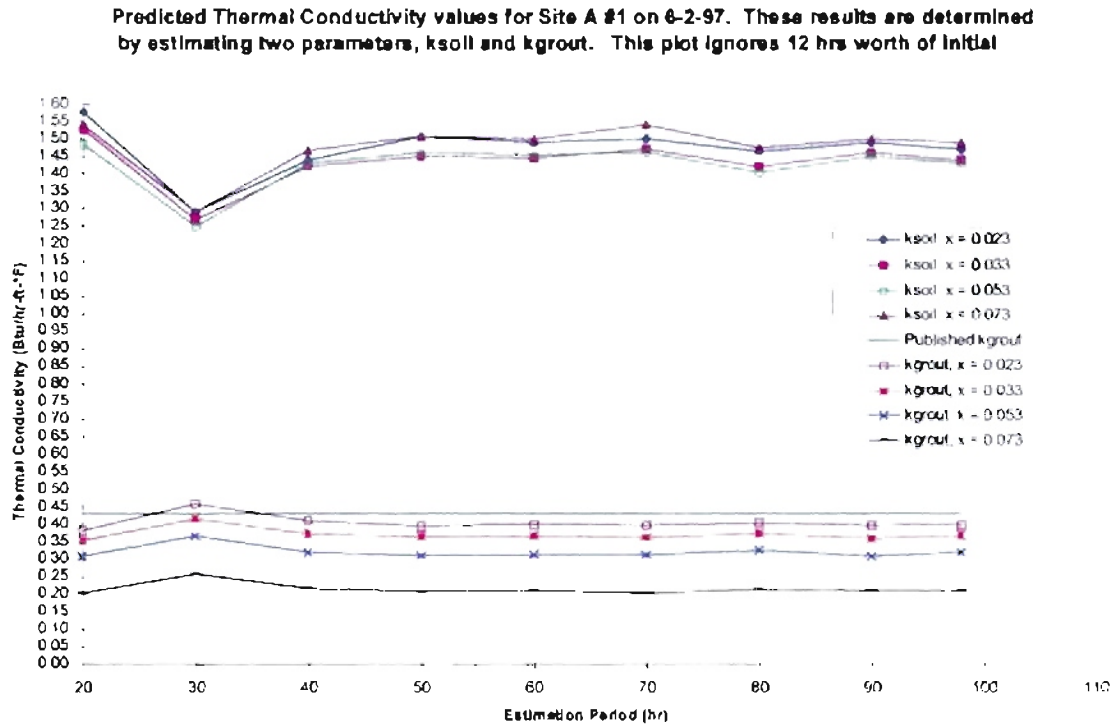
Figure 5-36. Thermal Conductivity Estimations

Interestingly though, they all have an estimation error that lay on top of each other.
The error is about 0.13°F per data point. This is a further indication that allowing the
grout conductivity to be varied (and estimated), nearly the same ground conductivity can
be predicted.

Another case is Site A #2 on 5-28-97. In this case on two shank spacing values
were chosen, but the results are about the same. Figure 5-38 depicts the thermal
conductivity estimations. The ground conductivity estimations are a little different but
only by 1%. This data set did estimate a higher conductivity than the results presented in
the previous two figures. The results of the ground conductivity predictions are an
increase of about 15% of the results of Site A #1 on 6-2-97. However, the error for this
data set is much lower as shown in Figure 5-39. The estimation error is 0.09°F per data

119

point. In this data set, the two shank spacing values estimation errors lay on top of one another as in the case previously presented.

Both data sets indicate that the estimated grout conductivity compensates for different assumed shank spacing. This gives us increased confidence that uncertainties in how the U-tube is placed in the borehole can be accounted for with the grout conductivity.

Error for Site A #1 on 6-2-97. These error Ignore the first 12 hours worth of data.
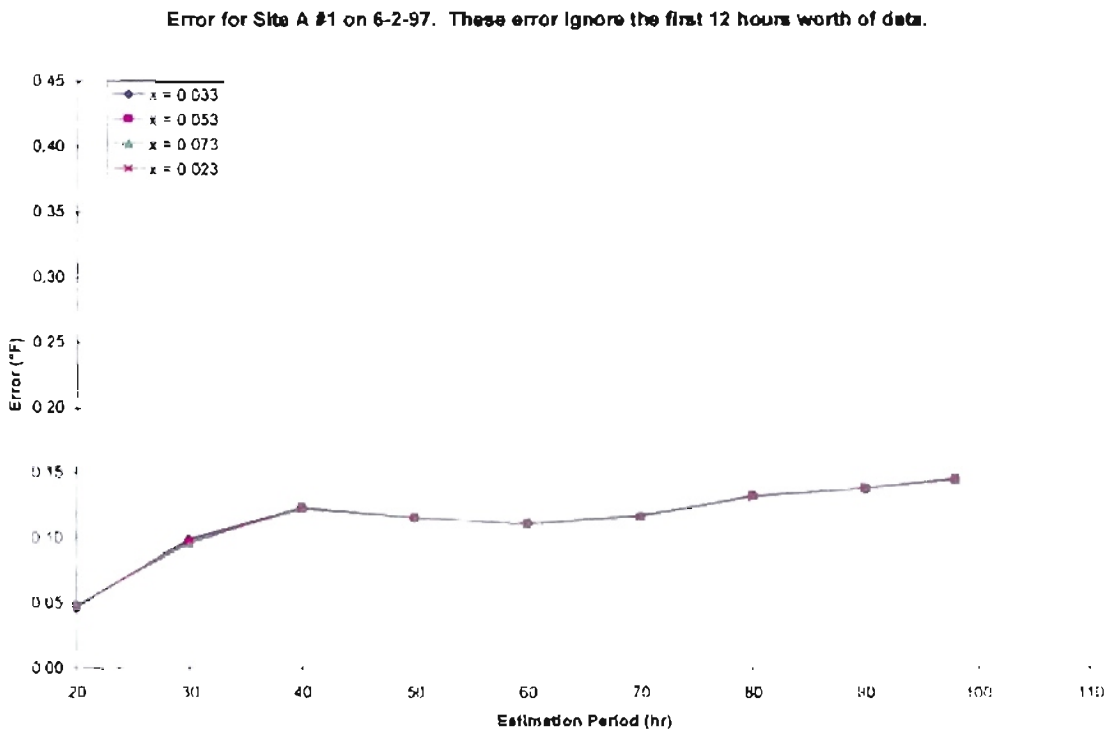
Figure 5-37. Average Error Estimations

Predicted Thermal Conductivity values for Site A #2 on 5-28-97. These results are determined by estimating two parameters, ksoil and kgrout. This plot ignores 12 hrs worth Initial data.
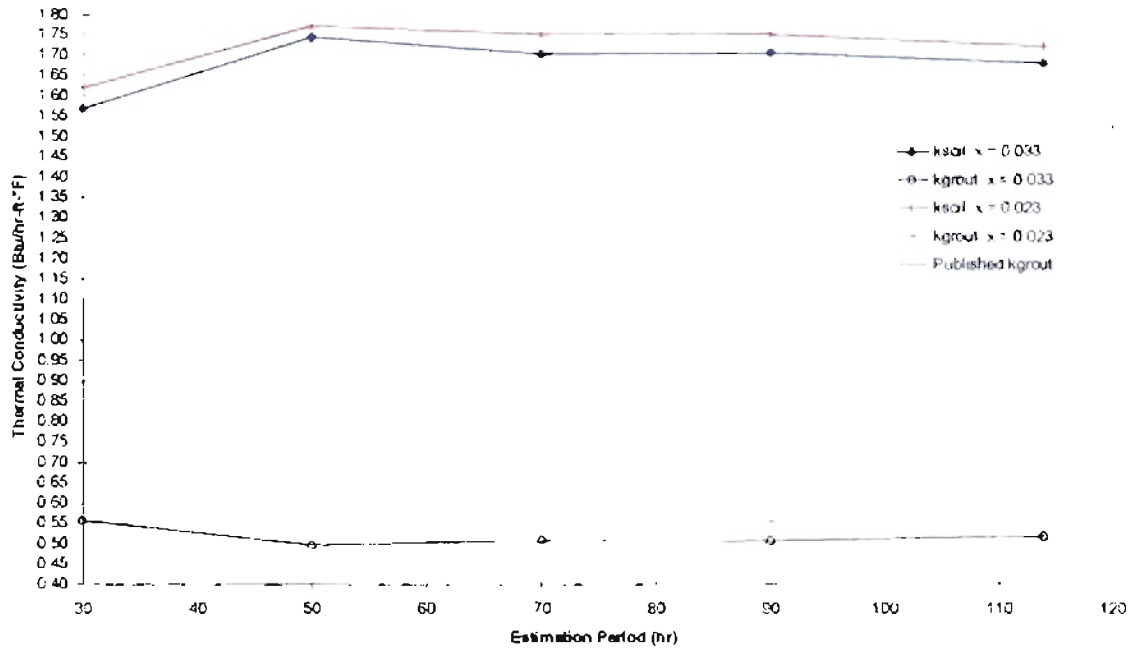
Figure 5-38. Thermal Conductivity Estimations

Error for Site A #2 on 5-28-97. This estimation ignore the first 12 hours worth of data.
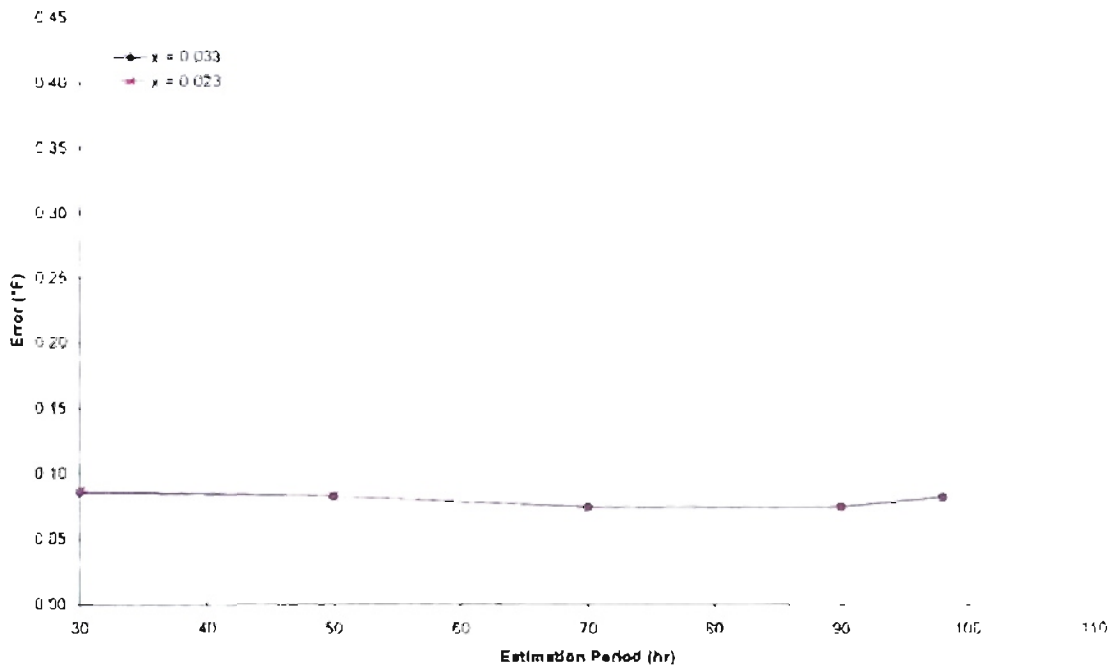
Figure 5-39. Average Error Estimations

121

5.7.3. Two Variable Optimization for Different Times of Year

Another question that should be addressed is how sensitive are the results to the time of year. The temperature profile of the ground, especially near the surface changes throughout the year. This section presents two borehole locations, Site A #1 and #2, each tested at different times of the year. The best shank spacing approximation is 0.023 ft and, therefore, used in the results of this section (The best shank spacing is the one that resulted in the estimated grout conductivity nearest to the published grout conductivity). The results in this section are also two variable estimations that ignore the first 12 hours of initial data.

Results presented in Figure 5-40 are the Site A #1 data sets. The time of the year does not seem to have a significant impact. Both data sets appear to have the same problem discussed earlier with estimating a ground conductivity value in the initial estimation period, but after the 45-50 hour time period, they are nearly the same. As can be seen in Figure 5-41, the error for each data set is essentially the same over the entire estimation period.

Site A #1 Comparison of two tests performed. Test 1 was performed on 1-6-97 and test 2 was performed on 6-2-97. This comparison ignores the first 12 hours of initial data.
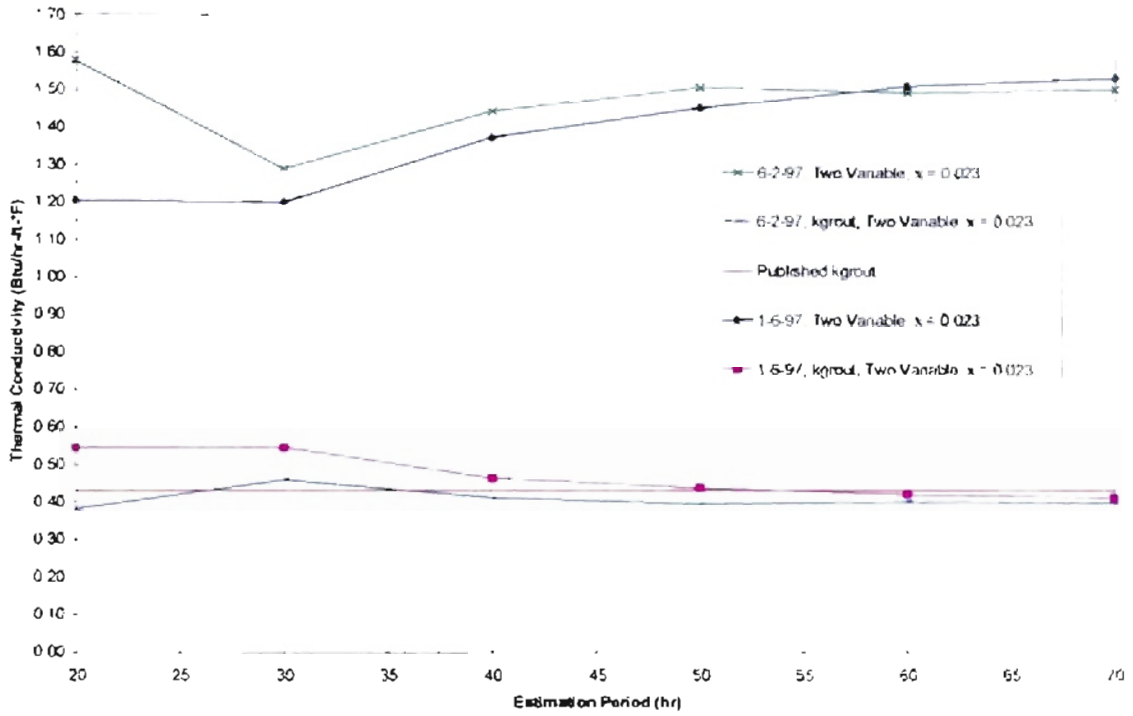
Figure 5-40. Thermal Conductivity Estimations

This plot is the average error of Site A #1 for two different tests. The first test was performed on 1-6-97 and the second test was performed on 6-2-97. This comparison ignores the first 12 hours of initial data.
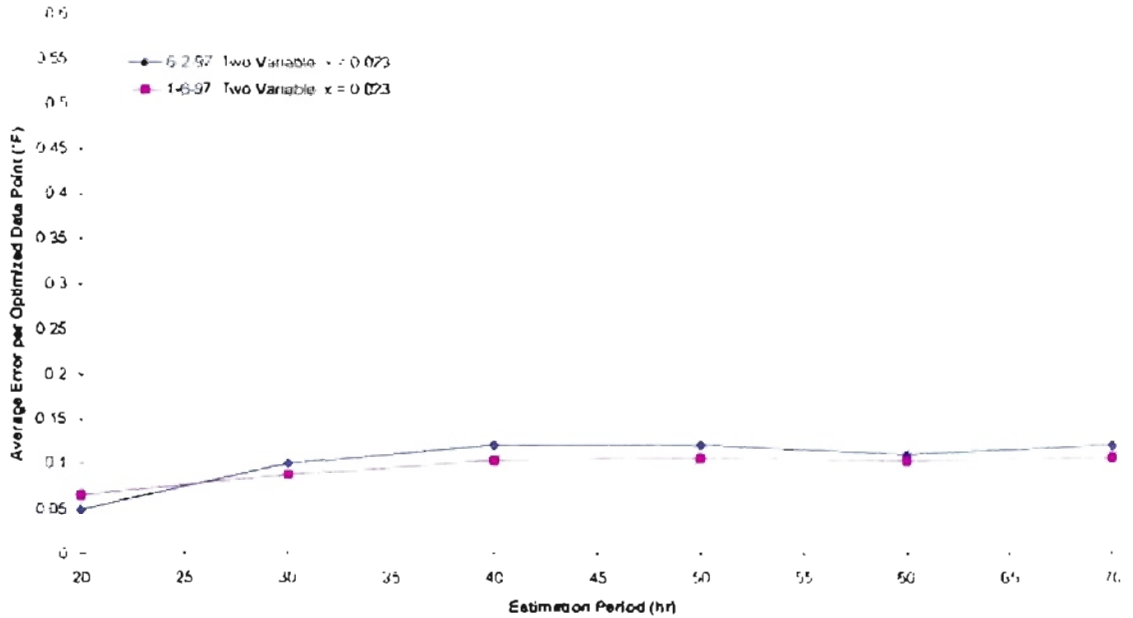
Figure 5-41. Average Error Estimations

123

The second case to present is Site A #2 tested on 1-9-97 and 5-28-97 shown in Figure 5-42. These data sets estimate the ground conductivity to be different by about 10%.

Site A #2 Comparison of two tests performed. Test 1 was performed on 1-9-97 and test 2 was performed on 5-28-97. This comparison ignores the first 12 hours of initial data.
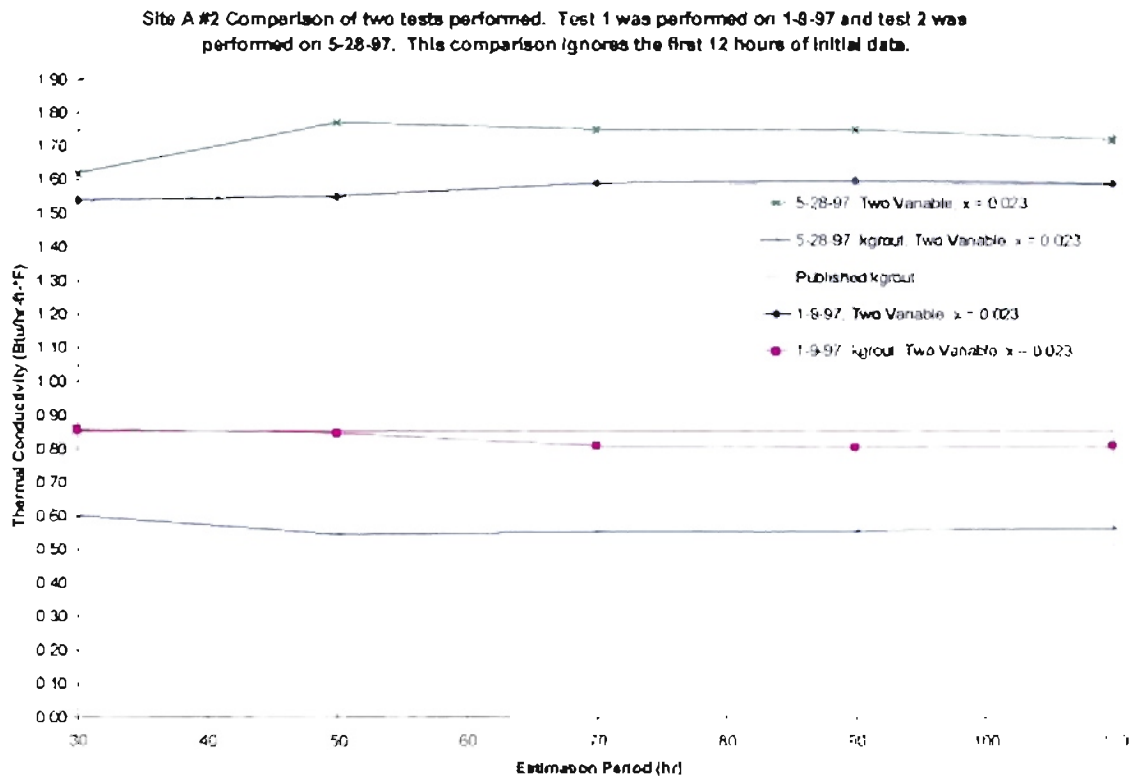
Figure 5-42. Thermal Conductivity Estimations

The errors for the two data sets are shown in Figure 5-43. One data set has an error of 0.06°F and is nearly constant. The data set taken on 5-28-97 has a higher error of about 0.08°F and changes slightly over time. It is difficult at this point in time to draw a conclusion as to which result is more accurate.

124
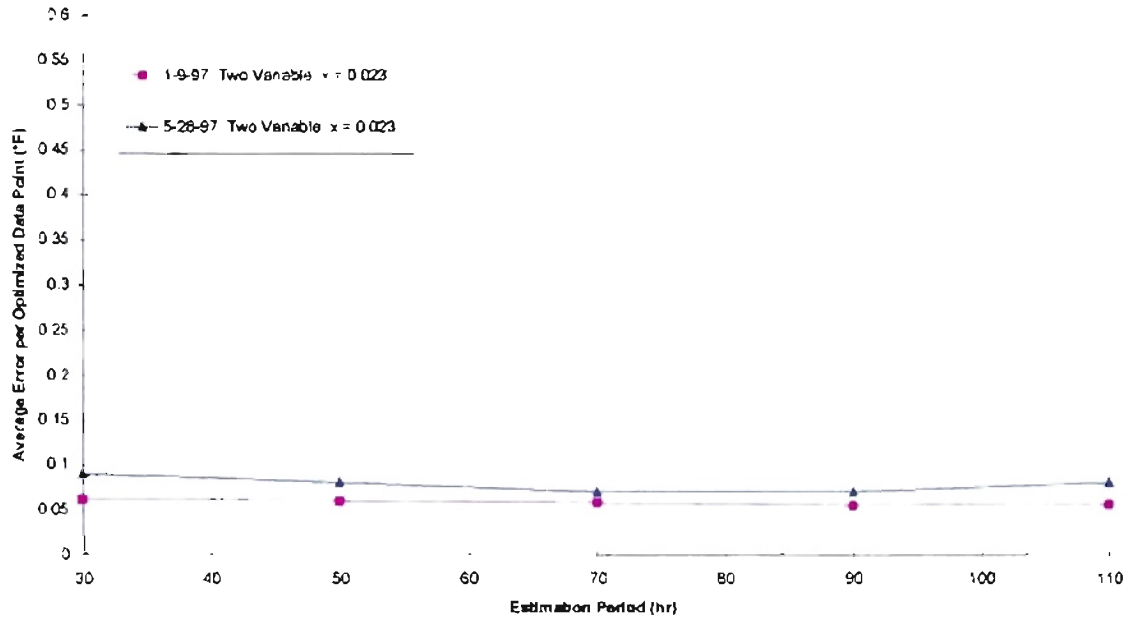
Figure 5-43. Average Error Estimations

5.7.4. Length of Test

The two variable estimation results are summarized in Table 5-8. These results are from one shank spacing value of 0.023 ft for Site A cases and 0.033 ft for the Chickasha case. All sets ignore the first 12 hours of estimation data. Using the two variable estimation approach, the question of how long to test is approximated by a percentage of the final ground conductivity value in each data set. If a ±2% estimation of the ground conductivity is sufficient. then for Site A #1 on 1-6-97 testing the borehole for approximately 50 hours would give results of 98% confidence in the ground conductivity value. If a ±5% confidence were desired. then for the same data set case.

125

45 hours of testing would be sufficient. The percentages with the associated time frame are also given in Table 5-8.

Table 5-8. Results of Two Variable Estimation with One Shank Spacing and Ignoring 12 Hours of Initial Data.

Location	Date of Test mm-dd-yy	k_{soil} (Btu/hr-ft-°F)	Length of Test (hr)	Time at ±2%(hr)	Time at ±5% (hr)
Site A # 1	01-06-97	1.50	72	50	45
Site A # 2	01-09-97	1.55	170	50	30[*]
Site A # 2	05-28-97	1.76	114	48	42
Site A # 1	06-02-97	1.50	98	45	38
Chickasha	09-26-97	1.55	99	50	30[*]

* It may be possible to extrapolate to an earlier time prior to the 30 hour estimation period, but it was not calculated before that 30 hour estimation value. Since no estimations were made with less than 30 hours of data, this was not estimated.

Overall, Table 5-8 suggests that for the time of year with different borehole configurations, the ground conductivity can be estimated within a 15% range of 1.50 to 1.76 Btu/hr-ft-°F.

5.7.5. Sensitivity of Two Variable Estimation to Volumetric Specific Heat

After presenting the results of single parameter estimations varying the volumetric specific heat, a two-parameter estimation is presented in this section for different volumetric specific heats. Three separate volumetric specific heat values were varied while estimating two parameters, k_{soil} and k_{grout}. Values of ρc_p reported in EPRI (1991) and GLHEPRO (Spitler, et al. 1996) for all soil and rock types range from about 18 to 40 Btu/ft^3-°F. The results from the two-parameter estimation are shown in Table

5-9. The different conductivity predictions are approximately 3.4% apart. The errors associated with the estimations do not vary; all three errors are 0.08°F (more digits would reveal a slight variation) as shown in Table 5-9. Because of the independence between k_{soil} and ρc_p, this difference in estimated soil conductivities is not as significant as it might seem.
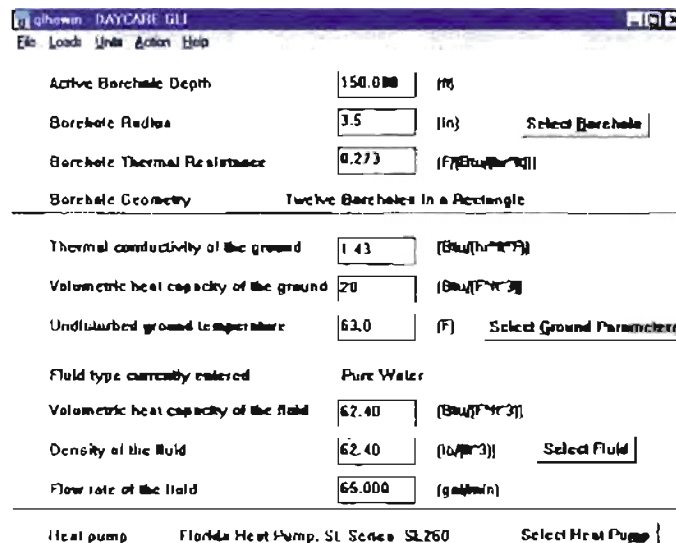
Figure 5-44. GLHEPRO Main Input Screen

Again, to illustrate the point, each estimated ground conductivity and grout conductivity (represented in the borehole resistance value), coupled with the varied volumetric specific heat were used as input values in GLHEPRO. The same daycare center used in Chapter 1 is used in this example. There are 12 boreholes spaced in a rectangular configuration. The GLHEPRO input file can be seen in Figure 5-44 with the load-input file shown in Figure 5-45. Table 5-9 contains the results of the borehole sizing option of GLHEPRO.

Figure 5-45. GLHEPRO Load Input File

Table 5-9. GLHEPRO Results for $k/\rho c_p$ Combinations.

Volumetric Specific Heat (Btu/ft^3-°F)	Estimated k_{soil} (Btu/hr-ft-°F)	Estimated k_{grout} (Btu/hr-ft-°F)	Flow Rate (gpm)	Borehole Length (ft)
20	1.80	0.61	65	3125.82
30	1.77	0.55	65	2967.42
40	1.74	0.53	65	2855.16

The borehole lengths in Table 5-9 are within 9.5% of each other. Note that the range 20-40 Btu/hr-ft-°F covers nearly the entire range of expected values. Using an intelligent estimate of ρc_p should allow the impact on the ground loop heat exchanger design to be relatively minor.

128

5.7.6. Sensitivity to Experimental Error

This section investigates the sensitivity of the results to experimental error. The experimental error of most concern is that associated with measurement of power. Three data sets were simulated with power increased artificially by 5%. Table 5-10 shows the resulting change in estimated thermal conductivity due to the artificial 5% power increase.

The mean error for each data set did not change with the power increase. However, the 5% increase in the power input yields roughly a 5% increase the estimated ground thermal conductivity. Additional anecdotal evidence suggests that a change in power resulted in a proportional change in estimated thermal conductivity. This highlights the need to carefully measure the power. The watt transducer is rated by the manufacturer as having an error of ±1% of the reading and ±0.5% of full scale, so the resulting effect on the thermal conductivity estimate is about ±1%.

Table 5-10. Sensitivity of Results to Power Increase

Location	Date of Test (mm-dd-yy)	k_{soil} (Btu/hr-ft-°F)	k_{grout} (Btu/hr-ft-°F)	Estimation Mean Error (°F)	% Change
Normal Power File					
Site A #1	6-2-97	1.51	0.39	0.12	
Site A #2	5-28-97	1.77	0.54	0.08	
Site A #3	2-27-97	1.60	0.70	0.04	
5% Power Increase					
Site A #1	6-2-97	1.57	0.43	0.12	4.0
Site A #2	5-28-97	1.85	0.58	0.08	4.5
Site A #3	2-27-97	1.69	0.76	0.04	5.6

5.8. Summary of Results- Two Parameter Results

This section contains results from every test performed with the final experimental configuration[*] that was over 50 hours in length at Site A in Stillwater, OK. Estimates of the ground conductivity based on the "best procedure" as recommended in section 5.7:

- Length of test: 50 hours (In this case, only the first 50 hours of the data set were used, regardless of the length of the test.)
- Initial data ignored: 12 hours
- Two parameters estimated: ground thermal conductivity and effective grout thermal conductivity.

Once each data set had been analyzed, the results were used to design a ground loop heat exchanger for the daycare facility described in Chapter 1. The first approach used the estimated ground thermal conductivity, but did not use the estimated effective grout thermal conductivity. The results for this approach are summarized in Table 5-11. As can be seen in Table 5-11, the highest predicted thermal conductivity value is about 22% higher than the lowest. When the conductivities are used in GLHEPRO, the highest resulting borehole length is 14.4% higher than the lowest. Still, a narrower spread between the predictions would be desirable.

Therefore, a second approach was used; one in which the estimated ground thermal conductivity was also used. (Because there is some trade-off between the effects of

---

[*] As discussed in Chapter 2, tests performed prior to January 1, 1997 did not have adequate insulation on the exposed piping. They are not included in this section, but a brief summary is made in Appendix C

borehole resistance and ground thermal conductivity, all other things being equal, tests with higher predicted ground thermal conductivity tend to have lower estimated grout thermal conductivity. Likewise, in the design process, there is a similar trade-off.) In order to make use of this information, the same grout, piping, borehole diameter, etc. should be used in the test borehole as will be used in the final installation. In the test boreholes at Site A, there were two substantially different configurations: holes #2 and #3 used thermally enhanced grout, while holes #1, #4, and #5 used standard Bentonite grout. The two groups of boreholes were analyzed separately.

Table 5-11. Results of Two Variable Estimation with One Shank Spacing and Ignoring 12 Hours of Initial Data of All Data Sets that have at Least 50 Hours of Data.

Location	Date of Test (mm-dd-yy)	k_{soil} (Btu/hr-ft-°F)	k_{grout} (Btu/hr-ft-°F)	Estimation Mean Error (°F)	Borehole Resistance (°F-hr-ft/Btu)	Borehole Length (ft)
Site A # 1	01-06-97	1.45	0.44	0.11	0.415	3081.47
Site A # 1	06-02-97	1.51	0.39	0.12	0.415	3035.98
Site A # 2	01-09-97	1.55	0.84	0.06	0.415	3010.66
Site A # 2	05-28-97	1.77	0.54	0.08	0.415	2844.26
Site A # 3	02-27-97	1.60	0.70	0.04	0.415	2972.90
Site A # 4	03-05-97	1.68	0.46	0.15	0.415	2909.88
Site A # 5	04-21-97	1.56	0.41	0.15	0.415	3255.48
High		1.77				2844.26
Low		1.45				3255.48

Table 5-12 contains results for the boreholes that utilized thermally enhanced grouts. For this group of tests, the highest estimated thermal conductivity is 14% higher than the lowest value. However, the highest borehole length is only 5.5% different from the lowest. Use of the effective grout thermal conductivity significantly reduces the spread in design borehole lengths.

Table 5-12. Results of Two Variable Estimation with One Shank Spacing and Ignoring 12 Hours of Initial Data of All Data Sets that have at Least 50 Hours of Data for an Estimated Grout Conductivity of about 0.85 Btu/hr-ft-°F.

Location	Date of Test (mm-dd-yy)	k_{soil} (Btu/hr-ft-°F)	k_{grout} (Btu/hr-ft-°F)	Estimation Mean Error (°F)	Borehole Resistance (°F-hr-ft/Btu)	Borehole Length (ft)
Site A # 2	01-09-97	1.55	0.84	0.06	0.275	2859.89
Site A # 2	05-28-97	1.77	0.54	0.08	0.377	2896.62
Site A # 3	02-27-97	1.60	0.70	0.04	0.371	2744.38

Table 5-13 contains results for the boreholes that utilized standard Bentonite grouts. For this group of tests, the highest estimated thermal conductivity is 16% higher than the lowest value. However, the highest borehole length is only 11.2% different from the lowest.   Again, use of the effective grout thermal conductivity significantly reduces the spread in design borehole lengths.

Table 5-13. Results of Two Variable Estimation with One Shank Spacing and Ignoring 12 Hours of Initial Data of All Data Sets that have at Least 50 Hours of Data for an Estimated Grout Conductivity of about 0.43 Btu/hr-ft-°F.

Location	Date of Test (mm-dd-yy)	k_{soil} (Btu/hr-ft-°F)	k_{grout} (Btu/hr-ft-°F)	Estimation Mean Error (°F)	Borehole Resistance (°F-hr-ft/Btu)	Borehole Length (ft)
Site A # 1	01-06-97	1.45	0.44	0.11	0.443	3308.61
Site A # 1	06-02-97	1.51	0.39	0.12	0.488	3348.50
Site A # 4	03-05-97	1.68	0.46	0.15	0.518	3011.89
Site A # 5	04-21-97	1.56	0.41	0.15	0.468	3255.48

As demonstrated in this section, use of the estimated grout conductivity in the design process gives significantly better results. Therefore, it is recommended that the test borehole be configured (grout, piping, diameter) the same way as the final boreholes will be configured and that the effective grout conductivity be utilized.

5.9. Experimental Error Analysis

Several sources of uncertainty were identified and quantified. A summary of the uncertainties is given in Table 5-14. The estimated uncertainties are based on a limited number of tests, so the estimates may change with more testing.

Table 5-14 Estimated Uncertainties

Source	Estimated uncertainty in value of k_{ground}	Estimated uncertainty in borehole length
Length of test – 50 hours	±2%	±1%
Power measurement when high accuracy watt transducer is used	±1.5%	±1%
User estimate of volumetric specific heat. The value typically ranges from about 20 Btu / ft³ °F for a very dry soil to about 40 Btu / ft³ °F for a very wet soil or dense rock. If the user can estimate to within ±5 Btu / ft³ °F, the effect on the borehole length is about ±3%	±1.5%	±3%
Assumed shank spacing. With the two parameter estimation, the effect of the spacing is small	±1%	±0.5%
The numerical model. Based on the validations against the cylinder source, in most cases the error in the estimated conductivity would be no more than ±2%. However, it is greater in a few cases.	±4%	±2%
Estimate of far-field temperature. The parameter estimation process is very sensitive to the far-field temperature. However, as long as the far-field temperature used for the parameter estimation is also used in the ground loop design, the uncertainty in borehole length is substantially reduced. (The uncertainty is based on an assumed error of ±1°F in the far-field temperature.)	±11%	±3%

133

Since the uncertainties described above are all independent or nearly independent from each other, they may be added in quadrature. Therefore, the total estimated uncertainty in the value of the ground thermal conductivity is +12%. The total estimated uncertainty in the resulting borehole length is ±5%. This compares well with the range of values that we obtained for 7 tests in nearby boreholes in Stillwater previously described. The highest value of thermal conductivity was 14% higher than the lowest value, and the highest value of borehole length for our test building was 5.5% higher than the lowest value.

6. Conclusions and Recommendations

6.1. Conclusions

As stated in the objectives, there are three issues, which this project focused on: the experimental apparatus and procedure, the development of a numerical model, and the parameter estimation.

In situ experimental test and procedure

Approximately 36 in situ tests were conducted over the span of one year for this research project. As time progressed from the first experimental test conducted in June of 1996, we were able to make several observations. Some observations are pitfalls to watch out for, while other observations are specific steps that need to be taken in certain areas of the experimental apparatus or testing procedure.

- The following instrumentation and equipment should be included in an "in situ" measurement system:

  Equipment

    1. Power Supply. The power drawn from a utility hook-up or portable generator is sufficient. The power does not need to be drawn from a voltage regulator, although it would be a nice feature to have.

    2. Screw-threaded water heater elements with at least 2.5kW power rating. This particular type of water heater element is suggested so that the element can be screwed into a pipe tee. It is recommended that a water tank not be used during the test as it adds an undesirable time lag.

3. Circulating/Purge Pump. Careful calculation and selection should be made to ensure the chosen pump(s) can provide enough head to meet the purging flow standard of 2ft/sec for any given size of pipe diameter.

4. Flow Controls. Although it is an obvious requirement, proper flow valves, connectors, and control schemes are considered part of the necessary equipment.

5. Water supply tank. A water tank is needed for tests made at undeveloped job sites and for purging the system

Instrumentation

1. Temperature Measurement. The inlet and outlet temperatures of the borehole should be measured. Use temperature sensors that can be immersed in the flow of the circulating fluid. When combined with the data acquisition system, temperature should be measured within $\pm0.5°F$ or better.

2. Fluid Flow Measurement. The flow rate of the system should be measured. Although it is not directly required, if the flow is used as an input to the numerical model, the model can calculate a convective resistance, which will yield a better parameter estimation.

3. Power Input. The watt input to the water heater elements and the circulating pumps should be directly measured by some form of a high accuracy watt transducer that measures the voltage and the current. The power can be much more accurately measured with a watt transducer than with a $mc_p\Delta T$ calculation, given a relative small ΔT. Since the error in conductivity is directly proportional to the error in power measurement, a high accuracy watt transducer is highly desirable.

- Test Procedure

1. Drill and grout the borehole. This would include taking any information on known geologic conditions, borehole depth, borehole diameter, pipe diameter, and grout material used to fill the borehole. The loop should be filled with water[*]. Allow the borehole with the loop installed to return to the ambient conditions (temperature, moisture content) surrounding the borehole[**].

2. Insulate any exposed piping. This includes the exposed HDPE legs and the test apparatus piping, if not already insulated.

3. Connect the experimental apparatus to the borehole. Fill up the entire piping system with water.

4. Purge the system per the standard determined by IGSHPA. Depending on the piping configuration, this could purge the borehole first, then purge the test apparatus or purge both at the same time. It is recommended that each line be purged for at least 15 minutes.

5. Once the system is purged, close off all open-loop ends. At this point, it is possible to have a slight temperature increase due to the heat input to the pumps. If time permits, allow the circulating fluid to re-approach the undisturbed ground temperature.

6. Begin data collection. In order to ensure the first temperature increase and power input are read, turn on the data collection device and begin collecting data *before* the power to the water heater elements and circulating pumps is turned on. **Test for at least *50* hours.**

7. Turn on circulating pumps and heater elements. As the test begins, make any necessary adjustments to the system to provide the correct flow that will result in the desired ΔT. The normal difference between the inlet and outlet temperatures (ΔT) for the tests we performed was 6 °F. We suggest using about 2500 Watts of total power input for a 250' deep borehole; other boreholes should be scaled similarly. Due to low voltages, this is equivalent to a water heater element rated at 2500 Watts, but only providing 2000 Watts and 500 Watts of pump power in our test apparatus. Using the suggested power input and the desired ΔT, this will result in a required flow rate of 3 gpm. (The flow rate may vary for other lengths of boreholes.

---

[*] This is usually done before the loop is inserted in the ground.
[**] No research has been done into how long this might take. Presumably this is a relatively short amount of time, say a day for cases where the drilling/grouting does not saturate dry ground or dry damp grout.

8. Once the test period is terminated, the power to the water heater elements should be turned off prior to turning off the circulating pumps. Once the power to the water heater elements is turned off, the data collection can be terminated also, but *not before.*

9. Test Shutdown

   - Disconnect from the loop pipe legs. Then, seal the pipe ends with duct tape, end caps, or fusion welds.
   - Drain all piping, especially if testing in near or below freezing climate conditions.

10. Analyze data and write report on findings. The analysis begins by first writing down the estimated parameter values. Then review the estimation errors printed on the same output file by back-calculating the error per estimated temperature point using a spreadsheet. Next, plot the temperature profile of the experimental and the parameter estimation values. Using all of these analysis tools will enable the designer to gain useful knowledge for the design of the ground loop heat exchanger. but some reasonable rationale will still need to be used.

Numerical Model

- The model is sensitive to the shank spacing parameter. It is clear that for different shank spacing values, there are different parameter estimations with different estimation errors. As the shank spacing changes, the thickness of low conductivity grout between the pipe and the ground can vary significantly. With current installation practices, the precise location of the U-tube is unknown. The U-tube can be right next to the borehole wall or located in middle. A possible improvement for in situ testing would be to control the shank spacing.

- The numerical model is a better representation of the borehole configuration than a line source or cylinder source approach. The U-tube pipes, grout material, soil, and circulating fluid are separate entities that can all be represented by the numerical model. The line source approach groups all of these separate components into one

138

element allowing for a large amount of uncertainty in the manner in which the borehole can be configured. The cylinder source approach is slightly better than the line source, but it, too, makes a gross approximation by creating an equivalent pipe diameter from the two U-tube pipe legs.

- In validating the numerical model, it does reasonably model the borehole configuration. The pie-sector representation is a reasonable starting point, but some improvements might be made, either by adjusting the shape or using boundary-fitted coordinates.

Parameter Estimation Procedure

Different approaches to determine the best analysis procedure were performed on several data sets. After estimating one parameter, then two parameters, I was able to draw several conclusions about the length of test required, the number of and the type of parameters to estimate, and the initial number of data hours to ignore.

- The Nelder-Mead simplex algorithm can be improved. This algorithm usually finds a good solution, but it does not always find the absolute or global minimum, even after a restart. An algorithm that will more reliably find the global minimum should be considered.

- The length of test should be no less than 50 hours to obtain a value of ground conductivity that would be within 2% of that obtained with a much longer tests.

- The best estimates are made when approximately 12 hours of initial data are ignored. The parameter estimations that ignored the first 12 hours approach the final soil thermal conductivity value more quickly than the parameter estimations that used the entire data set. This is partly due to the initial heat transfer being dominated by the contents of the borehole. As time increases, the heat transfer becomes more dominated by the soil thermal properties rather than the borehole, though the borehole contents are still a factor in the heat transfer rate.

- The single variable approach is not a good estimation procedure for this problem because there are too many unknown factors that influence the estimation, e.g. shank spacing.

- The two-variable estimation for k_{soil} and k_{grout} can adequately represent some of the unknown parameters such as the shank spacing. In the data sets that were evaluated, the estimation of the grout thermal conductivity resulted in more steady soil conductivity estimations and lower estimation errors.

- The time of year is not significant if precautions are made to highly insulate and control the environment surrounding an in situ test unit. The data sets analyzed in this thesis did not show any significant changes in the estimation due to the warmer climate versus the colder climate. It is possible that in other geographical locations, the thermal conductivity changes depending on the time of the year.

- The two-variable parameter estimation predicted the ground thermal conductivity within a range of about 20% for 12 tests at the same site. If the borehole used in the in situ test is also used in the final ground loop design, the effective grout conductivity can be used in the ground loop design process. In this case. the range of borehole lengths is substantially reduced.

- Because there is no absolute truth model yet available, it is difficult to assign an exact final value to the uncertainty of the measurement prediction. However, based on examination of the parameter estimation procedure's sensitivities to various experimental inputs, the estimated uncertainty in the value of the ground thermal conductivity ±12%. The resulting uncertainty in borehole design length is estimated to be ±5%, when consistent values for the undisturbed ground temperature and ρc_p of the soil are used in both the parameter estimation procedure and the ground loop heat exchanger design program.

6.2. Recommendations

- Develop a more compact experimental apparatus. This apparatus could be very portable, such as the size of a small strong box, small crate, or a suitcase, although an auxiliary power source and purging system would be needed.

- If possible, develop a system that does not require purging.

- Further validate the pie sector approximation of the half-cylindrical pipe and/or develop an improved numerical model. An improved numerical model might allow for shorter tests.

- The current model uses 2/3 power dissipation in the leg as it flows down into the borehole and 1/3 power in the pipe leg that flow up and out of the borehole. A three-dimensional model would not require this assumption. The assumption could be checked with a three-dimensional model or by inserting a temperature sensor in the fluid flow at the bottom the U-tube.

- Improve the parameter estimation algorithm by incorporating a new minimization function instead of the current Nelder-Mead simplex. Nelder-Mead works reasonably well and is very robust, but a better technique might be found.

- To attempt to scientifically validate the parameter estimation results, one approach would be to assemble a long (maybe 60 ft) trench box with a U-tube heat exchanger. The box could be filled with some known material, such as fine quartz sand, with an independently measurable thermal conductivity value for dry and wet (saturated) conditions. The heat exchanger would be centered in the middle of the box surrounded by the sand material. The U-tube could then be attached to an in situ

testing unit. After the test is complete, the results could be compared to published values if the test were kept under a controlled environment.

- There should be some further investigation into controlling the shank spacing that appears to be extremely important to parameter estimation. This would involve the use of spacers installed in between the two pipes.

- Use the same grout and piping in the in situ test as will be used in the final design. This will give reduced uncertainty in the final result.

- Finally, the ultimate validation will be to perform some in situ tests at sites where buildings with monitored GSHP systems are installed. If the systems are correctly monitored, the long term performance (temperature response due to known heat inputs) can be compared to that predicted with the design software, using input values determined from the in situ test. This comparison will serve as the ultimate validation of both the in situ test procedure and the design software.

References

ASHRAE. 1997. (Kavanaugh, S.P. and K. Rafferty, Authors) Ground Source Heat Pumps- Design of Geothermal Systems for Commercial and Institutional Building

Bose, J.E. 1984. *Closed-Loop Ground-coupled Heat Pump Design Manual.* Stillwater, OK: Oklahoma State University, Engineering Technology Extension.

Choudhary, A. 1976. "An approach to determine the thermal conductivity and diffusivity of a rock in situ" Ph.D. dissertation, Oklahoma State University.

Dittus, F.W., and L.M.K. Boeleter. 1930. *University of California publications on engineering,* vol. 2. Berkeley, CA: University of California.

EPRI. 1989. (Bose, J.E., Editor) Soil and Rock Classification for the Design of Ground-Coupled Heat Pump Systems—Field Manual. Electric Power Research Institute Special Report, EPRI CU-6600.

IGSHPA. 1991. (Bose, J.E., Editor) Design and Installations Standards.

Ingersoll, L.R. and H.J. Plass. 1948. Theory of the Ground Pipe Heat Source for the Heat Pump. Heating, Piping & Air Conditioning. July. pp. 119-122.

Ingersoll, L.R., O.J. Zobel and A.C. Ingersoll. 1948, 1954. *Heat Conduction with Engineering, Geological, and other Applications.* New York: Mc Graw-Hill.

Kavanaugh, S.P. 1984. "Simulation and experimental verification of vertical ground-coupled heat pump systems" Ph.D. dissertation, Oklahoma State University.

Kavanaugh, S.P. and J.D. Deerman. 1991. *Simulation of vertical U tube ground coupled heat pump systems,* ASHRAE Transactions, Volume 97, pages 287-295.

Mogensen, P. 1983. Fluid to Duct Wall Heat Transfer in Duct System Heat Storages. Proceedings of the International Conference on Subsurface Heat Storage in Theory and Practice. Swedish Council for Building Research. June 6-8.

Patankar, S.V. "Computation of Conduction and Duct Flow Heat Transfer", Innovative Research Inc., Maple Grove, MN. 1991.

Paul, N. 1996. "The effect of Grout Thermal Conductivity on Vertical Geothermal Heat Exchanger Design and Performance" Master's thesis, South Dakota State University.

Press, W., Flannery, B., Teukolsky. S., Vetterling, W., 1994. "Numerical Recipes in FORTRAN- The Art of Scientific Computing" (2nd Ed., pp. 436-448), New York: Press Syndicate of the University of Cambridge.

Sass, J.H., et al. "Thermal Conductivity of Rocks from Measurements on Fragments and Its Applications to Determination of Heat Flow." <u>Journal of Geophysical Research</u>, Vol. 76, No. 14 (May, 1971), 3391-3401.

Spitler, J.D., C. Marshall, R. Delahoussaye, M. Manicham. 1996. *Users Guide of GLHEPRO*, School of Mechanical and Aerospace Engineering, Oklahoma State University, Stillwater, OK.

Yavuzturk, Cenk. Private Communication. 1996.

Appendix A

Date	Location	Description	Duration(hr)
6-5-96	Richardson, TX	4 ½" borehole, 200' deep, grouted with Thermal Grout 85	11
6-6-97	Richardson, TX	4 ½" borehole, 200' deep, grouted with Ben-seal	10
6-27-96	Stillwater, OK Site A	Vertical #1, 250' deep, ¾" HDPE pipe, grout unknown, but assumed Bentonite	24
7-1-96	Stillwater, OK Site A	Vertical #2, 240' deep, ¾" HDPE pipe, grout unknown but assumed Bentonite	24
7-22-96	Stillwater, OK Site A	Vertical #2, 240' deep, ¾" HDPE pipe, grout unknown but assumed Bentonite	24 Test not completed due to instrumentation failure
7-30-96	Stillwater, OK Site A	Vertical #1, 250' deep, ¾" HDPE pipe, grout unknown, but assumed Bentonite	48
8-5-96	Brookings, SD	#1- 4 ½ " borehole, 200' deep, grouted with 30% solids Bentonite. Power Supply from Building hookup.	16
8-6-96	Brookings, SD	#2- 4 ½ " borehole, 200' deep, grouted with Thermal Grout 85. Power Supply from Building hookup.	12
8-7-96	Brookings, SD	#3- 6 " borehole, 200' deep, grouted with 30% solids Bentonite. Power Supply from Building hookup	12
8-8-96	Brookings, SD	#4- 6 " borehole, 200' deep, grouted with Thermal Grout 85. Power Supply from Building hookup.	12
8-9-96	Brookings, SD	#5- 4 ½ " borehole, 200' deep, grouted by air injecting 30% solids Bentonite. Power Supply from Building hookup. Partial collapsed near bottom of the borehole.	12
9-5-96	Stillwater, OK Site A	#1- 3 ½" borehole, 244' deep, grouted with 30% solids Bentonite. Powered by generators.	20
9-7-96	Stillwater, OK Site A	#2- 3 ½" borehole, 252' deep, grouted with Thermal Grout 85. Powered by generators.	24
9-11-96	Stillwater, OK Site A	#3- 4 ½" borehole, 252' deep, grouted with Thermal Grout 85. Powered by generators.	28
9-13-96	Stillwater, OK Site A	#4- 4 ½" borehole, 250' deep, grouted with 30% solids Bentonite. Powered by generators.	22

Date	Location	Description	Duration(hr)
9-23-96	Stillwater, OK Site A	#5- 3 ½" borehole. 252' deep, grouted with Benseal. Powered by generators.	24
10-2-96	Stillwater, OK Site A	#6- 3 ½" borehole. 258' deep, grouted with Benseal. * Powered by generators. Grout level is 20' below grade	24
10-9-96	Stillwater, OK Site A	Vertical #1- 250' deep, grout unknown, but assumed to ** be Bentonite. Powered by generators.	30
10-11-96	Stillwater, OK Site A	Vertical #2- 250' deep, grout unknown, but assumed to ** be Bentonite. Powered by generators.	23
11-6-96	Stillwater, OK Site A	#2- 3 ½" borehole, 252' deep, grouted with Thermal Grout 85. Powered by electric line.	75
11-12-96	Stillwater, OK Site A	#1- 3 ½" borehole, 244' deep, grouted with 30% solids Bentonite. Powered by electric line.	71
11-17-96	Stillwater, OK Site A	#3- 4 ½" borehole, 252' deep, grouted with Thermal Grout 85. Powered by electric line.	73
11-21-96	Stillwater, OK Site A	#4- 4 ½" borehole, 250' deep, grouted with 30% solids Bentonite. Powered by electric line.	73
11-25-96	Stillwater, OK Site A	#5- 3 ½" borehole, 252' deep, grouted with Benseal. Powered by electric line.	76
12-9-96	Stillwater, OK Site A	Vertical #1- 3 ½" borehole, 252' deep, grouted with Bentonite. Powered by electric line. Power shutdown.	26
12-30-96	Stillwater, OK Site A	Vertical #2- 3 ½" borehole, 240' deep, grouted with Bentonite. Powered by electric line. Power shutdown. *	26
1-6-97	Stillwater, OK Site A	#1- 3 ½" borehole, 244' deep, grouted with 30% solids Bentonite. Powered by electric line.	72
1-9-97	Stillwater, OK Site A	#2- 3 ½" borehole. 252' deep, grouted with Thermal Grout 85. Powered by electric line.	170
2-27-97	Stillwater, OK Site A	#3- 4 ½" borehole, 252' deep, grouted with Thermal Grout 85. Powered by electric line.	120

Date	Location	Description	Duration(hr)
3-5-97	Stillwater, OK Site A	#4- 4 ½" borehole. 250' deep, grouted with 30% solids Bentonite. Powered by electric line.	73
3-10-97	Bartlesville, OK	Well #17- 4 ½ " borehole, 300' deep, grouted with Thermal Grout 85. Power supply from portable generators. Cored Sample taken from this well.	24
3-11-97	Bartlesville, OK	Well #16- 3 ½ " borehole, 300' deep, grouted with Thermal Grout 85. Power supply from portable generators.	24
3-12-97	Bartlesville, OK	Well #15- 3 ½ " borehole, 300' deep, grouted with 30% Bentonite. Power supply from portable generators. Grouting problems; grouted to 250'	24
3-14-97	Bartlesville, OK	Well #14- 3 ½ " borehole, 300' deep, grouted with Ewbank's Enhanced Grout. Power supply from portable generators.	24
4-21-97	Stillwater, OK Site A	#5- 3 ½" borehole, 252' deep, grouted with Benseal. Powered by electric line.	93
5-28-97	Stillwater, OK Site A	#2- 3 ½" borehole. 252' deep, grouted with Thermal Grout 85. Powered by electric line.	170
6-2-97	Stillwater, OK Site A	#1- 3 ½" borehole, 244' deep, grouted with 30% solids Bentonite. Powered by electric line.	93
9-26-97	Chickasha, OK	Test Well for Smart Bridge Project- 3 ½" borehole, 250' deep grouted with 30% solids Bentonite. Power by Electric Generators	99

Note:
*   Data was not analyzed due to circumstances beyond our control.
**   Power was randomly turned on and off to see if model could handle the changes.

Appendix B

Temperature Rise for Site A #1 for 1-6-97 to 1-9-97.
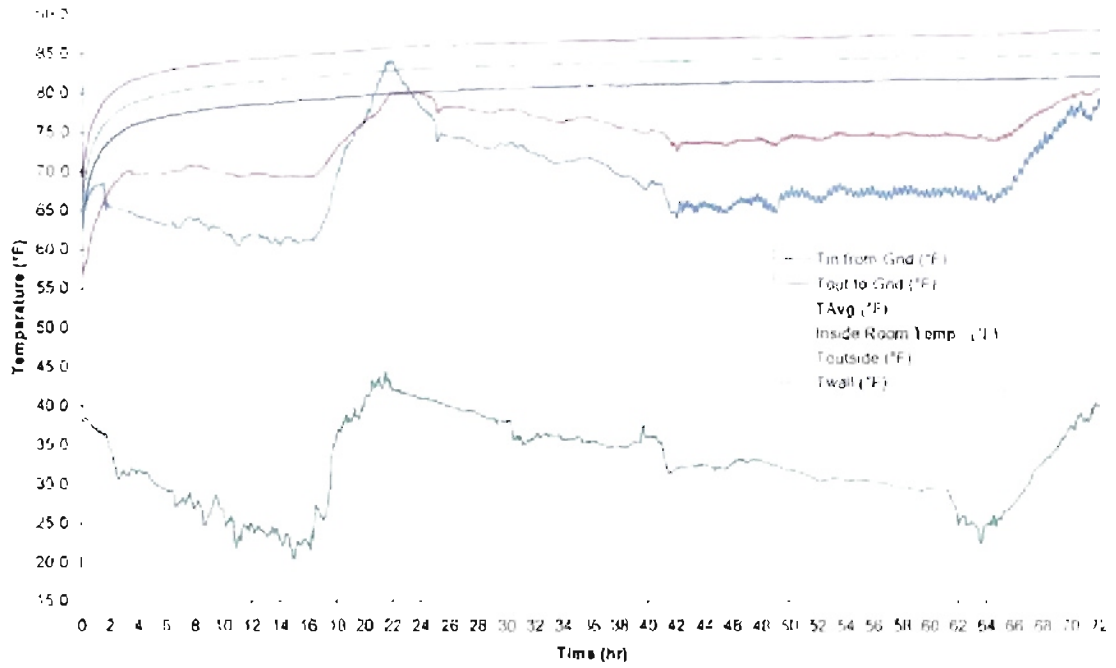
Power and Flow Rates for the test of Site A #1 on 1-6-97.

151
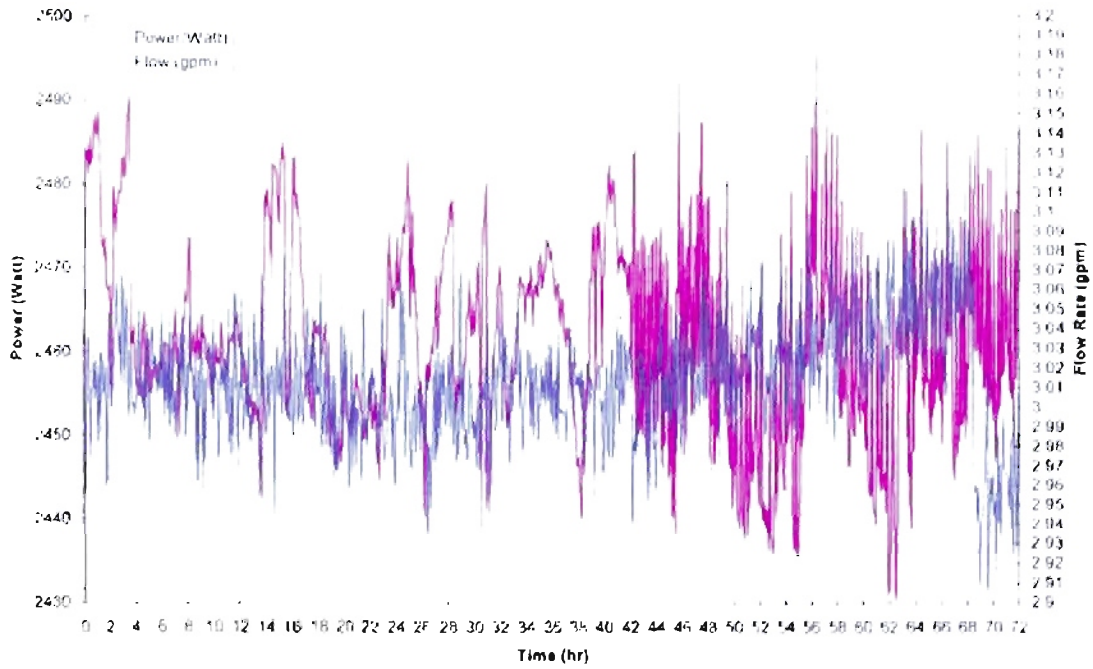
## Temperature Rise for Site A Well #1 on 6-2-97 to 6-6-97

Legend:
- Tin from Gnd (°F)
- Tout to Gnd (°F)
- TAvg (°F)
- Inside Room Temp (°F)
- Toutside (°F)
- Twall (°F)

X-axis: Time (hr)
Y-axis: Temperature (°F)
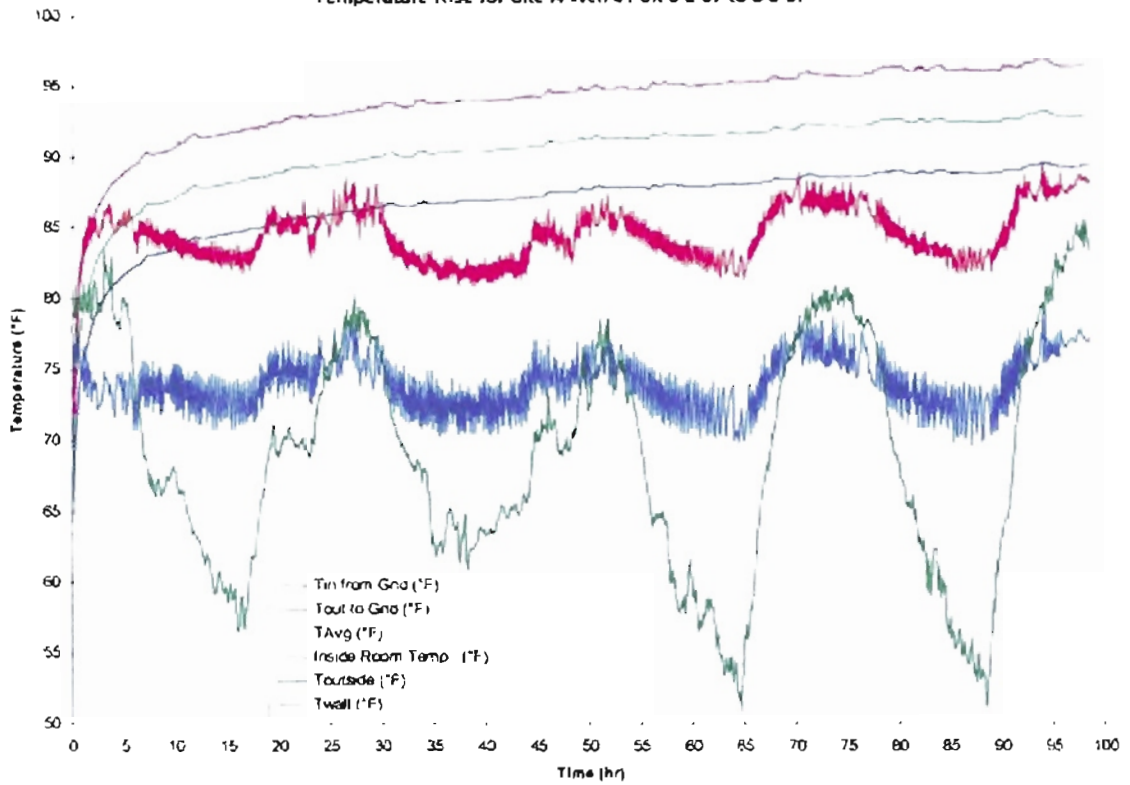
Power and Flow Rates for the test of Site A Well #1 on 6-2-97

Legend:
- Power (Watt)
- Flow (gpm)

X-axis: Time (hr)
Y-axis (left): Power (Watt)
Y-axis (right): Flow Rate (gpm)
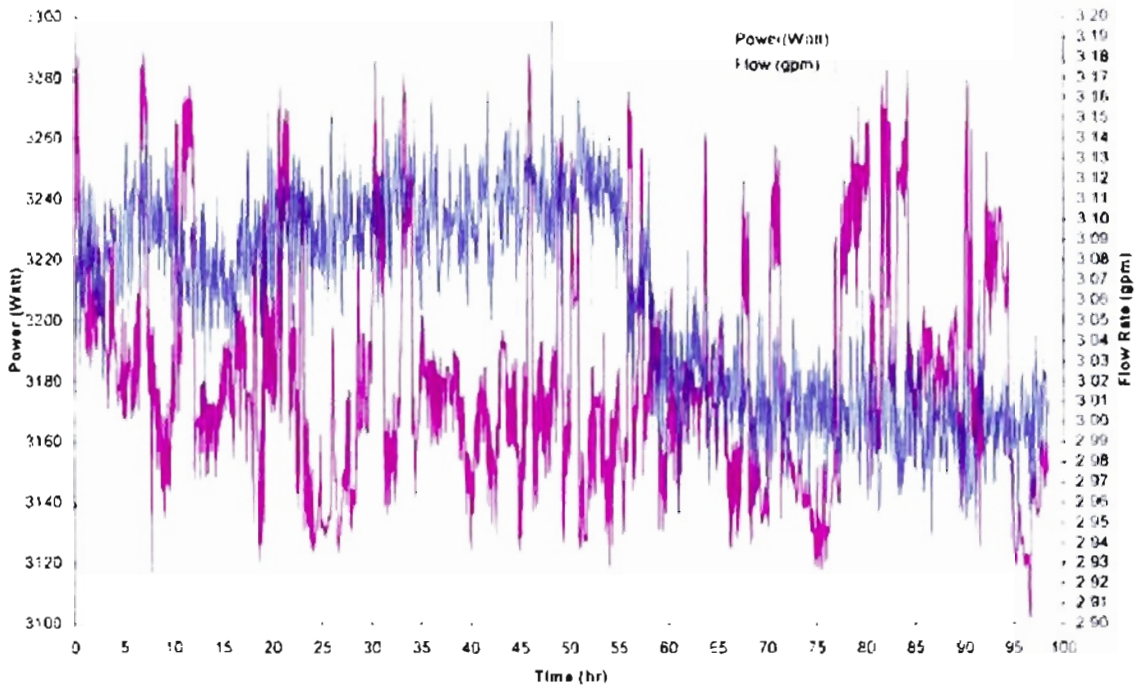
Temperature Rise for Site A Well #2 on 5-28-97 to 6-2-97
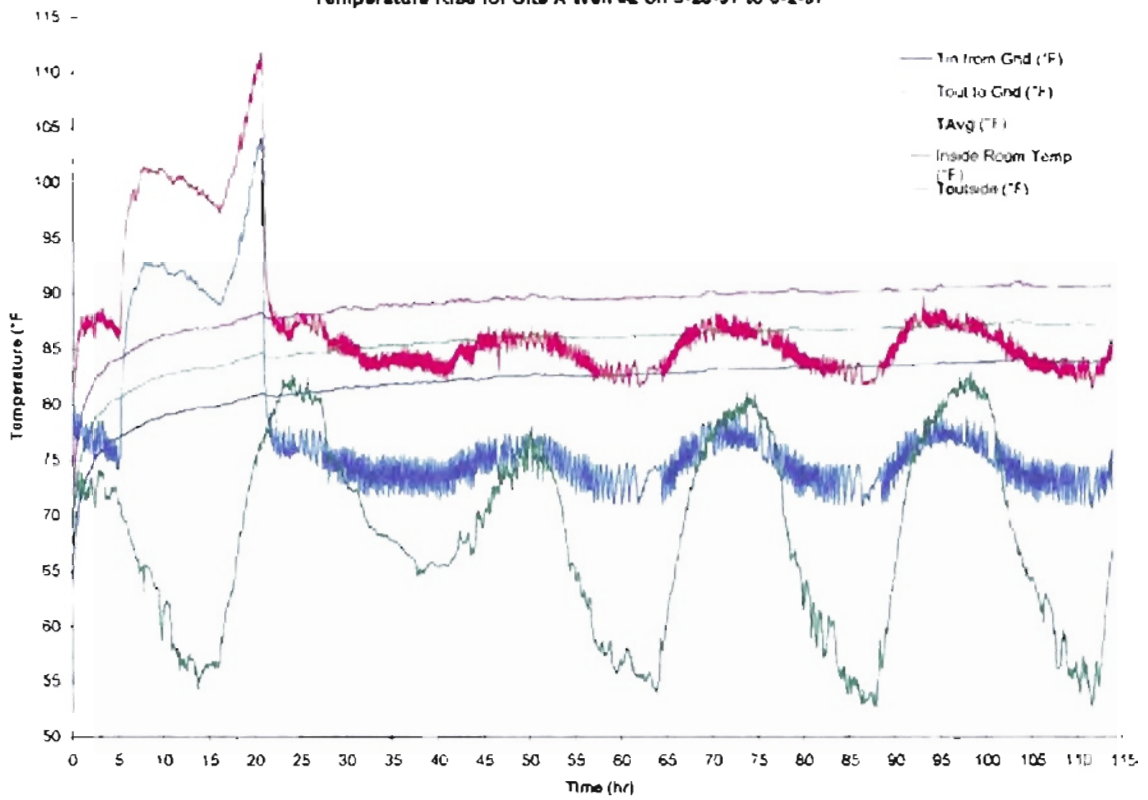
Power and Flow Rates for the test of Site A Well #2 on 6-28-97
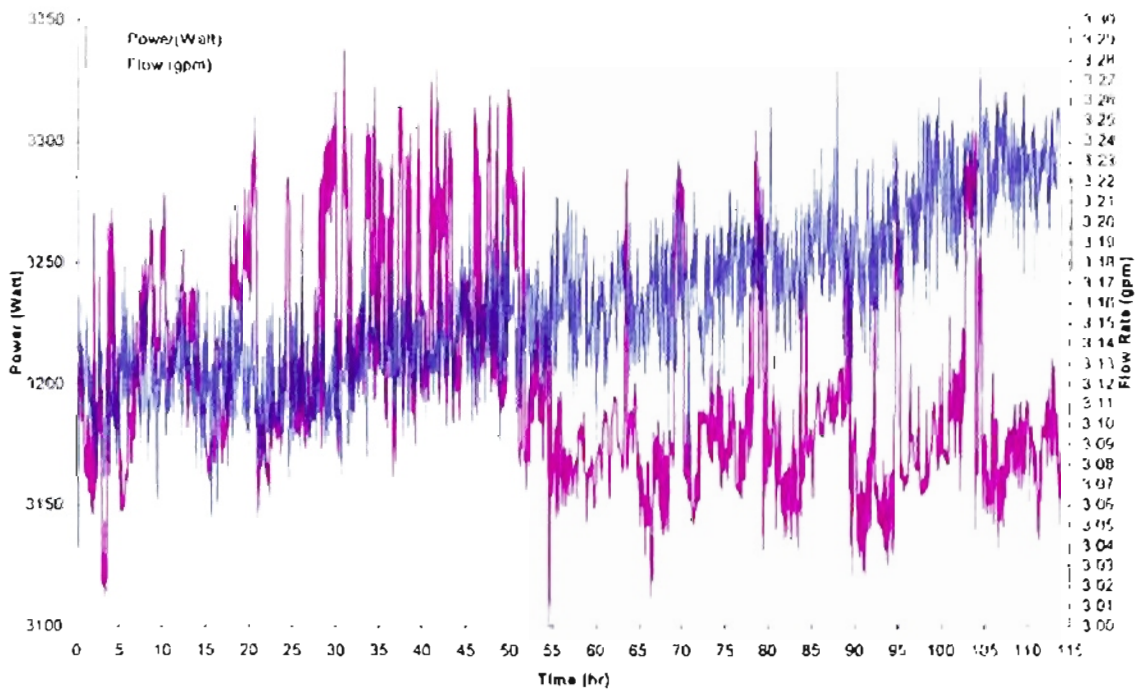
Temperature Rise for Site A #2 for 1-9-97 to 1-16-97.
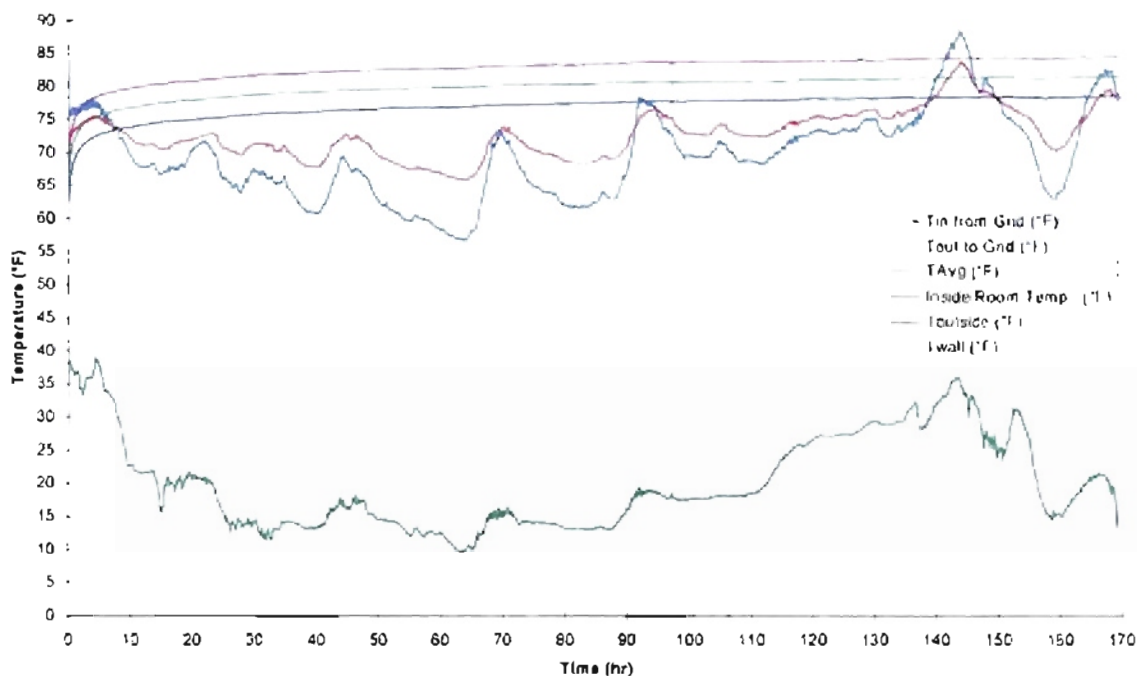
Power and Flow Rates for the test of Site A #2 on 1-9-97.

154
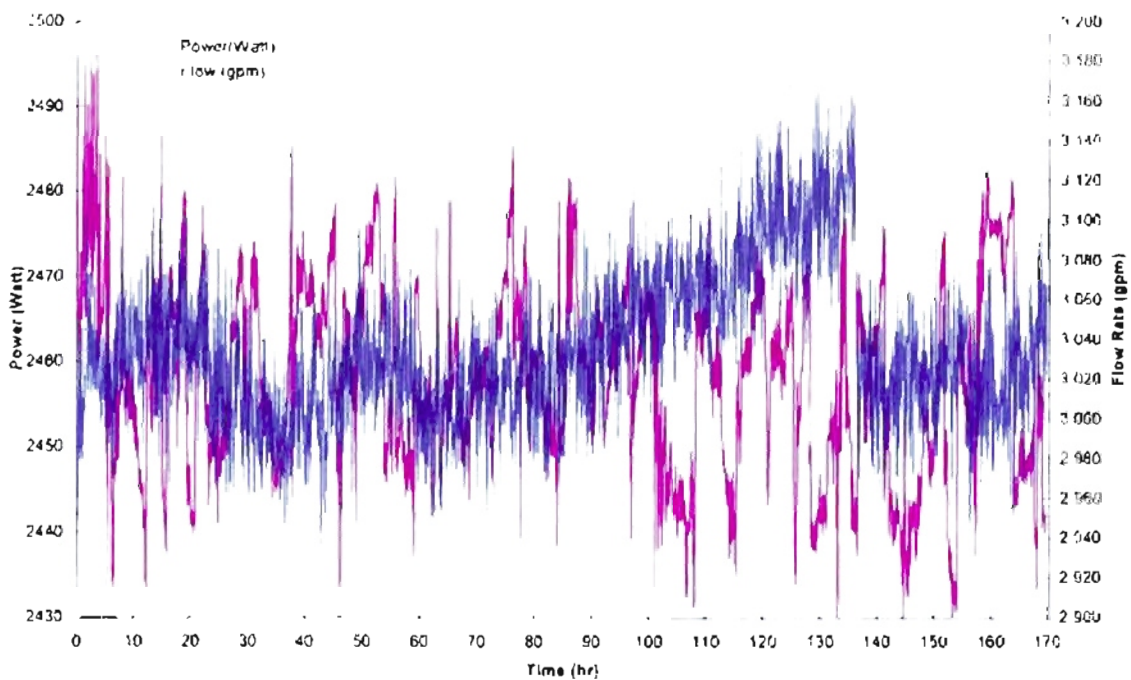
Temperature Rise for Site A #3 for 2-27-97 to 3-4-97.
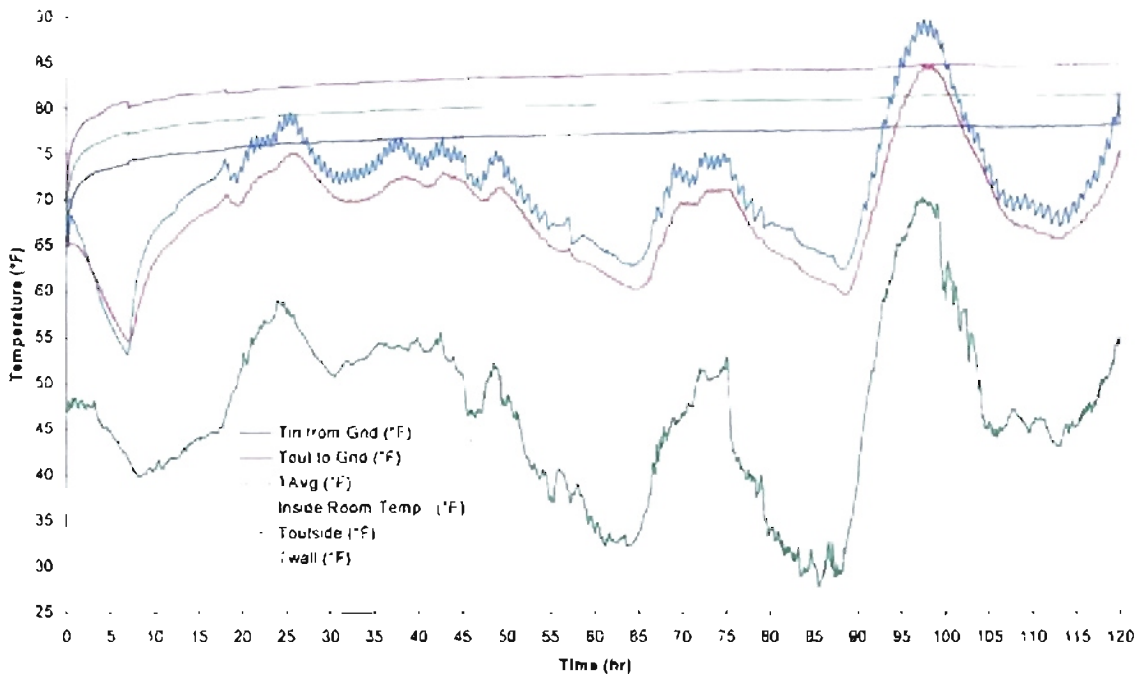
Power and Flow Rates for the test of Site A #3 on 2-27-97.
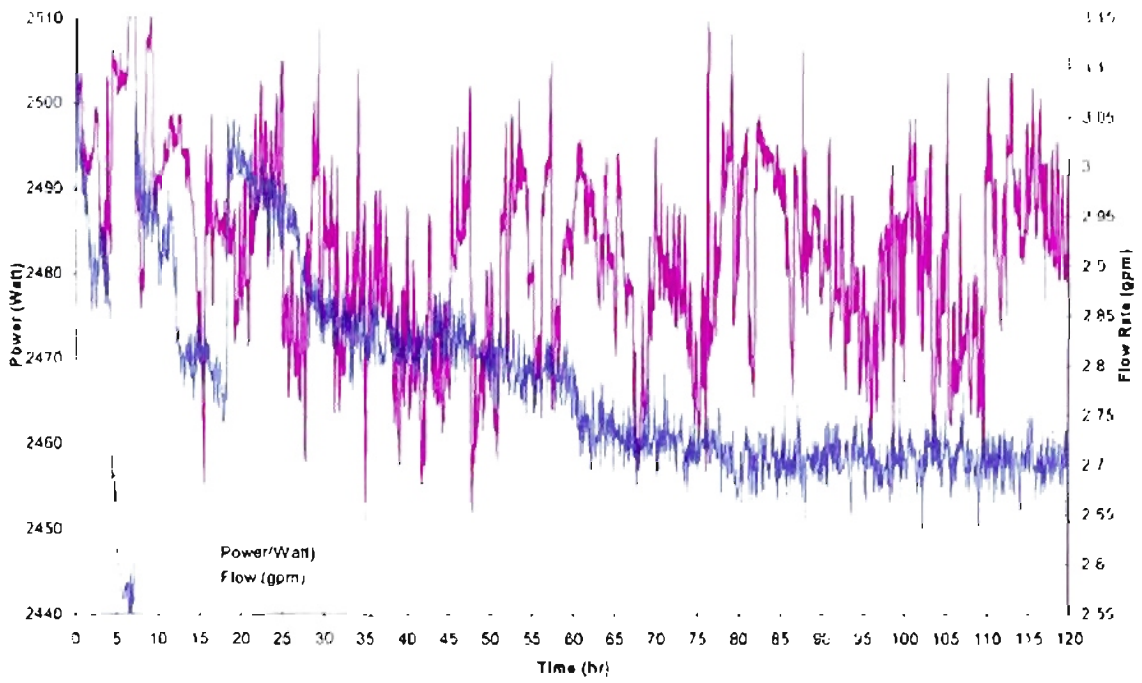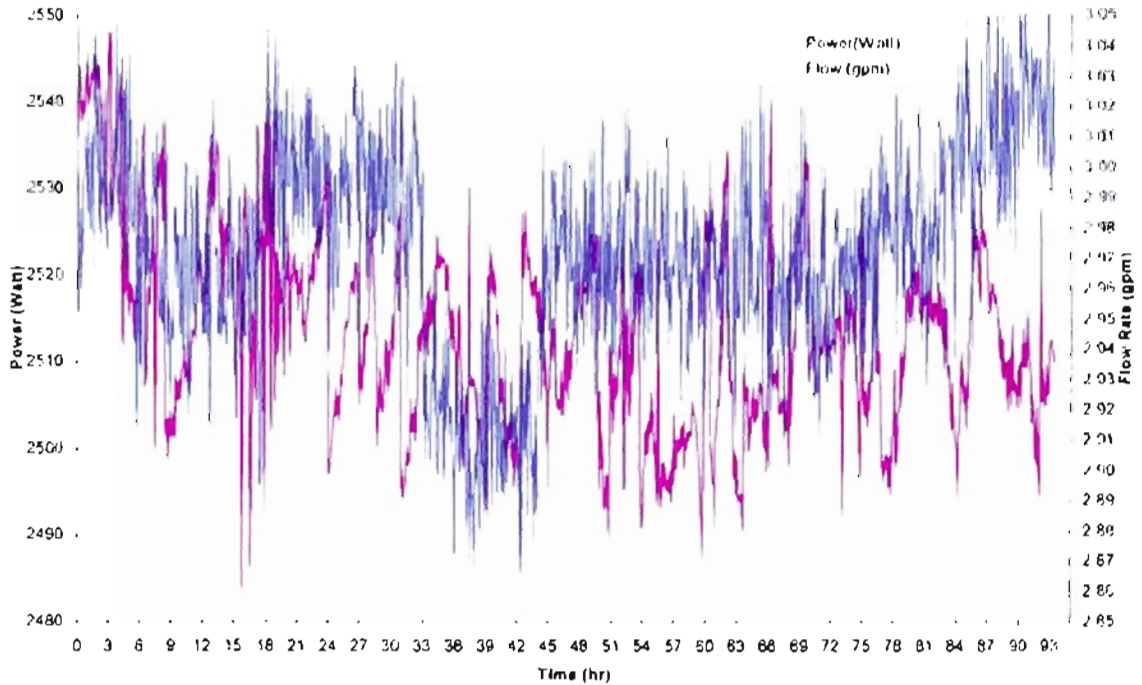
Temperature Rise for Site A #4 for 3-5-97 to 3-8-97.
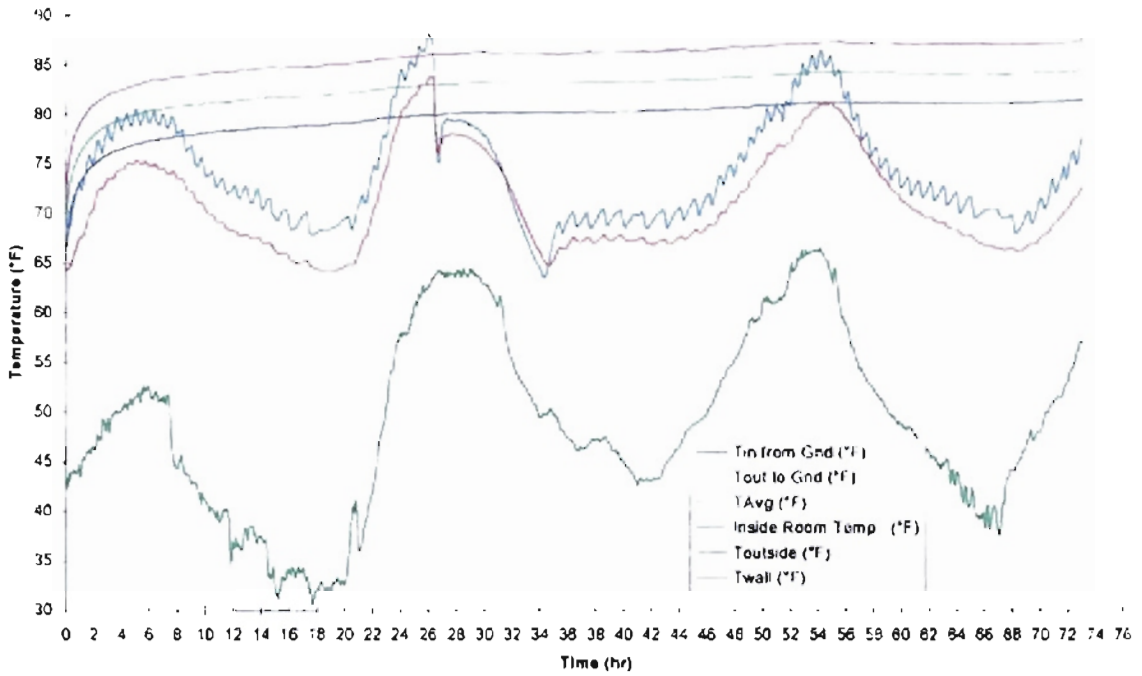
Power and Flow Rates for the test of Site A #4 on 3-5-97.

156
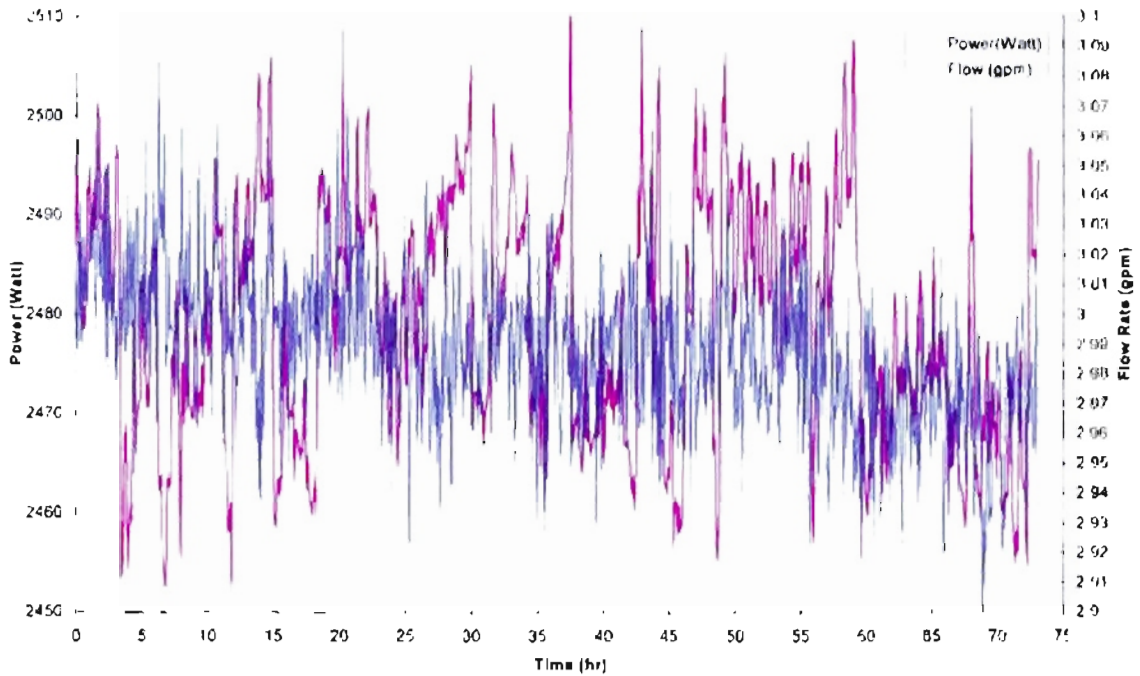
Temperature Rise for Site A #5 on 4-21-97 to 4-25-97

Tin from Gnd (°F)
Tout to Gnd (°F)
Tavg (°F)
Inside Room Temp (°F)
Toutside (°F)
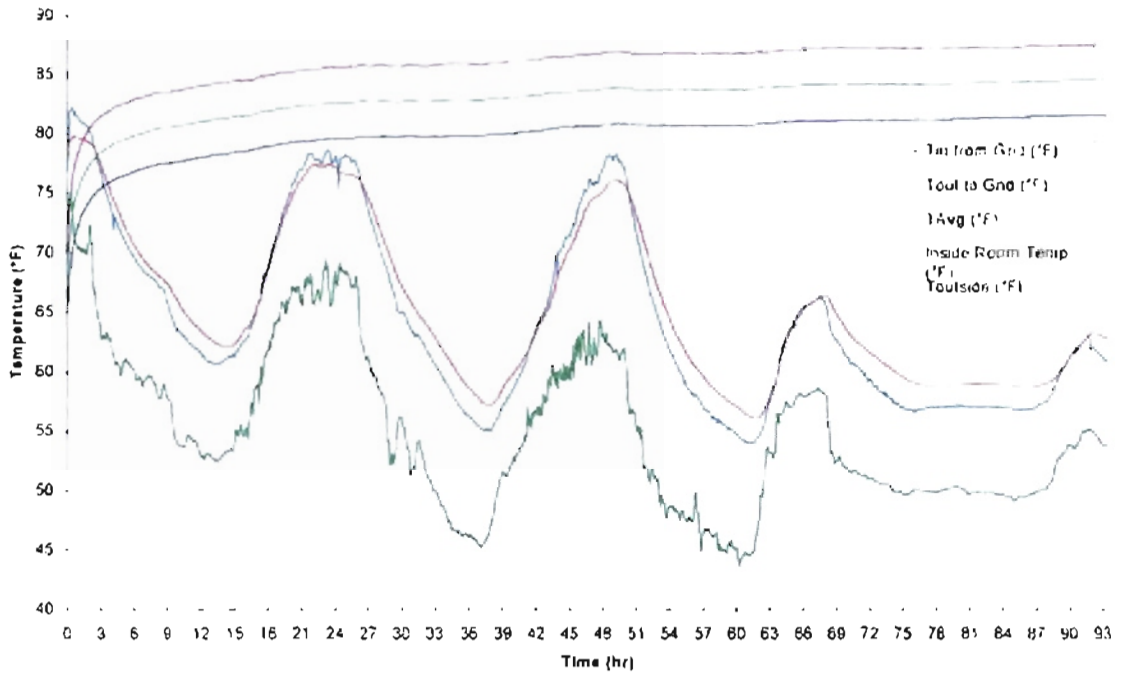
Power and Flow Rates for the test of Site A #5 on 4-21-97

Power(Watt)
Flow (gpm)

Appendix C

Table C-1 shows results that can be determined from compromised experimental tests. The data in this Appendix were analyzed in the same manner as Section 5-8. These results show the erratic estimations when poor insulation is applied to the experimental apparatus. The poor insulation allowed either the outside temperature or the inside temperature to influence the average fluid temperature. The parameter estimation method has matched unreliable estimation parameters based upon the average fluid temperature that in turn over predicts or under predicts the parameters. The raw data from these tests follow.

Table C-1. Results of Two Variable Estimation with one shank spacing and ignoring 12 hours of initial data of all data sets that have at least 50 hours of data. *

| Location	Date of Test (mm-dd-yy)	k_{soil} (Btu/hr-ft-°F)	k_{grout} (Btu/hr-ft-°F)	Estimation Mean Error (°F)	Borehole Resistance (°F-hr-ft/Btu)	Borehole Length (ft)
Site A # 1	11-12-96	1.71	0.36	0.30	0.415	2887.91
Site A # 2	11-06-96	1.81	0.65	0.20	0.415	2812.00
Site A # 3	11-17-96	1.38	0.83	0.05	0.415	3147.61
Site A # 4	11-21-96	1.22	0.57	0.08	0.415	3315.55
Site A # 5	11-25-96	1.86	0.33	0.18	0.415	2777.94

Temperature Rise for Site #1 on 11-12-96. The borehole is 3.5" in diameter and is grouted with Bentonite.
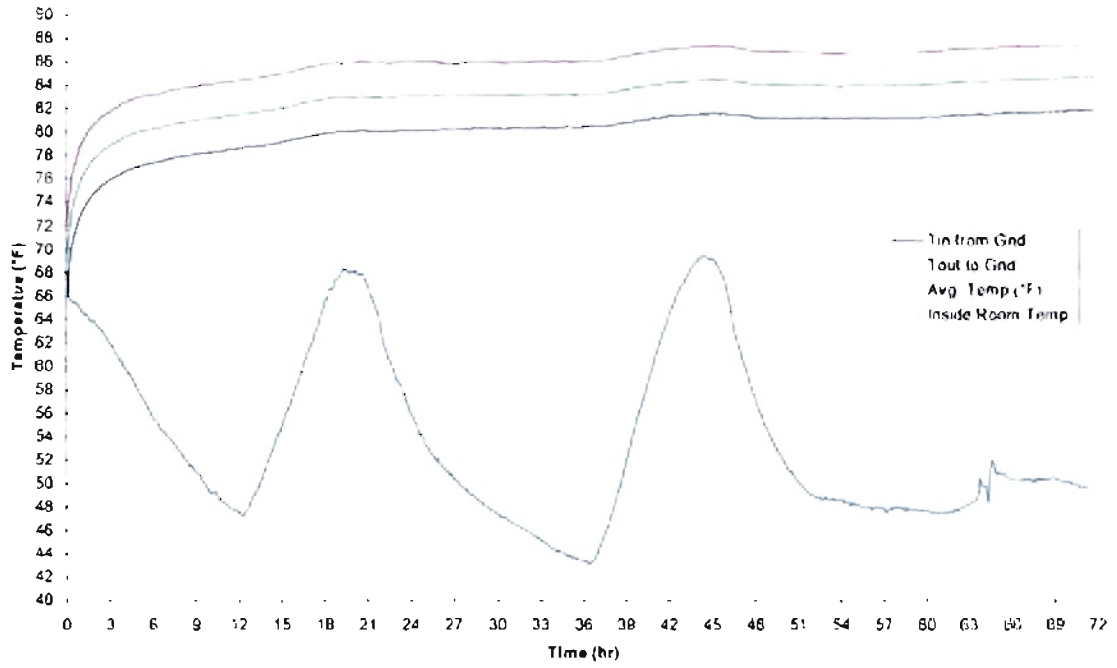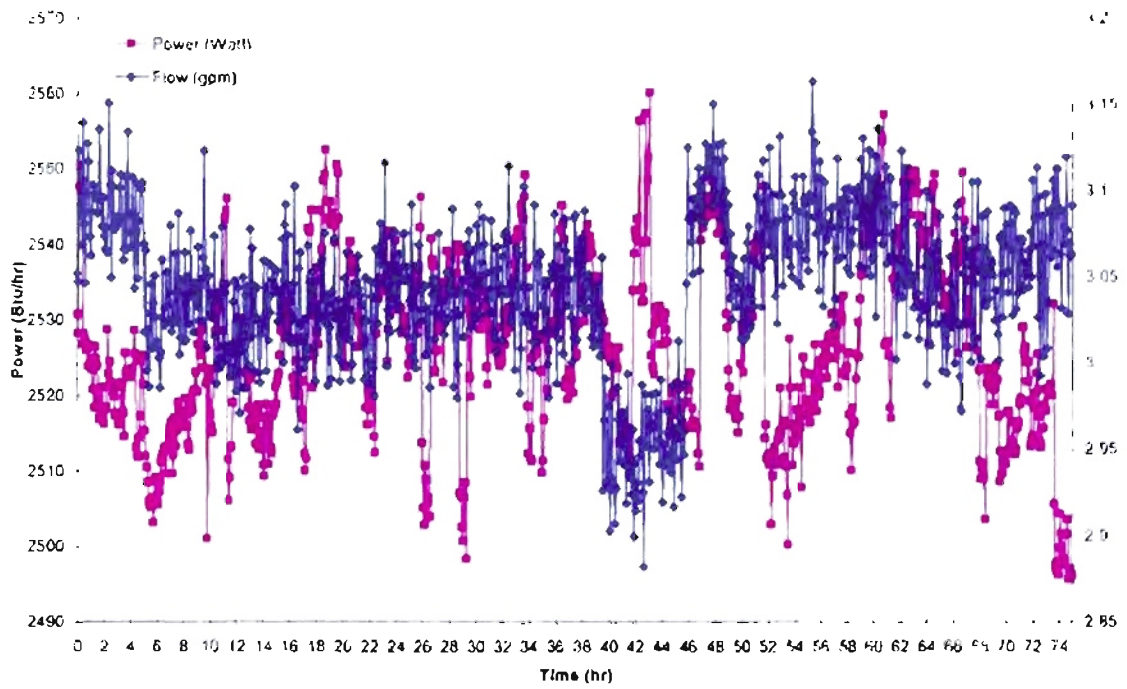

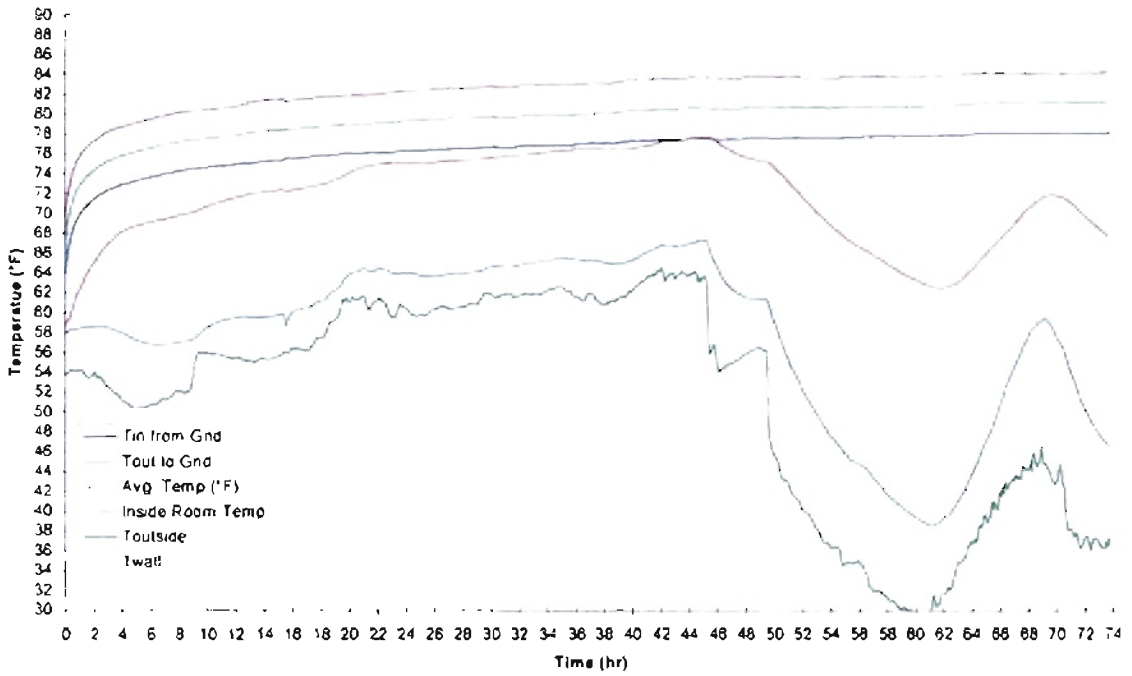Power and Flow Rates for the test of Site A #1 on 11-12-96

160
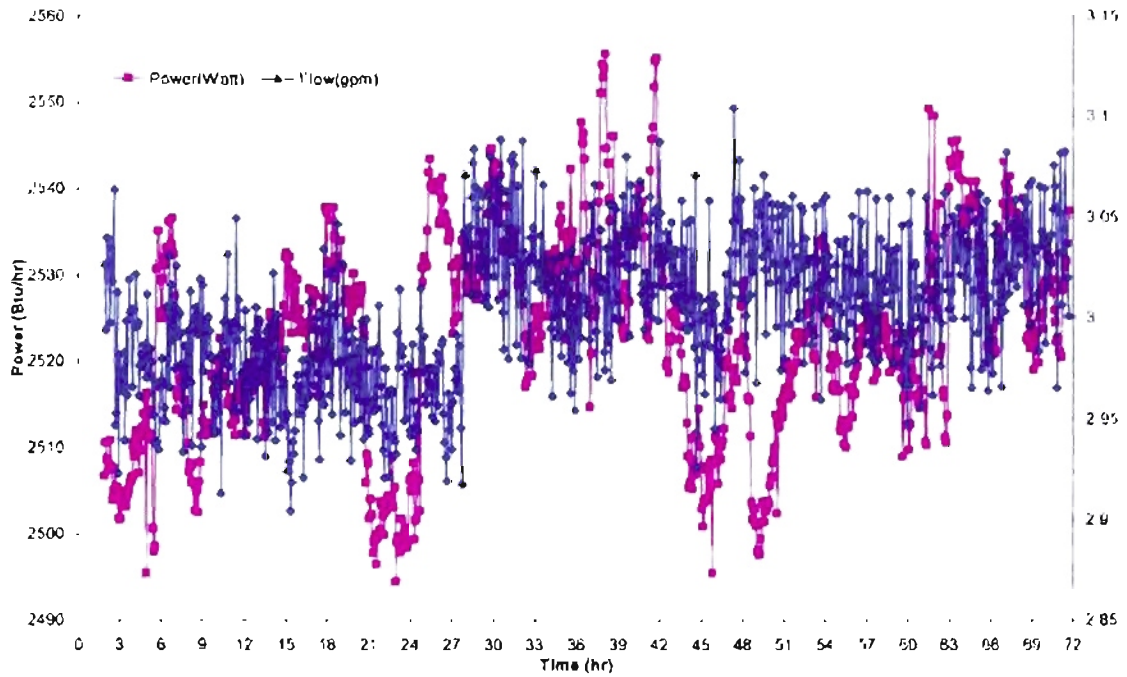
Temperature Rise for Site A #2 on 11-8-96. The borehole is 3.5" in diameter and is grouted with Thermal Grout 85.
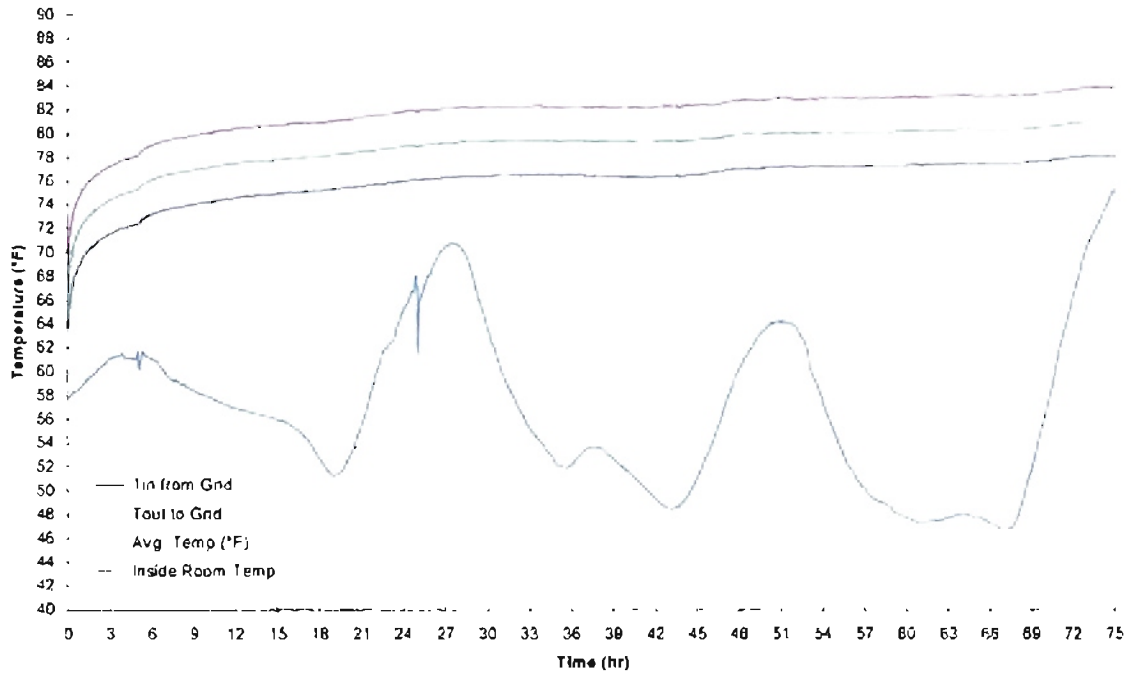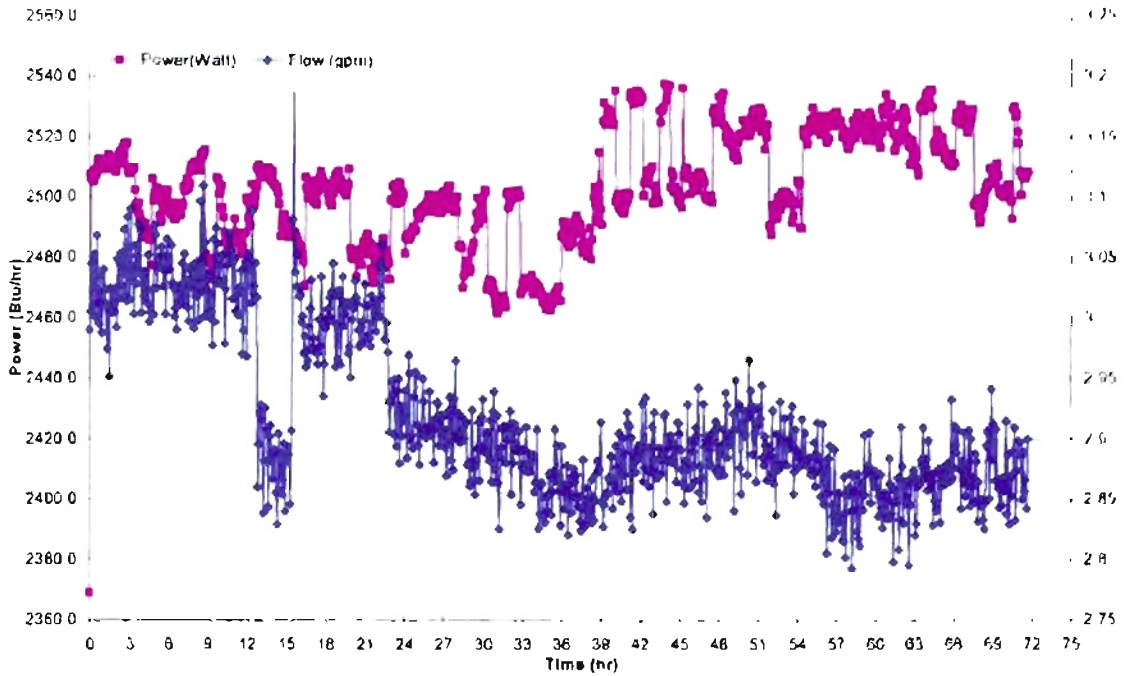

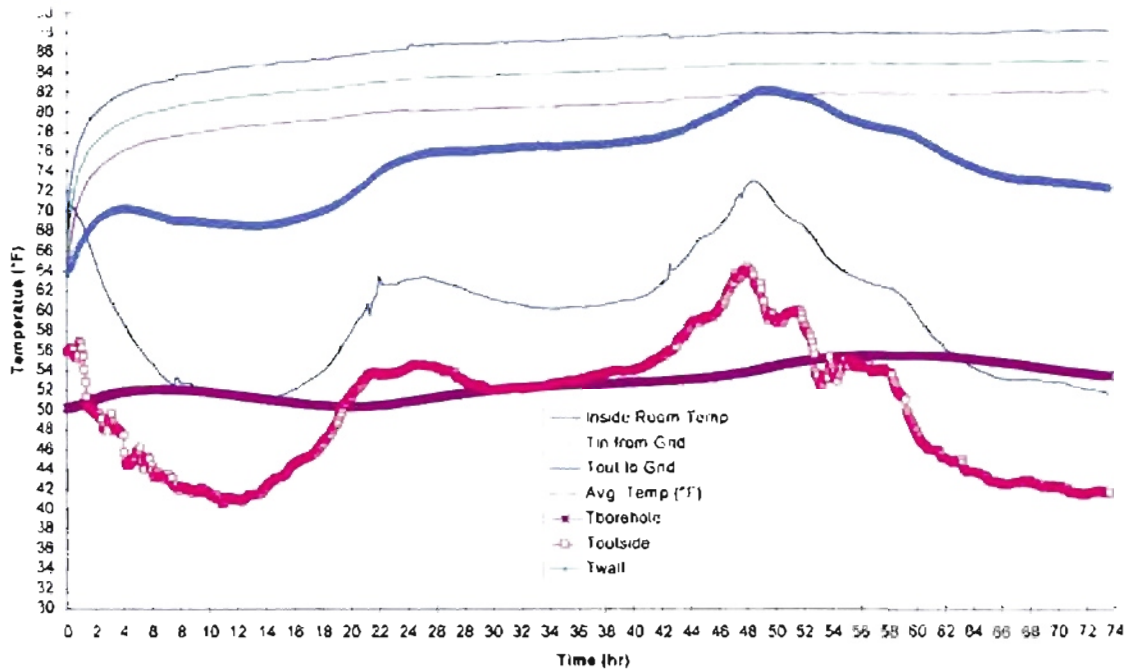## Power and Flow Rates for a test at Site A #2 on 11-8-96

Temperature Rise for Site #3 on 11-17-96. The borehole is 4.5" in diameter and is grouted with Thermal Grout 85.
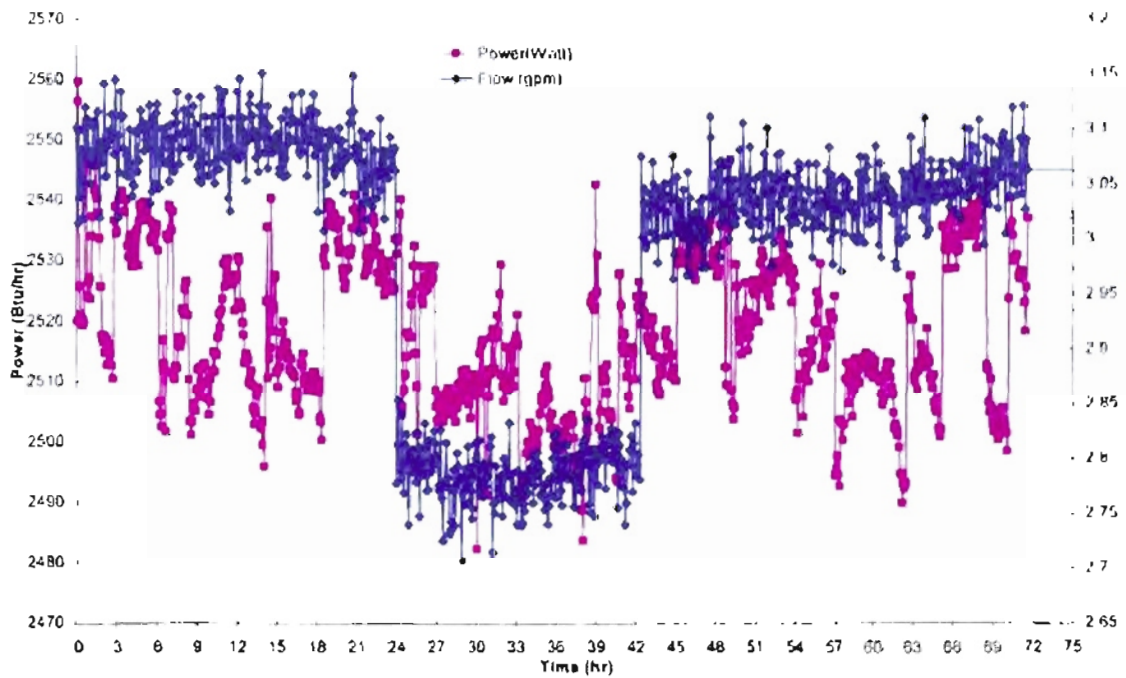

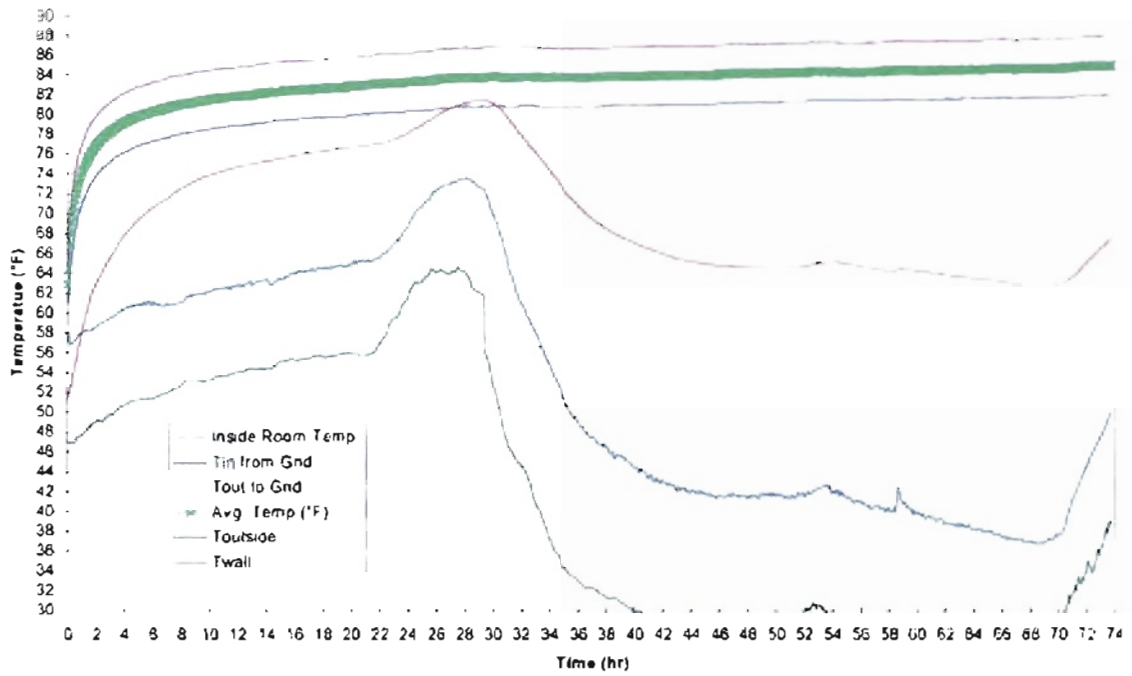Power and Flow Rates for the test of Site A #3 on 11-17-96

162

Temperature Rise for Site #4 on 11-21-96. The borehole is 4.5" in diameter and is grouted with 30% Bentonite.
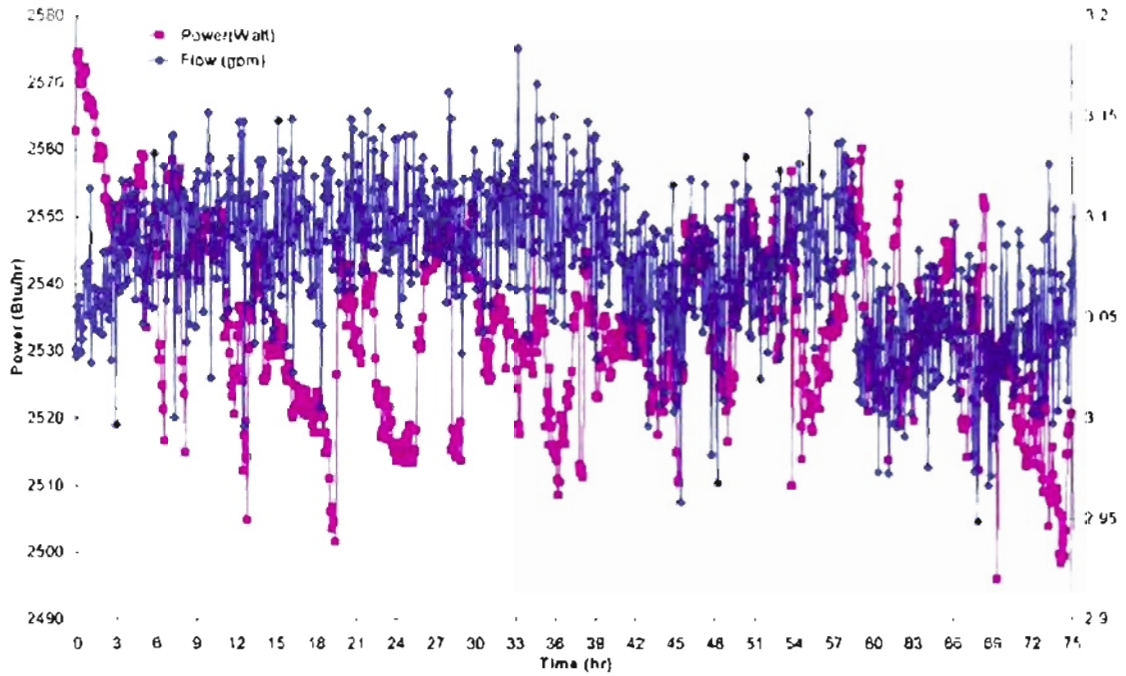

Energy Input to the Water by the Heater Elements and Circulating Pumps for Vertical Hole #4 on 11/21/96 at Site A

Temperature Rise for Site A #5 on 11-25-96.

Legend:
- Inside Room Temp
- Tin from Gnd
- Tout to Gnd
- Avg Temp (°F)
- Toutside
- Twall

Y-axis: Temperature (°F)
X-axis: Time (hr)

Power and Flow Rates for the test of Site A #5 on 11-25-96

Legend:
- Power(Watt)
- Flow (gpm)

Y-axis: Power (Btu/hr)
X-axis: Time (hr)

164

VITA

Warren A. Austin, III

Candidate for the Degree of

Master of Science

Thesis: DEVELOPMENT OF AN IN SITU SYSTEM FOR MEASUREMENT FOR GROUND THERMAL PROPERTIES

Major Field: Mechanical Engineering

Biographical:

Personal Data: Born in Oklahoma City, Oklahoma, On January 2, 1972, the son of Warren and Teri Austin; Married Dusti Stanley, On September 30, 1995.

Education: Graduated from Grace Christian Academy, Oklahoma City, Oklahoma in May 1990; received Bachelor of Science in Mechanical Engineering from Oklahoma State University, Stillwater, Oklahoma in December 1995. Completed the requirements for the Master of Science degree with a major in Mechanical Engineering at Oklahoma State University in May of 1998.

Experience: Worked two summers as a laborer for Naylor & Roberts Construction Company 1991 to 1992; employed three summers as a mechanical engineer summer intern for Ted Davis Manufacturing 1993 to 1995; employed by Oklahoma State University, Department of Mechanical Engineering as a graduate research assistant 1995 to 1997; currently employed by Geothermal Design and Engineering, a subsidiary of Oklahoma Gas and Electric, as a Engineering Project Manager.

Professional Memberships: American Society of Heating, Refrigerating, and Air Conditioning Engineers, Inc.; International Ground Source Heat Pump Association; Oklahoma Society of Professional Engineers.